1990

Simulational studies of the formation and properties of ring galaxies and leading one-arm spirals due to galaxy encounters

Pnina Lotan-Luban
Iowa State University

INFORMATION TO USERS

The most advanced technology has been used to photograph and reproduce this manuscript from the microfilm master. UMI films the text directly from the original or copy submitted. Thus, some thesis and dissertation copies are in typewriter face, while others may be from any type of computer printer.

The quality of this reproduction is dependent upon the quality of the copy submitted. Broken or indistinct print, colored or poor quality illustrations and photographs, print bleedthrough, substandard margins, and improper alignment can adversely affect reproduction.

In the unlikely event that the author did not send UMI a complete manuscript and there are missing pages, these will be noted. Also, if unauthorized copyright material had to be removed, a note will indicate the deletion.

Oversize materials (e.g., maps, drawings, charts) are reproduced by sectioning the original, beginning at the upper left-hand corner and continuing from left to right in equal sections with small overlaps. Each original is also photographed in one exposure and is included in reduced form at the back of the book.

Photographs included in the original manuscript have been reproduced xerographically in this copy. Higher quality 6" x 9" black and white photographic prints are available for any photographs or illustrations appearing in this copy for an additional charge. Contact UMI directly to order.

U·M·I

University Microfilms International
A Bell & Howell Information Company
300 North Zeeb Road. Ann Arbor. MI 48106-1346 USA
313 761-4700 800 521-0600

Order Number 9101364

Simulational studies of the formation and properties of ring galaxies and leading one-arm spirals due to galaxy encounters

Lotan-Luban, Pnina, Ph.D.

Iowa State University, 1990

U·M·I
300 N. Zeeb Rd.
Ann Arbor, MI 48106

Simulational studies of the formation and properties of ring galaxies and leading one-arm spirals due to galaxy encounters

by

Pnina Lotan-Luban

A Dissertation Submitted to the
Graduate Faculty in Partial Fulfillment of the
Requirements for the Degree of
DOCTOR OF PHILOSOPHY

Department: Physics
Major: Astrophysics

Approved:

Signature was redacted for privacy.

In Charge of Major work

Signature was redacted for privacy.

For the Major Department

Signature was redacted for privacy.

For the Graduate College

Iowa State University
Ames, Iowa
1990

TABLE OF CONTENTS

DEDICATION

Dedicated to my husband and best friend Marshall Luban, to our children Dekel, Aviv, and Sarit, and to my parents Ilana and Dov Harpak.

GENERAL INTRODUCTION

I. EXPLANATION OF DISSERTATION FORMAT

This dissertation is divided into six chapters. The first chapter consists of a general introduction which contains a literature survey of the field of interacting galaxies, and an overview of the original research described in this dissertation.

The second chapter describes the study of properties of ring galaxies conducted by my thesis advisor C. Struck-Marcell and myself. The description of this project as given in the second chapter, is based on an article titled "The Varieties of Symmetric Stellar Rings and Radial Caustics in Galaxy Disks", by Struck-Marcell and Lotan, to be published in the *Astrophysical Journal*, Volume **358**, in the July 20, 1990 issue

The third chapter deals with effects of multiple-passages and merger on the morphology and kinematics of a ring galaxy. It is written in a journal article format identical to a paper titled "Effects of Satellite Multiple Passages and Merger on a Ring Galaxy" by Lotan and Struck-Marcell, submitted to the *Astrophysical Journal* in May 1990. My main contribution to this journal article is the numerical modelling. This project also resulted in a contributed talk which I presented at the conference *"Evolutionary Phenomena in Galaxies"*, which took place in Tenerife, Canary Islands, in July 1988, as well as a publication as part of the conference proceedings, titled *"Classes of Ring Galaxies Generated by Dynamical Friction"* by Luban-Lotan and Struck-Marcell, published in *Astrophysics and Space Science* **156**: 229-234, 1989. The latter publication will not be included in its original form as part of the dissertation, since its content and scope are superseded by the more complete project article which constitutes this

chapter. This chapter, which is written in a journal format, and includes introductions to the topics, as well as conclusions and suggestions for future investigation, should thus stand as self-contained.

The fourth chapter of the dissertation describes a new scenario for the formation of leading one-arm spirals. It is similar to a journal article on this topic titled "Long-Lived Leading One-Spiral Arm Produced in a Head-On Off-Center Galaxy Collision" by P. Lotan, currently in preparation for submission to the *Astrophysical Journal.*

The fifth chapter describes an efficient method for the accurate evaluation of the gravitational field arising from a flattened exponential density distribution. A journal article titled "A Computational Method for the Gravitational Field of Disk Galaxies" on this topic, by P. Lotan and M. Luban, is currently in preparation for submission to a journal.

Since the numerical model, namely the restricted three-body code, is used in all three projects described in the second, third and fourth chapters of this dissertation, I will describe the method once in the third chapter, and refer to this description in the other two chapters.

The last chapter contains a summary of the dissertation, the major conclusions, and future research directions.

II. LITERATURE SURVEY OF INTERACTING GALAXIES

Until the 1970s the widespread view among astronomers was that galaxies are "island universes" which are born, evolve, and die in isolation. Since then, however, it has been realized that galaxies frequently interact with their environment which consists of neighboring galaxies, satellites, and gas clouds. The various types of interactions are now believed to be responsible for a host of phenomena, including a variety of morphologically fascinating galaxies and merger remnants, the triggering of vast star formation in galaxies, and the fueling of nuclear activity in quasars.

The growing realization, prior to the 1970s, that galaxies are susceptible to significant mutual influence was based on two main premises. (1) The mean separation between galaxies is only of the order of 10 to 100 their diameters. This ratio is roughly seven orders of magnitudes smaller than the equivalent ratio for stars. (2) Unlike stars, galaxies are composite systems and thus are subject to sizable tidal deformations, and consequently, loss of orbital energy. As a result the galaxies' relative orbits may shrink, and the participating galaxies might merge.

The first astronomer who tried to put these ideas to work was Holmberg (1940), who executed the first simulation of interacting galaxies by using two sets of several dozens moving lamps, which were computerized to move according to the mutual gravity mathematically assigned to them. In this first of its kind simulation Holmberg demonstrated the role of tidal forces between the galaxies, and the resulting loss of orbital energy. On the observational front, Holmberg pointed out the important fact that galaxies tend to reside in small groups of typically two or three galaxies, rather than

in isolation, while Zwicky (1956, 1959) contributed a rich collection of photographs of interacting galaxies.

The next leap in the understanding of interacting galaxies occurred no less than thirty years after Holmberg's pioneering work. In 1972, Alar and Juri Toomre conducted restricted three-body simulations which demonstrated that pure gravitational forces acting between two colliding galaxies, can give rise to the "bridges and tails" already known from the observations of Zwicky (1956, 1959) and Arp (1966).

The growing understanding of the mechanisms of violent relaxation and tidal friction laid the theoretical groundwork for realizing the importance of orbital decay and merger. Chandrasekhar (1943) first showed that a body moving through an infinite homogeneous background of stars, will be subject to a drag force brought about by the wake of enhanced density behind it, which is induced due to the gravitational attraction of the body on the surrounding stars. Further theoretical work on tidal friction - the extension of dynamical friction to two interacting extended systems - demonstrated the surprising fierceness of this force. Satellites were found to spiral rapidly into their parent galaxies, and two galaxies of comparable size were shown to merge even within one orbital period, in particular following penetration or slow close encounters.

Due to progress in numerical modelling of galaxies, and advances in computation capabilities, an entire array of peculiar galaxies could be explained as collision remnants. Approximately 6% of all galaxies are classified as peculiar, mainly on the basis of an unusual, rare morphology. Among these are galactic bridges and tails, which were shown (Toomre and Toomre 1972) to consist of material tidally stripped from the interacting galaxies, and arranged in long and skinny structures. Shells or arc-like structures were interpreted (Quinn 1984) as the debris of a small galaxy

which "fell" into an elliptical galaxy, and whose material oscillates back and forth inside the elliptical, with the turning points marking the arc-like features. A different interpretation of arcs in SO galaxies is that these are tidal distortions of a disk galaxy following a nearly central passage of a small galaxy through the disk (Wallin and Struck-Marcell 1988). Some elliptical galaxies, previously believed to be relics from the era of galaxy formation which probably took place shortly after the big-bang, were shown to be piles of stars left over from the merger of two spiral galaxies (Toomre and Toomre 1972, and Toomre 1977). Polar rings surrounding some S0 galaxies are believed to be the debris left over from an orbiting satellite which was tidally disintegrated, or material tidally stripped from a disk galaxy, upon its passage close to an S0 galaxy (Schweizer, Whitmore and Rubin 1983). Cd galaxies, which are supergiant bright ellipticals residing near the centers of some galaxy clusters, are suspected to be "cannibals" which gradually consume other galaxies in the cluster (Ostriker and Tremaine 1975). Due to dynamical friction acting on the cluster members, they end up spiraling toward the cluster center, and being "swallowed" by the Cds. Supporting evidence for this scenario is provided mainly by the presence of "multiple nuclei" in approximately one-quarter to one-half of all Cds (Schneider, Gunn and Hoessel 1983). However, this hypothesis is still doubtful, and it is possible that these supergiants are simply the brightest galaxies in the cluster. Star-burst galaxies, characterized by an unusally high central activity, have been shown to often correlate with interacting and merging galaxies (Balick and Heckman 1982, and Joseph *et al.* 1984). The hypothesis is that new hot massive stars form in a burst in these galaxies, and heat up the surrounding gas and dust from which they were born. The heated dust then reemits this enormous flux of energy, in the infrared wavelength. The Infra-Red Astronomical Satellite (IRAS) launched in 1983, which scanned the sky for

10 months, detected enormous amounts of energy from these sources in the infrared wavelength, to which the earth's atmosphere is largly opaque. Quasars, which are extremely distant objects and emit energy at rates which are orders of magnitude greater than "normal" galaxies, have also been shown to be associated with interacting galaxies (Stockton 1982, Hutchings 1983, and Crampton 1984).

It has been estimated that a typical galaxy has experienced a couple of mergers in its lifetime, and has accumulated additional mass roughly equal to its original mass. Thus, it appears that galaxy interactions over the age of the universe, are the rule, rather than the exception, which makes the realm of galaxies yet more complex, and richer than previously believed.

In the context of this dissertation, two rare types of peculiar galaxies are of special interest. These are ring galaxies, and leading one-arm spiral galaxies, with occurence of approximately 1 in 10,000 and 5 in 10,000 of all galaxies, respectively. Ring galaxies, so named due to their distinct ring-like structure, where most of their luminous energy output originates, were interpreted as the aftermath of a nearly head-on collision between a disk galaxy and an arbitrary galaxy (Theys and Speigel 1976, Lynds and Toomre 1976), or possibly as the remnant of a collision between a disk galaxy and an intergalactic gas cloud (Freeman and de Vaucouleurs 1974).

Whereas most grand-design spiral galaxies contain two trailing arms, and are symmetric under a revolution of 180^{o}, a portion of spiral galaxies contain one, three, or a greater number of arms. Also, a small minority of spiral arms are leading, namely, the tip of their arms point in the direction of the disk rotation. Most of these peculiar spirals are believed to owe their unique structure to an external influence, in particular forcing from a neighboring galaxy. Specifically, the rare family of leading one-arm spirals was demonstrated, in both analytic and numerical calculations, to result from

a co-planar retrograde encounter of a disk galaxy with another arbitrary galaxy (Athanassoulla 1978, Thomasson *et al.* 1989).

In summary, in the last two decades it has been realized that the universe, on all scales, is extremely dynamic and violent. Interacting, colliding and merging galaxies are the main entities that contribute to this property of the universe.

III. TOPICS OF DISSERTATION

In my dissertation I will concentrate on two rare types of interacting galaxies already referred to in the literature survey in the previous section. These are ring galaxies and leading one-arm spiral galaxies. My research was conducted in three different, yet interrelated areas.

The first project concentrates on an in-depth analysis of the morphology and kinematics of ring galaxies within the conventional collisional model of Theys and Speigel (1976) and Lynds and Toomre (1976). Two numerical tools are employed in this research. The first is a restricted three-body method, which we use to simulate single-collision ring galaxies. This code invokes realistic, time-independent, bulge, disk and halo potentials. Inclusion of a flattened disk potential approximates the effect of disk self-gravity, and serves as an *effective field* felt by the disk test particles. This makes for a significant improvement over the spherical potentials used in the pioneering restricted three-body simulations of Toomre and many others who followed. The second method we utilized is an analytic method, which is an elaboration of a simple kinematic model developed by Toomre (Lynds and Toomre 1976, and Toomre 1978) for ring formation. The purpose of this project is to gain a better understanding of the fine structure of ring galaxies and its dependence on various parameters, including target-to-companion mass ratio, and the structures of the target and companion galaxies. The results of the two methods are compared to each other, in particular in order to test the validity of the approximations made in the kinematic model. Comparison of the results of both methods to observations may clarify the formation mechanism, and possibly put constraints on the collision parameters, and the

structures of the colliding galaxies.

The second project is an investigation of effects of multiple passages of a companion through a disk galaxy. In the literature survey (Section II above) we stressed the importance of mergers between galaxies. Since ring galaxies are the aftermath of highly central and slow collisions, they are excellent candidates for merger. The investigation of effects of the merger process on a disk galaxy is conducted using the numerical and analytical methods described above, as well as numerical hydrodynamical calculations. In this work we find that ring-forming collisions, within a certain range of realistic parameters, may lead to the merger of the ring galaxy with its intruding galaxy. This result implies a classification into a class of merged ring galaxies, and another class of ring galaxies whose intruding companion escaped, and thus is expected to be apparent in the vicinity of the ring galaxy. The two classes are found to differ in various morphological and kinematic characteristics, in addition to the existence or non-existence of an apparent companion. This classification is probably closely related to an empirical classification of Few and Madore (1986) which has up till now lacked a satisfactory explanation.

Another rare type of interacting galaxies, referred to in the literature survey, is leading one-arm spiral galaxies. Dozens of numerical restricted three-body simulations I have conducted, exhibited the formation of simulated leading one-arm spirals for a domain in parameter space, previously unreported, and different from the production mechanism discussed in the existing literature. In the numerical simulations I found that leading one-arm spirals share a similar production mechanism with ring galaxies, the difference being the amount of off-centeredness of the nearly head-on collision. In the existing literature, only co-planar retrograde encounters are reported to result in leading one-arm spirals. I find that,

similar to ring galaxies, the basic phenomenon responsible for this unique structure, is the radial epicyclic oscillations of the disk stars excited by the temporary increase in the inward gravitational pull created by the passage of the companion. In addition, the detailed structure of the single arm is found to depend on the collision parameters, target to companion mass ratio, and the structures of the colliding galaxies.

The fourth research area deals with an efficient numerical methods for calculating the gravitational field created by a flat density distribution. The motivation for this project was provided by the multiple-passage research project. In the course of the latter research it became clear that inclusion of a flattened disk potential is absolutely essential in order to prevent unrealistic behavior of the particles in the restricted three-body code. Specifically, multiple passages give rise to extensive heating and thickening of the disk in the direction normal to the disk plane. While thickening of the disk will indeed take place in real galaxies, exaggeration of this phenomenon is prevented due to the large restoring force exerted by a flat planar density distribution. The numerical method we present for calculating the disk potential overcomes great difficulties originating in the slow convergence of the integrals appearing in the expressions for the field components. These complexities have been overcome with the use of the Levin (1973) method for accelerating the convergence of an infinite series. This method turns out to be especially helpful in achieving highly accurate numerical values of the disk field.

IV. REFERENCES

Arp, H. C. 1966, *Atlas of Peculiar Galaxies* (Pasadena: California Institute of Technology)

Athanassoula, E. 1978, *Astron. Astrophys.*, **69**, 395.

Balick, B. and Heckman, T. M. 1982, *Annu. Rev. Astron. Astrophys.*, **20**, 431.

Chandrasekhar, S. 1943, *Ap. J.* , **97**, 255.

Crampton, B. C. 1984, *Ap. J.*, **280**, 41.

Few, J. M. and Madore, B. F. 1986, *M.N.R.A.S.*, **222**, 673.

Freeman, K. C. and de Vaucouleurs, G. 1974, *Ap. J.*, **194**, 569.

Holmberg, E. 1940, *Ap. J.*, **92**, 200.

Holmberg, E. 1941, *Ap. J.*, **94**, 385.

Hutchings, J. B. 1983, *Publ. Astron. Soc. Pacific*, **95**, 799.

Joseph, R. D. *et al.* 1984, *M.N.R.A.S.*, **209**, 111.

Levin, D. 1973, *Int. J. Computer Math.*, **3**, 371.

Lynds, R., and Toomre, A. 1976, *Ap. J.*, **209**, 382.

Ostriker, J. P., and Tremaine, S. P. 1975 *Ap. J. Lett.*, **202**, L113.

Quinn, P. J. 1984, *Ap. J.*, **279**, 596.

Schneider, D. P., Gunn, J. E., and Hoessel, J. G. 1983, *Ap. J.*, **268**, 476.

Schweizer, F. 1986, *Science*, **231**, 227.

Schweizer, F., Whitmore, B. C., and Rubin V. C. 1983, *A. J.* , **88**, 909.

Stockton, A. 1982, *Ap. J.*, **257**, 33.

Theys, J. C. and Speigel, E. A. 1976, *Ap. J.*, **208**, 650.

Thomasson, M., Donner, K. J., Sundelius, B., Byrd, G. G., Huang, T.-Y., and Valtonen, M. J. 1989, *Astron. Astrophys.*, **211**, 25.

Toomre, A. 1977, in *The Evolution of Galaxies and Stellar Populations* (New Haven, CT: Yale University Observatory) p. 401.

Toomre, A. 1978, *The Large Scale Structure of the Universe*, ed. M. S. Longair and J.Einasto (Dordrecht: Reidel), p. 109.

Toomre, A. and Toomre, J. 1972, *Ap. J.*, **178**, 623.

Wallin, J. F. and Struck-Marcell, C. 1988, *A.J.*, **96**, 1850.

Zwicky, F. 1956, *Ergeb. Exakten. Naturwiss.*, **29**, 344.

Zwicky, F. 1959, *Handb. Phys.*, **53**, 373.

14

THE VARIETIES OF SYMMETRIC STELLAR RINGS AND RADIAL CAUSTICS IN GALAXY DISKS

ABSTRACT

Numerical restricted-three-body and analytic calculations are used to study the formation and propagation of cylindrically symmetric stellar ring waves in galaxy disks. These calculations assume a number of different gravitational potentials or potential components in the target galaxies, including softened point-mass, Hubble-like, and Plummer potentials, exponential disks, and a nearly isothermal halo. A variety of ring morphologies are found depending on the collisional disturbance amplitude, and the form of the potentials. Alternately, the models suggest that morphological features, including: the number of separate nonoverlapping stellar rings, ring widths, and ring-to-ring separations, can provide useful information about the gravitational potential in ring galaxies.

The application of singularity theory techniques to the kinematic radial oscillation model for rings of Lynds and Toomre (1976) and Toomre (1978) allows the analytic derivation of ring formation time; ring width as a function of time, position, ring number, and collisional perturbation amplitude; and the relative overdensities of rings versus inter-ring regions. Good agreement is found between the analytic and numerical results which indicates that the approximations made in the simple kinematic model are valid, at least to the degree that the restricted three-body method represents real galaxies. Comparison of the models to real ring galaxies may provide certain knowledge of the properties of these galaxies, as well as impose constraints on the collision parameters responsible for their formation.

I. INTRODUCTION

The basic collisional model of ring galaxies was presented by Lynds and Toomre (1976) and Theys and Spiegel (1976), and elaborated by Toomre (1978). The model resolved the mystery of the ring in the famous Cartwheel galaxy, and implied that other rings with nearby companions are likely to be collision remnants. The publication of the Arp and Madore catalog (1987) greatly increased the number of catalogued ring galaxies, and emphasizes the variety of ring morphologies. Since Toomre's pioneering work, there has been little systematic theoretical exploration of the dependence of ring morphology on the orbital and structural parameters of the colliding galaxies. Yet several recent papers (Hernquist and Quinn 1988, Huang and Stewart 1988, Wallin and Struck-Marcell 1988, Appleton and James 1989, and Lotan and Struck-Marcell 1990) indicate that a variety of unusual morphologies, including thick rings, "diamond" rings, and outer disk ripples, might be the result of collisions like those that produce more "classical" ring galaxies. This point is demonstrated and extended with additional examples of collisional morphology by the numerical, restricted three-body simulations.

Lynds and Toomre (1976) noted that the basic ring phenomenon results from the simple kinematic epicyclic oscillations of the disk stars, following an impulsive disturbance. This suggests that it would be worthwhile to pursue and test analytic results based on the Toomre kinematic model, as well as to compare them to numerical simulations. Such a comparison clarifies the degree to which the kinematical model can be applied to real disk galaxies, and helps to understand the results of the numerical simulations themselves.

The latter point is particularly important since only a finite number of simulations can be carried out in the large parameter space. These analytic, kinematic models are described in Section II and Section III, and compared to numerical results in Section III - Section IV.

II. ANALYTIC APPROXIMATIONS

In this section, we review simple analytic models based on Toomre's kinematic model for the case of a direct collision between a rotating disk and a companion traveling along the disk symmetry axis, where both galaxies have time-independent potentials. (Thus, it is assumed that the change in the galaxy potentials in the encounter has a negligible effect on the subsequent evolution of the target disk.) As a specific example, we study the case of a family of potentials that includes both the softened point-mass and the Plummer potential, and in later sections briefly give results for other potentials. The acceleration of a point particle in these potentials is given by

$$g = \frac{-GM\, r^{2p-2}}{(r^2 + \varepsilon^2)^p}, \tag{1}$$

where ε is the softening length of the potential, and it is assumed that $p \geq 1$. ($p = 1$ is the softened point-mass potential, and $p = 3/2$ is the Plummer potential.) The advantage of this form is that it is relatively simple, but still possesses a rotation curve with qualitative features similar to those observed in many disk galaxies. These include the following: (1) an increasing rotation velocity as a function of radius at small radii, (2) a fairly broad turnover region which mimics a flat rotation curve, and (3) a Keplerian falloff at radii much larger than the softening length. Another practical advantage of these potentials is that they have been used frequently in numerical simulations.

A. The Disturbance

Two limiting types of disturbance are considered which are simple enough to allow an explicit estimate of the magnitude of the disturbance

caused by the intruder galaxy on the stellar orbits in the target galaxy. The first of these special cases is the usual impulse approximation, where it is assumed that the disturbance occurs very rapidly relative to stellar orbital or relaxation times (see e.g., Alladin 1965, Toomre 1977, Tremaine 1981).

Consider the case of an intruder moving rapidly along the disk symmetry axis. In the impulse approximation a star's position changes negligibly during the encounter, and is treated as a fixed number. The net change in the velocity of a star located in the plane of the disk at a position *(x,y,0)* due to an intruder of mass M_C moving on the disk symmetry axis is

$$\Delta\vec{v} = \frac{-2GM_c}{rV_{rel}}\ \hat{r}\,, \tag{2}$$

where $r = (x^2 + y^2)^{1/2}$, and where V_{rel} is the relative velocity between the mass M_C and the disk galaxy.

Among the problems in applying the impulse approximation to galaxy-galaxy collisions is the fact that most collisions are more likely to be marginally bound, rather than highly unbound (e.g., Chatterjee 1987). Thus, the underlying notion of an instantaneous, impulsive hit is not correct. This fact does not necessarily make it impossible to approximate the disturbance, but the approximation must be based on slightly different assumptions. Specifically, if the collision occurs on a timescale comparable to the epicyclic period of a fiducial star, we expect roughly the following sequence of events. First, the star falls radially inward in response to the additional gravity of the companion as the latter approaches the disk center. Once the companion passes through the center, the star continues to fall inward against the centrifugal barrier until it is brought to rest. By this time, the companion is far enough away that its gravity is unimportant relative to the unbalanced centrifugal force, so the star is released to pursue epicyclic oscillations. In

this picture, unlike the impulse case, the star has time to respond to the disturbance.

In a collision where the following conditions are satisfied: (1) The collision is axisymmetric or nearly so, (2) The perturbation on a disk star in the target galaxy is small enough that the star remains approximately confined to the disk plane, then the *magnitude* of the total angular momentum is approximately conserved. This fact can be used as the basis for a simple analytic estimate for the amplitude of the epicyclic motion of a star in the disk plane in response to the perturbation. To begin we assume that the star's minimum radius is the point where the centrifugal force would balance both the disk galaxy gravity and the companion's gravity when it is located at the disk center. This approximation is likely to lead to a slight overestimate of the disturbance. Under these assumptions the radial force balance equation for the star at minimum radius is approximately,

$$\frac{-GM_c}{r^2} - \frac{GM\, r^{2p-2}}{(\varepsilon^2 + r^2)^p} + \frac{h^2}{r^3} = 0, \qquad (3)$$

where subscript c refers to the intruding companion, and h is the magnitude of the angular momentum per unit mass of a star in the target disk. Using the initial unperturbed force balance equation (e.g., eq. [3] with $M_C = 0$) we can eliminate h in equation (3). Then, letting $\xi = r/q$, where q is the initial unperturbed position of the disk star (following Zeldovich's notation for the Lagrangian coordinate) we have the following equation for ξ,

$$-\left(\frac{M_c}{M}\right)\xi\left(\frac{\varepsilon^2}{q^2} + \xi^2\right)^p - \xi^{2p+1} + \left(\frac{\frac{\varepsilon^2}{q^2} + \xi^2}{\frac{\varepsilon^2}{q^2} + 1}\right)^p = 0. \qquad (4)$$

In the limit that $q >> \varepsilon$, the gravity of the parent galaxy reduces to Keplerian form, so that to first order in ε/q the expression for the oscillation amplitude is the same as that for a point mass (i.e., no ε/q term), and is given by

$$\frac{\delta r}{q} = 1 - \xi = \frac{\left(\frac{M_c}{M}\right)}{1+\left(\frac{M_c}{M}\right)} \tag{5}$$

Thus, under the above assumptions, the relative amplitude of the disturbance is independent of the initial position q within the target disk. In the opposite limit, $q << \varepsilon$, the amplitude is dependent on the companion potential, and it does generally depend on q.

Equation (2) gives Δv in the impulse approximation, and the parallel expression in the present centrifugal balance approximation can be derived as follows: $\Delta v \propto \delta r/\Delta t \propto q/\Delta t$ (using eq. [5]). Also $\Delta t \propto 1/\omega$, and $\omega \propto (GM_G/q^3)^{1/2}$ (see eq. [8] below when $q/\varepsilon >> 1$). Therefore, $\Delta v \propto (GM_G/q)^{1/2}$. A comparison between this expression and equation (2) indicates that the disturbance in the outer disk is much greater in this case than in the impulse approximation. Therefore, a significant amount of (orbital) energy is deposited in the outer disk whenever this approximation is valid. Note that the solution to equation (4) is also the equilibrium radius of a disk star following an axisymmetric merger with the companion.

With the results above, we can describe the perturbation amplitude in a variety of limiting cases. However, in most of the analytic work below we will limit ourselves to the simple approximation that the perturbation amplitude is a constant independent of radius. This approximation is not very accurate in the inner parts of the disk, but we have no special interest in those

regions in this work. As a heuristic exploration of the possible dynamical behaviors, this approximation will suffice.

B. Stellar Free Oscillations in a Simple Potential

In response to a low-amplitude, quasi-impulsive perturbation, a star in the target disk will execute radial harmonic oscillations in addition to its initial (circular) orbital motion. As a first approximation we can assume that stars located throughout the disk are essentially noninteracting. The frequencies and relative phases of these epicyclic oscillators, as a function of position within the disk, are the key parameters for determining the structure and evolution of rings or similar waves, as Lynds and Toomre (1976) pointed out.

The oscillation frequency as a function of radius is readily derived from the radial component of the linearized equation of motion (also see Saslaw 1985, Binney and Tremaine 1987). Let the perturbed radius be given by

$$r = q - Aq\sin(\omega t + \phi). \tag{6}$$

where the (constant) amplitude A equals $\delta r/q$. The radial equation of motion is given by

$$\frac{d^2r}{dt^2} = \frac{-GM\,r^{2p-2}}{(r^2 + \varepsilon^2)^p} + \frac{h^2}{r^3}, \tag{7}$$

where we take $h(q)$ to be conserved during the encounter. Substituting equation (6) into equation (7), expanding in powers of the amplitude A, retaining only terms to first order in A, and using the equilibrium version of equation (7) ($d^2q/dt^2 = 0$), leads to the following expression for the epicyclic frequency,

$$\omega^2(q) = \frac{GM\,q^{2p-3}}{(q^2+\varepsilon^2)^p}\left(\frac{q^2+(2p+1)\varepsilon^2}{q^2+\varepsilon^2}\right). \tag{8}$$

Equations (6) and (8) specify the radial kinematics of a disturbed stellar orbit. In exploring the properties of the simple model represented by these two equations we will make the following simplifications: set the amplitude A constant independent of q throughout the disk as discussed above, and set all of the initial phases $\phi(q)$ equal to zero (i.e., assume no initial radial motions).

C. Ring Singularities

In a cylindrically symmetric system, the mass continuity equation gives the following expression for the local star density in terms of the initial unperturbed density $\rho_0(q)$

$$\frac{\rho}{\rho_0} = \left(\frac{r}{q}\frac{\partial r}{\partial q}\right)^{-1}. \tag{9}$$

Note that the density formally goes to infinity when

$$\frac{\partial r}{\partial q} = 0. \tag{10}$$

Equation (10) is essentially an orbit crossing or caustic condition for the radial motion, and we will henceforth take it as our definition of a singularity. However, equation (9) shows that such caustics are also strong density waves. The infinite densities implied for a solution of equation (10) are certainly not realized physically. The finite number of stars in a galactic disk and the fact that the stellar ensemble has a nonzero velocity dispersion are not accounted for in the kinematic motion equation (6). In any case,

equation (10) determines the Lagrangian mapping which describes the location and structure of strong circular density waves, as will now be shown.

Substituting equation (6) into the caustic condition (10) gives,

$$1 - A\sin(\omega_c t) - Aq_c t\cos(\omega_c t)\left(\frac{d\omega}{dq}\Big|_{q=q_c}\right) = 0. \qquad (11)$$

The structure of the gravitational potential of the target galaxy, which must play a key role in determining the propagation of waves and caustics, enters into equation (11) through the radial gradient of the epicyclic frequency. For the potentials specified by equation (1), and using equation (8), this gradient can be written

$$\frac{d\omega}{dq} = -\left(\frac{\omega}{q}\right)\left[\frac{3q^4 + 2(4p+3)q^2\varepsilon^2 - (2p-3)(2p+1)\varepsilon^4}{2(q^2+\varepsilon^2)(q^2+(2p+1)\varepsilon^2)}\right] \qquad (12a)$$

$$= -\left(\frac{\omega}{q}\right) f_1(q/\varepsilon), \qquad (12b)$$

where the function f_1 is defined as the quantity in square brackets in the first equation. Substituting equation (12) into equation (11) we have

$$f_1(q_c/\varepsilon) = \frac{A\sin(\omega_c t) - 1}{A\,\omega_c t\cos(\omega_c t)} = W(A, \omega_c t), \qquad (13)$$

where we have written this in a form that reveals the separability into a function f_1 of the unperturbed structure of the galaxy on the left-hand-side, and a function W of the amplitude and frequency on the right-hand-side.

Equation (13) is a quadratic equation in the quantity $(q_c/\varepsilon)^2$, whose solution is

$$\frac{q_c^2}{\varepsilon^2} = \frac{2W(p+1)-(4p+3)}{3-2W} \pm \frac{2p^{1/2}}{(3-2W)}\left[pW^2-2(3p+1)W+(7p+3)\right]^{1/2}. \quad (14)$$

Recall that q is the initial, unperturbed radius or Lagrangian coordinate of the star, which thereafter labels the ensemble of stars located initially at that radius. Equation (14) specifies the location of a caustic in terms of the Lagrangian coordinates of the stars contained within it. The radial position of the caustic is obtained by substituting equation (14) into equation (6). These equations specify q_c and r_c as complicated functions of the phase ωt (and amplitude A). Since ω is itself a nontrivial function of q, equation (14) cannot be solved explicitly for $q_c(t)$.

There is some simplification in the limiting cases. First, note that equation (14) has real positive solutions only for $(3\text{-}2p)/2 < W < 3/2$, and $3/2 < W < [(3p+1) - (2p^2+3p+1)^{1/2}]/p$ ($\approx 3/2$, *for* $1 \leq p \leq 3/2$). Inspection of equation (13) reveals that this limitation on W implies that the cosine in that equation has a negative sign when $p \leq 3/2$, and so $(2n\text{-}1)\pi - \pi/2 < \omega t < (2n\text{-}1)\pi + \pi/2$, with $n = 1, 2, 3, \ldots$. This means that at a given time caustics can only occur for values of ω (and therefore q) within these intervals. [If $p>3/2$ it is possible to have *inward propagating* ring waves with phase ωt centered on $2\pi n$, rather than $(2n\text{-}1)\pi$.] Whether or not caustics actually form within the allowed phase interval depends on the amplitude A of the perturbation. In any case, each allowed phase interval will be a compressed region, so we will refer to the n^{th} interval as the n^{th} ring.

In the limit $q_c/\varepsilon >> 1$, equations (12) and (13) reduce to $W \approx 3/2$, and

$$A\sin(\omega_c t) - 1 \approx \frac{3}{2}A(\omega_c t)\cos(\omega_c t). \quad (15)$$

On the other hand, if $q_c/\varepsilon << 1$, then $W \approx (3\text{-}2p)/2$ and,

$$A \sin(\omega_c t) - 1 \approx \left(\frac{3-2p}{2}\right) A (\omega_c t) \cos(\omega_c t) . \qquad (16)$$

Equations (15) and (16) constitute the implicit $q_C - t$ relation in their respective limits. Unfortunately, even in these limiting cases we cannot separate $\omega(q_C)$ from t, to solve explicitly for $q_C(t)$. Yet a graphical representation reveals much of the essence of these equations. This is shown in Figure 1 (for the softened point-mass case $p=1$), where the left hand side of the equations (divided by $A = 1/7$) is graphed as a thick curve while the right hand sides are graphed as thin curves. The solid curve corresponds to equation (15) and the dotted curve to equation (16). The intersections between thick and thin curves mark the solutions to the equations. The thickened intervals on the phase axis designate the allowed regions, where caustics can occur.

D. Ring Structure and Fold Singularities

For the arbitrarily chosen amplitude $A = 1/7$ in Figure 1, there are no caustics for the first allowed interval ($n=1$). There are caustic solutions to equation (16) for $n=2$, but not for equation (15). This suggests the possibility that in some cases, a ring may originate in the inner regions as a mere density enhancement, and only later as it propagates to the outer disk, develop caustics. (Such a case is also evident in the second ring for $A = 0.1$ (solid curve) in Fig. 7 below.) Caustic solutions exist in both cases for higher values of n, if $p < 3/2$. (If $p = 3/2$, the Plummer model, caustics can never form in the limit of eq. [16], and if $p > 3/2$ inward propagating caustics can form in this limit.) It is also evident from the figure that caustic solutions appear in the intervals corresponding to small values of n as the amplitude

Fig. 1 - Solutions to the caustic condition as a function of oscillation phase in the limiting cases given by eqs. (15) and (16) divided by A (and with dummy variable $t' = \omega t$). The thick solid curve represents the left-hand-side of those eqs. when the amplitude $A = 1/7$. The thin solid and dashed curves represent the right-hand-sides of eqs. (15) and (16) respectively. Intersections between the thick curve and either the thin solid curve or the dashed curve imply the existence of caustics in the outer and inner disk, respectively. These intersections are highlighted with open circles. Intersections can only occur in permitted phase intervals which are marked as thick lines on the $f(\omega t) = 0$ line. For smaller amplitudes A the thick curve is translated downward, making caustics less likely in the first few rings, while for larger amplitudes the thick curve is translated upward.

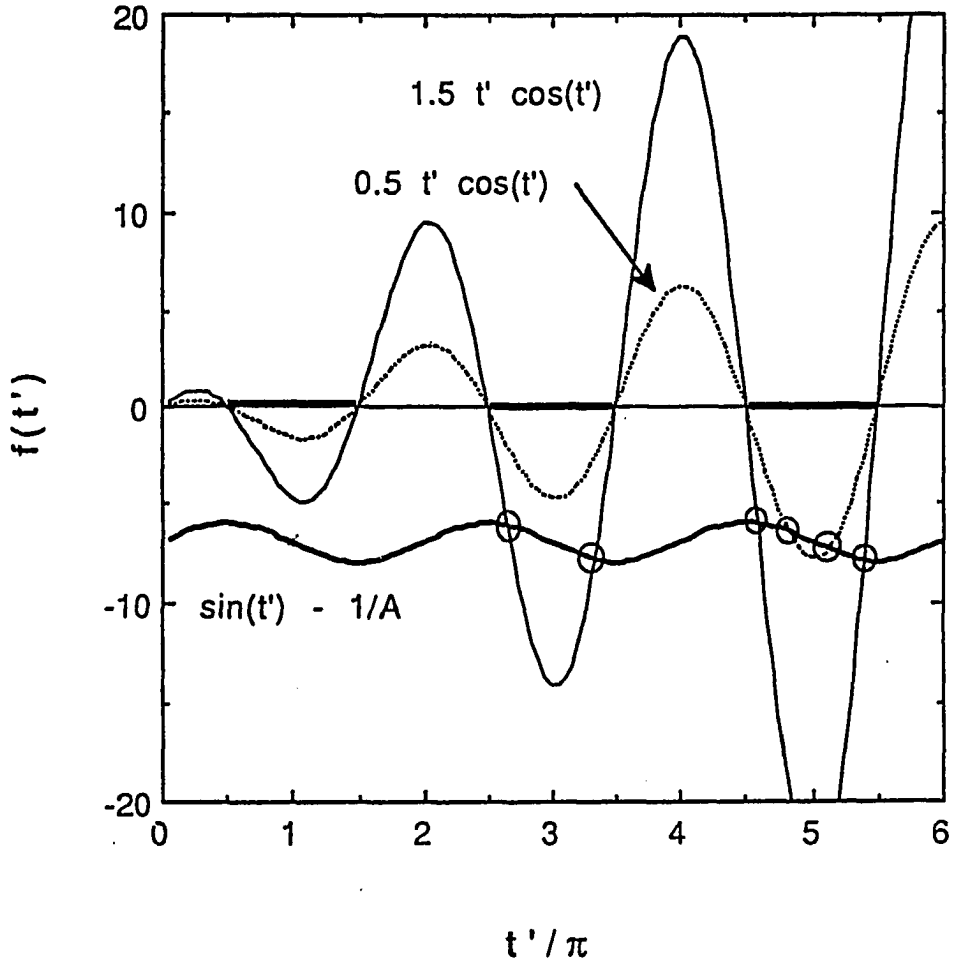
20
10
0
-10
-20
0
1
2
3
4
5
6
f(t')
t ' / π
1.5 t' cos(t')
0.5 t' cos(t')
sin(t') - 1/A

A is increased. (In the figure, the thick solid curve is pushed upward as the amplitude is increased.) Alternately, for the n^{th} interval there exists some minimum value of the amplitude A^n_{min} for the appearance of a caustic in that interval. If $A = A^n_{min}$ then the curves for the left hand side and the right hand side of equation (15) or (16) will intersect at a point, with $\omega_c t \approx (2n-1)\pi$. For A slightly greater than A^n_{min} there will be paired caustic solutions within the relevant interval, one on each side of the phase $\omega t = (2n-1)\pi$, and quite close to it. These are the inner and outer edges of the ring. Define this phase difference as θ, such that $\omega t = (2n-1)\pi \pm\theta$. For A slightly greater than A^n_{min}, θ is small, so we can approximate

$$\sin(\omega t) = \pm\sin(\theta) \approx \pm(\theta - \frac{1}{6}\theta^3), \text{ for } \theta = \pm((2n-1)\pi - \omega t),$$
$$\text{and, } \cos(\omega t) = -\cos(\theta) \approx -1 + \frac{1}{2}\theta^2. \qquad (17)$$

Substituting $\omega_c t$ into equation (15) and expanding to third order in θ yields,

$$\frac{11}{12}(\pm\theta)^3 + \frac{3}{4}\pi(2n-1)\theta^2 - \frac{1}{2}(\pm\theta) + \frac{1}{A} - \frac{3}{2}(2n-1)\pi = 0. \qquad (18)$$

First of all, we note that if $\theta = 0$, this equation implies that $A^n_{min} = [3\pi(2n-1)/2]^{-1}$, or $A^n_{min} = [\pi(2n-1)(3-2p)/2]^{-1}$ if we use equation (16). These values for A^n_{min} imply some interesting consequences for collisions with very low mass companions. For example, with $M_c/M = 0.05$ and $p \approx 1$ we would not expect the caustic condition to be met until the third or fourth ring. Also the ring would be thin and contain very little mass (see below). These conclusions are confirmed in numerical simulations (described below).

To first order in θ, the solution to equation (18) is

$$\pm\theta^{(n)} \approx 2\left(\frac{1}{A} - \frac{1}{A^n_{min}}\right) = 2\left(\frac{A^n_{min} - A}{A\,A^n_{min}}\right), \qquad (19)$$

which is a useful estimate for the spreading behavior of the two caustic branches as A increases beyond $A^n{}_{min}$. The symmetry between the positive and negative θ is retained at least to the second order solution.

The double-branched nature of the ring caustics is confirmed by Figures 2 and 3, in which equations (6) and (8), with $A = 0.2$ are plotted in two different ways. Figure 2 shows radius r as a function of initial radius q at a fixed (late) time. The singularities are, by definition, points where the curve has zero slope. It is apparent from Figure 2 that, in general, these points come in pairs, as expected. We also can see in Figure 3 that these singularities make-up the inner and outer boundaries of the ring, defined as an overdense region.

Figures 2 and 3 (see also Fig. 6 of Toomre 1978) show that there are three streams of particles at any position within a ring. These include: (1) stars falling through the ring toward their innermost radius, (2) stars moving up through the ring after reaching their lowest point, (3) stars falling from their maximum radius, back through the ring, and then out through the inner edge of the ring.

Another point that is obvious in Figure 3 is that the outer edge of a high-order ring can move through the inner edge of the previous ring. Figures 1 and 3, as well as equation (19), do indicate (through the dependence of $A^n{}_{min}$ on n) that the first few rings will be progressively broader, at least in terms of the opening angle θ. More precisely, if we assume that the Lagrangian position of all particles within the ring are roughly equal, then the ring half-width Δr is approximately $r_c - q$, namely the difference between the

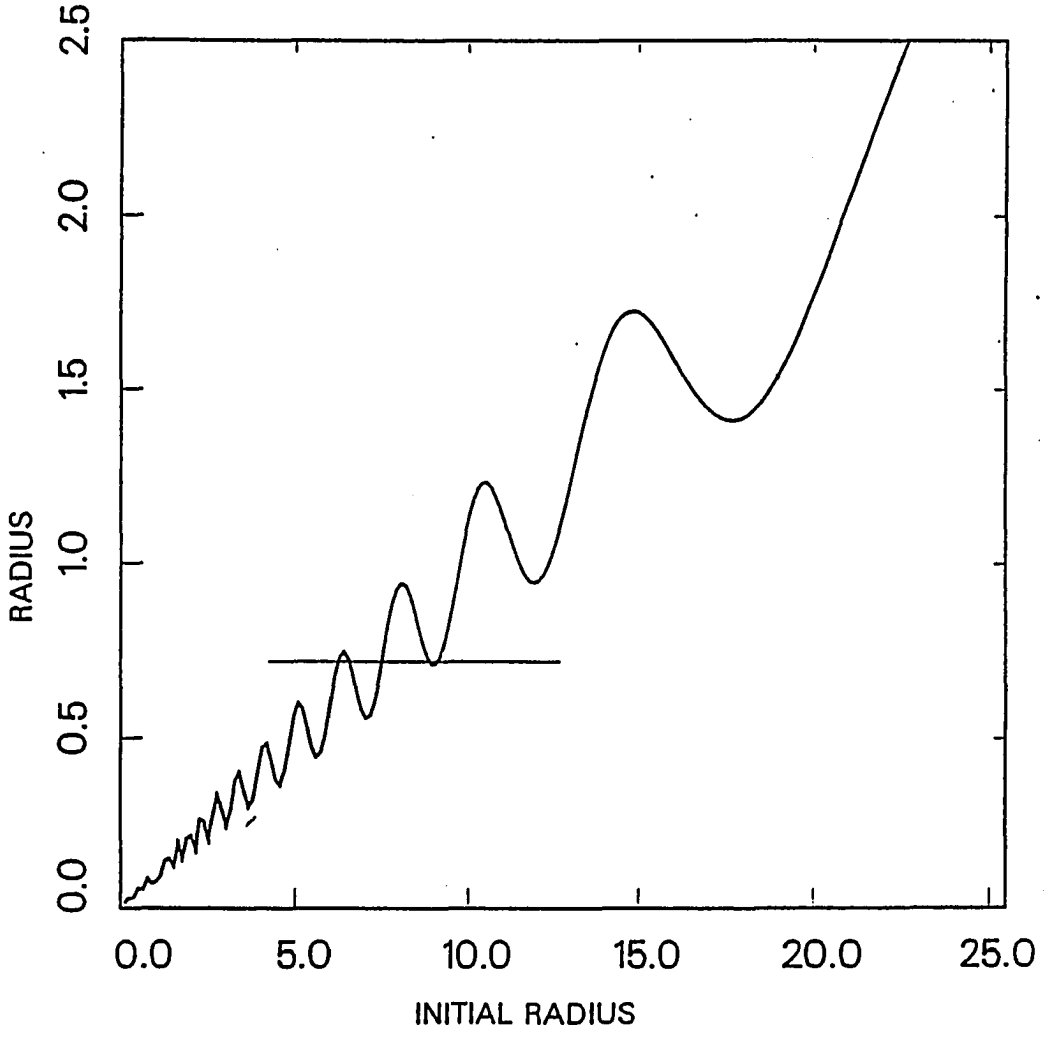

Fig. 2 - Radius $r(q)$ as a function of initial (Lagrangian) radius q at a time of $t = 16\tau_{ff}$, with a perturbation amplitude of $A = 0.2$ ($p = 1$), showing the fold singularities as local peaks and valleys. r and q values are in units of the softening length ε. The horizontal line segment shows a region of overlapping rings, where there are five distinct particle streams.

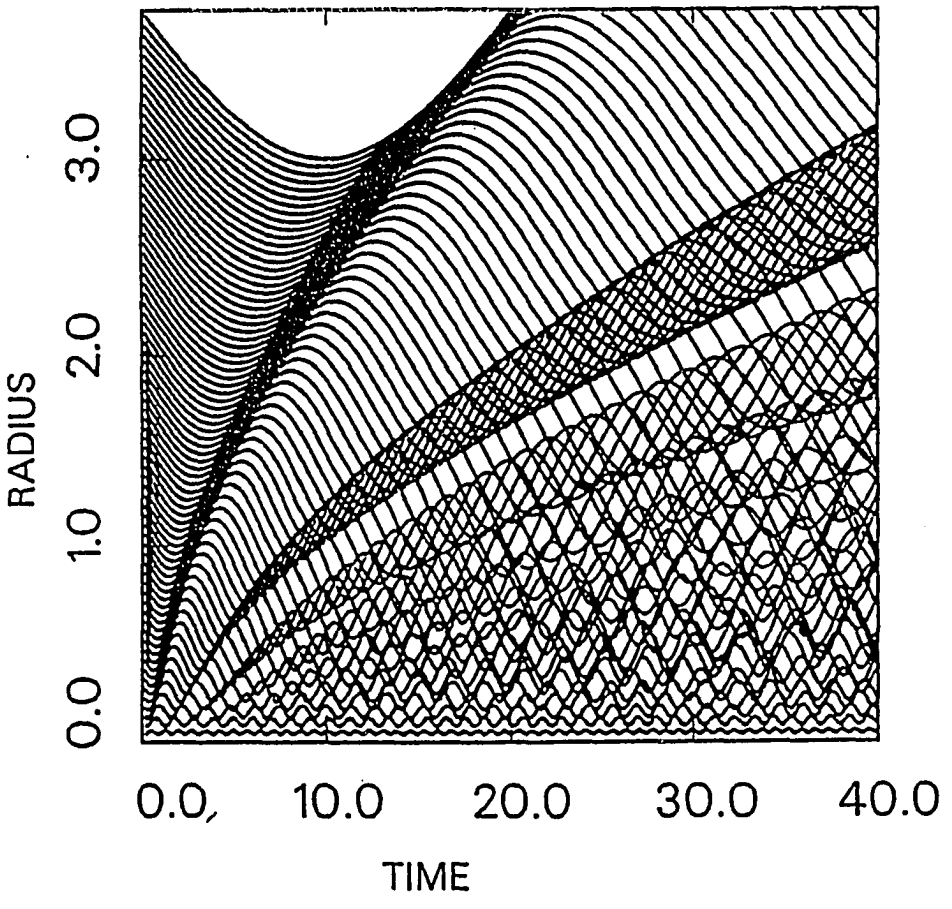

Fig. 3 - Radius-time plots of the stellar trajectories $r(q,t)$, calculated according to eqs. (6) and (8) with $p = 1$. The values of r and t are in units of ε and τ_{ff}, the free-fall time at $r=\varepsilon$, respectively. Each case has a different value of the amplitude A: (a) $A = 0.2$, (b) $A = 0.3$, and (c) $A = 0.1$.

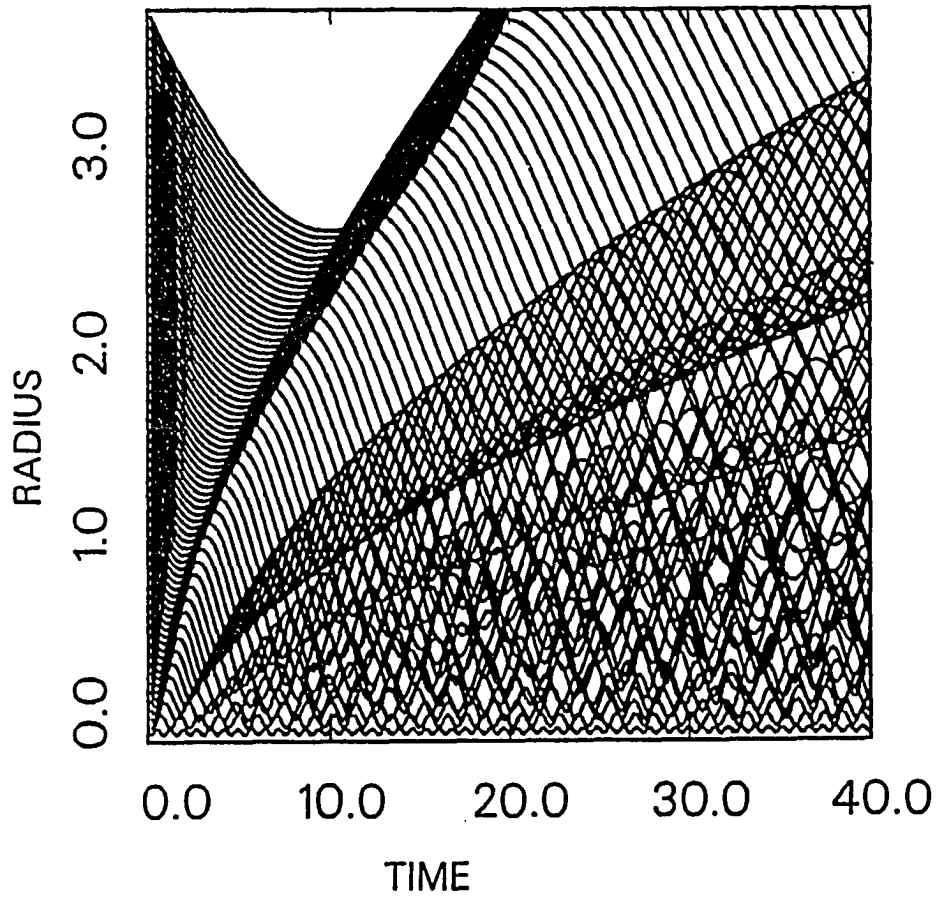

Fig. 3 (continued)

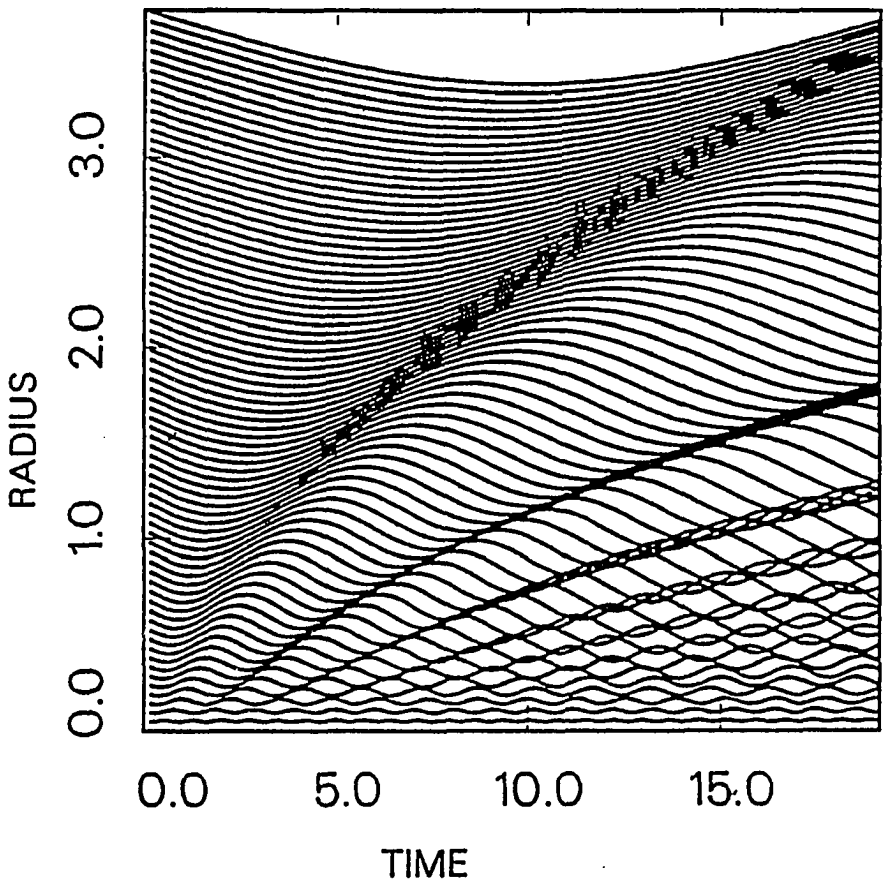

Fig. 3 (continued)

position of a caustic particle and its unperturbed radius. Then, using equations (14), (6) and (17) we get

$$\frac{\Delta r}{\varepsilon} = A\frac{q}{\varepsilon}\sin(\theta). \qquad (20)$$

The width increase of a ring as it propagates outward is dominated by the q/ε factor, while the θ factor is responsible for the increase in width from ring to ring for the first few rings (in this potential). Once the rings begin to broaden substantially they overlap other rings, so the latter effect can be difficult to discern in the simulations described below.

As can be seen from Figure 1 (or derived from eq. [19]), in the limit $n >> 1$, and for $A >> A^n_{min}$, the caustics occur at a phase differences $\theta \approx \pm\pi/2$. Since the phase ωt of the ring center is approximately an odd multiple of π (again see Fig. 1, and below), then the phases of the ring edges are approximately odd multiples of $\pi/2$. Equation (6) indicates that the extrema of a single particle's oscillatory motion also occur at odd multiples of $\pi/2$ in phase. This means that the outer (inner) caustic occurs at apoapse (periapse) of the radial oscillations of the particles in the ring. Also the ring width (from either eq. [14] or eq. [20]) is about Aq, with q equal to the average Lagrangian coordinate of the particles in the ring (cf., Figs. 3, 7). These results are independent of n, for n sufficiently large, so the width of all high-order rings is the same. The high n ring edges all behave like the epicyclic analogue Quinn's radial shells (Quinn 1984, Hernquist and Quinn 1987) in this limit.

III. RINGS IN GALAXIES WITH SINGLE-COMPONENT POTENTIALS

A. Restricted Three-Body Models with Realistic Potentials

The accuracy of the Lynds and Toomre (1976) kinematic model of the stellar dynamics in colliding galaxies appears to depend on many approximations. These include: (1) either the impulse approximation or the centrifugal release approximation (eq. [7]) to the disturbance, (2) the epicyclic approximation to the perturbed stellar orbits (eq. [8]), (3) that the gravitational potential of the target galaxy is rigid, (4) that this is a single-component potential whose gradient is given by equation (1), for example, (5) that the effects of thermal diffusion due to the stellar random velocities are negligible over the lifetime of the rings, (6) that thermal diffusion resulting from dynamical heating in the encounter is negligible. Item 4. is trivial since other, multi-component potentials can equally well be used in kinematic models. The smoothing effects of thermal diffusion can be estimated simply (see Section V). However, most of the other effects cannot be evaluated so simply.

In this section, we will present the results of a number of restricted three-body type simulations of ring-making collisions. These give a direct indication of the validity of approximations 1, 2, and 5. A full evaluation of approximations 3 and 6 probably requires full N-body simulations. For example, only N-body simulations self-consistently calculate the effects of halo oscillations and dynamical friction. In order to check the validity of the restricted three-body method for describing the disk response in a ring galaxy, we have compared our simulations to the N-body simulations of Appleton and James (1989, and private communication, Department of

Physics, Iowa State University). The particle resolution of the graphical output of these simulations was not sufficient to permit quantitative comparison (but further work is underway). However, many of the qualitative features are similar, as detailed below. In the present work, we consider only single encounters, i.e., where the companion orbit is parabolic or hyperbolic and the dynamical friction of the target galaxy is insufficient to drag the companion back over the lifetime of the rings in the disk.

We have constructed a restricted three-body type code which we use to simulate the colliding galaxy. The target galaxy is made of three components: bulge, disk, and halo. The bulge is characterized by a mass density distribution of the form

$$\rho_B(r) = \frac{\gamma}{\pi^2} \frac{M_B}{(r^2+\gamma^2)^2} \tag{21}$$

(which will be termed a "Hubble-like" profile). The corresponding gravitational acceleration is

$$g_B = \frac{2}{\pi} \frac{GM_B}{r^2} \left[\frac{\frac{r}{\gamma}}{1+\left(\frac{r}{\gamma}\right)^2} - \tan^{-1}\left(\frac{r}{\gamma}\right) \right] . \tag{22}$$

The second component is a three-dimensional disk of mass density,

$$\rho(r,z) = \frac{M_D \alpha^2 \beta}{4\pi} \exp\left(-\alpha r - \beta |z|\right) . \tag{23}$$

The third component is a nearly isothermal halo of mass density distribution,

$$\rho(r) = \frac{\rho_o}{1+\left(\frac{r}{a}\right)^2}, \tag{24}$$

corresponding to the gravitational acceleration,

$$g(r) = \frac{-4\pi G\rho_o a^3}{r^2}\left(\frac{r}{a} - tan^{-1}\left(\frac{r}{a}\right)\right). \tag{25}$$

In all cases, the companion galaxy is simulated as a single Hubble-like profile (eq. [21]). Some of the simulations were carried out for a target galaxy containing all three (bulge, disk, and halo) components, while others used a single-component target. Detailed description of the code is given in Section III of the third chapter " Effects of Multiple...". Despite the fact that the potentials used in the numerical simulations do not accurately represent an entire disk galaxy, they allow closer, more quantitative comparison with the analytic results drawn from the same potentials.

B. Numerical Results

Figures 4 and 5 show the development of rings in a target disk consisting of 10,000 test particles following a collision with a 10% and 20% mass companion galaxy, respectively, where both galaxies are dominated by a single Hubble-like bulge component (eq. [21]). In both cases, the companion is in a moderately hyperbolic orbit and impacts the disk perpendicularly at the center.

Figure 4 shows a head-on view of the disk at selected times. Time is measured from the moment the companion passes through the target disk plane. The dimensionless time unit equals $0.34\ (R_0^3/GM)^{1/2}$. These conventions are followed in Figures 5, 10 and 11 below. In the first snapshot it can be seen that the first ring has already propagated about half-way

Fig. 4 - Head-on view of a disk consisting of 10^4 test particles following the central impact of a 10% mass companion. The potential of the target galaxy consisted of a single Hubble-like bulge component. Time indicated in each snapshot is measured from the moment the companion passes through the disk (see text for details). The radius of the disk is initially *10b*, where *b* is the potential scale length.

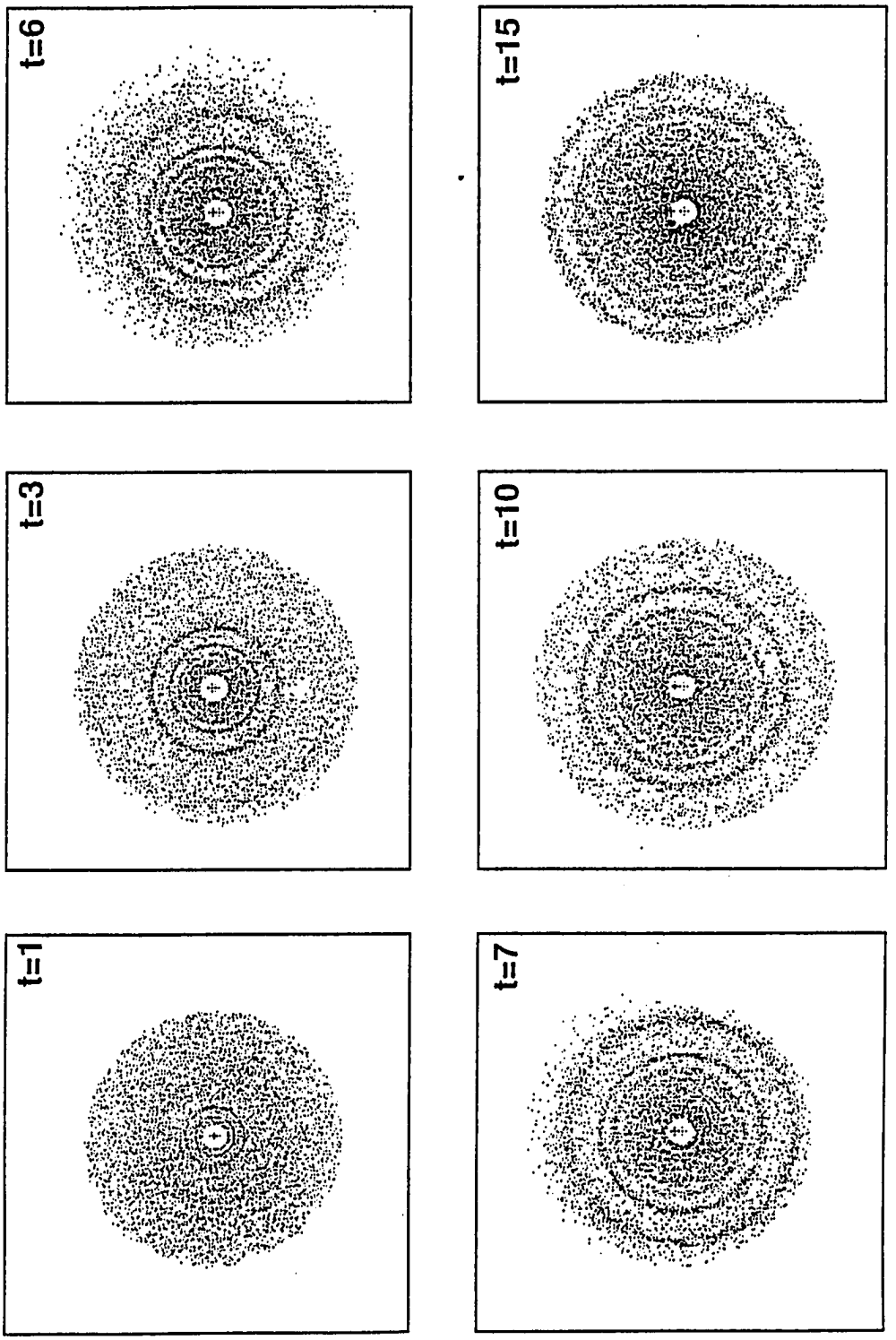
t=6
t=15
t=3
t=10
t=1
t=7

through the disk. However, this ring is so faint and diffuse that it is hardly visible until it begins to leave the disk in the second snapshot, as a result the disk is expanded considerably (compare frames 1 and 2). The second ring has also formed and moved a short ways out from the center. Between times 1 and 10 the second ring propagates through the disk. From early times, it is stronger than the first ring, with quite sharp edges. Note also how it gets steadily thicker as it moves outward. The third ring follows a very similar evolutionary sequence. At late times, there is increasing incoherence in the central regions. Although a fourth ring is discernible, the fifth and higher rings never free themselves from this confusion. Thus, by the last time shown the ringing is almost over, and in later times (not shown) the disk relaxes and smoothes out.

In Figure 5, although the companion is twice as massive, many of the same general features are apparent. The first ring, which is about to leave the disk in the first frame, is weak (though not *as* weak) and it propagates quickly through the disk. The overall size of the disk varies in a similar way. The second ring propagates more slowly than the first and gets thicker as it moves outward.

There are also interesting differences between Figures 4 and 5. The rings are apparently thicker in the latter case, and the density contrasts between ring and inter-ring regions are somewhat greater. Because the rings are substantially thicker in the second case it is hard to resolve the third and later rings. The incoherence in the central regions sets in earlier, and thus, the ringing phenomenon is rendered unrecognizable earlier. This result is interesting because of the somewhat paradoxical implication that larger amplitude disturbances lead to less persistent effects.

The caustics described by equations (6) and (14) can be identified with

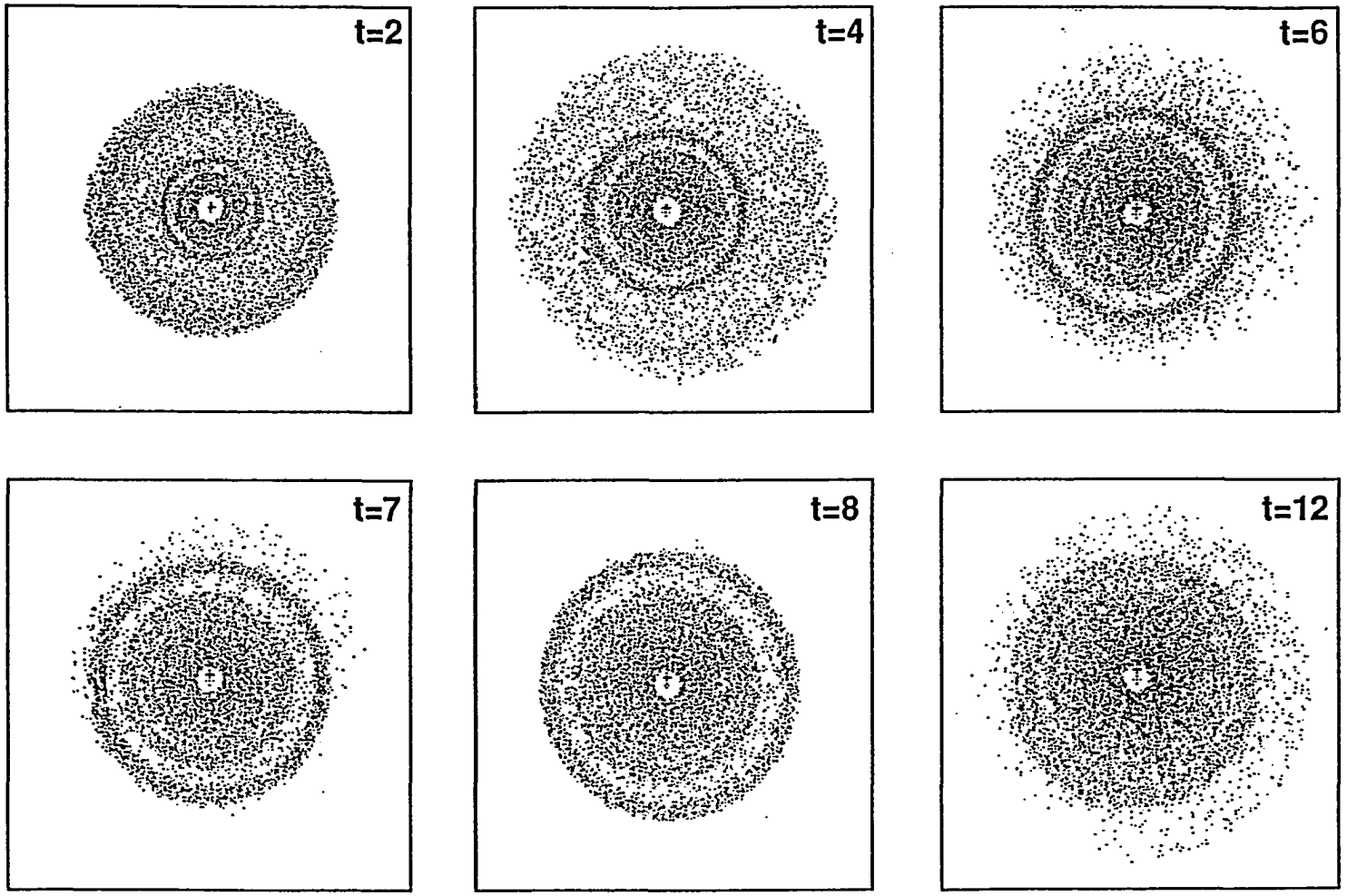

Fig. 5 - Same as Fig. 4, but with a *20%* mass companion.

the inner and outer ring edges in Figures 4 and 5 (see the following section). The finite thermal motions and limited particle resolution prevent these "caustics" from being infinite density surfaces in the numerical simulations, but the abrupt density change at these boundaries is obvious. It appears that the density within the rings is relatively constant. This point will also be discussed further below.

The last snapshot in Figure 5 shows that even though the confusion of overlapping rings makes their individual identification difficult, a ring wave can still lift the outer disk particles. This gives the appearance of a strong lens component superimposed on the disk. This feature is found in all of the simulations presented in this paper.

Many of the qualitative features of Figures 4 and 5 are also seen in the full N-body calculations of Appleton and James (1989) with similar target to companion mass ratio, including: the qualitative structure of the ring, the formation of the lens-like component, and the fact that the disk is not perturbed much perpendicular to its plane.

The simulations presented in Figures 4 and 5 were repeated with the softened point-mass potential (eq. [1] with p=1) in place of equation (21). The resulting ring waves and particle distributions in the disk plane resemble Figures 4 and 5 quite closely. There is some difference between the two cases in the direction perpendicular to the disk, in the sense that the heating in that direction and the resulting disk thickness are moderately greater with the softened point-mass potential. This behavior is expected since the gravitational acceleration on a test particle located close to the center ($\vec{r} \rightarrow 0$) is $\vec{g} \propto -/r/\hat{r}$ for a Hubble-like profile, and $\vec{g} \propto -\hat{r}$ for a softened point-mass ($\hat{r}$ is the radial unit vector). The greater acceleration in the latter case results in enhanced thickening in the direction perpendicular to the disk.

Some other differences in detailed morphology will be discussed below. However, the overall conclusion is that, the results discussed above are not particularly sensitive to the exact form of that potential.

C. Comparison to Analytic Models

In this section we will use the analytic models of Section II to help understand the numerical results presented above.

1. Particle Orbits and Ring Structure

In order to test the approximations adopted in the kinematic model we begin by analyzing individual particle orbits from a series of single-component (Hubble-like) simulations. The particle orbits were also used to check the quantitative predictions of equations (5), (6), and (8) for the amplitude, sinusoidal form and frequency of the epicyclic oscillations. The parameters that were varied in the simulations were the initial radius of the test particle, the mass of the main galaxy, and the mass ratio between the companion and the main galaxy. Figure 6 shows the radial motion of several test particles relative to their unperturbed guiding center orbits. The thick and thin solid curves refer to particles with initial radii of $15b$ and $7.5b$ (b is the scale length of the "Hubble-like" potential), respectively, in the case where $M_C/M_G = 0.1$. The dashed curve is for a particle with initial radius of in the case where $M_C/M_G = 0.2$, and where the mass of the target galaxy is twice that used previously. The radial oscillations in all of the simulations appear to be quite sinusoidal at all times after the impact at $t = 0$, in agreement with the epicyclic approximation (eq. [6]). However, note that the radial excursions are not completely symmetric about the initial guiding center radius. This is expected due to the increasing shallowness of the gradient of the effective potential with increasing radius.

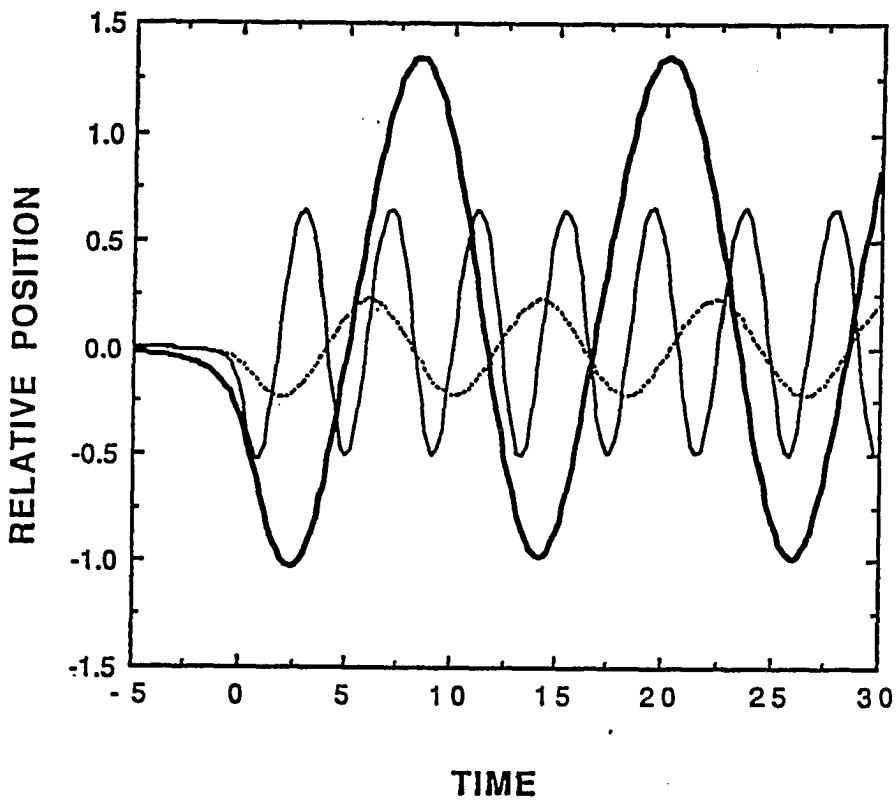

Fig. 6 - Epicyclic oscillations of a test particle initially located at q=*7.5 b* (solid curve), and *15.0b* (thick solid curve) following a collision with a 10% companion. The dashed curve shows the motion of a test particle with q = *15b* following a collision with a 2% mass companion, and where the mass of the target galaxy is twice that of the previous case. The sinusoidal form, the amplitude, and the frequency of all of these curves agree well with the predictions of eqs. (5), (6), and (8).

The amplitude of the oscillations in our simulations (e.g., compare thick and thin curves in Fig. 6) agrees with that predicted by equation (5), to within 1% as the initial radius of the particle is varied (with all other parameters fixed), and to within less than 10% as the companion-to-target mass ratio is varied over a factor of a few (compare solid and dashed curves in Fig. 6).

The oscillation frequency agrees with that predicted by equation (8) with $p=1$ to within 0.5% as the initial radius is varied (see the thick and thin curves of Fig. 6), and to within 7% when the companion-to-target mass ratio is varied. When the target galaxy mass is increased over a factor of a few, independent of the companion mass, there is always agreement to within 2% between the simulations and equation (8). These comparisons derive from a large number of orbital calculations, but the three examples shown in Figure 6 are representative.

Other comparisons can be made between the collective behavior of the 10^4 test particles used in the simulations described in the previous section and the kinematic model. The results include the following.

1. Since the condition that $A > A_{min}$ is not met in the first ring ($A^1_{min} = 0.21$ in the outer disk) in the cases shown in both Figures 4 and 5, we do not expect caustics to form in the first ring. At times $t = 1\text{-}3$ the figures do show that the first ring is a very weak compression with no clear edges. The critical amplitude for caustic formation in the second ring ($A^2_{min} = 0.07$) is close to the actual amplitude for the case shown in Figure 4, and is exceeded in the case shown in Figure 5. In both figures, the second ring has clear edges, and is stronger and broader in the latter case.

2. The modest broadening of the first few rings as they propagate outward is apparent in both the model predictions and the simulations (compare Figs. 3 and 4).

3. At a given time, there is quite good quantitative agreement between the ring widths predicted by equation (20) and the simulations. For example, at $t = 6$ in Figures 4, 5 the second ring has propagated well out into the disk. Solving the condition $\omega t = 3\pi$ (with $p = 1$) shows that particles within the ring have $q \approx 8\varepsilon$ (or b as in eqs. [21] and [22]). Then we can use equation (5) for A and equation (19) for θ in equation (20) to estimate the ring width as $2\,\Delta r \approx 1.3\varepsilon, 2.4\varepsilon$, for $M_c/M_G = 0.1, 0.2$, respectively. The actual widths at this time in Figures 4 and 5 are about $1.0\text{-}1.2\varepsilon$ and $1.4\text{-}1.7\varepsilon$, respectively. The estimate from equation (20) is quite good in the first case, and too large in the second case. In fact, it appears that the approximation that all ring particles have about the same value of the Lagrangian coordinate q, is not accurate in the latter case. A more careful calculation, using the conditions $\omega t = 2.5\pi, 3.5\pi$ to estimate the lower and upper values of q within the ring, gives a width estimate of 1.5ε, in good agreement with the simulation results.

4. Figure 3 suggests that when $A \approx 0.2$ the third and later rings will be strongly overlapping, while overlap won't occur before about the fifth ring when $A \approx 0.1$. These expectations are verified in Figures 4 and 5.

2. The Birth and Propagation of Rings

In the present context, a singularity is defined as satisfying both $\partial r/\partial q = 0$ (eq. [10]) and $\partial^2 r/\partial q^2 = 0$, and is effectively the birthplace of a nonlinear ring. Using equation (6) (or differentiating eq. [11]), we get

$$\omega t \tan(\omega t) = \frac{2\left(\frac{\omega}{q}\right)}{\frac{d\omega}{dq}} + \frac{\omega\frac{d^2\omega}{dq^2}}{\left(\frac{d\omega}{dq}\right)^2}. \qquad (26)$$

If we define a function f_2 such that

$$\frac{d^2\omega}{dq^2} = \frac{1}{\omega}\left(\frac{d\omega}{dq}\right)^2 - \frac{\omega}{q^2} f_2(q/\varepsilon), \tag{27a}$$

$$\text{then,} \quad f_2 = \frac{B_0 + B_2\left(\frac{q^2}{\varepsilon^2}\right) + B_4\left(\frac{q^4}{\varepsilon^4}\right) + B_6\left(\frac{q^6}{\varepsilon^6}\right) - 3\left(\frac{q^8}{\varepsilon^8}\right)}{2\left(\frac{q^2}{\varepsilon^2}+1\right)^2\left(\frac{q^2}{\varepsilon^2}+2p+1\right)^2}, \tag{27b}$$

$$\text{with} \quad B_0 = -(3 + 10p + 4p2 - 8p3) \ ,$$
$$B_2 = -2\,(6 + 11p - 8p2 - 12p3) \ ,$$
$$B_4 = -2\,(9 + 15p - 2p2) \ ,$$
$$B_6 = -6\,(2 + 3p) \ ,$$

and equation (26) can be written

$$\omega t \tan(\omega t) = \frac{f_1^2 - 2f_1 - f_2}{f_1^2}. \tag{28}$$

This form, like equation (13), reveals clearly the separability of the variables ωt and q/ε. However, there are a couple of important differences between equations (13) and (28). First, equation (28) is a quartic in $(q/\varepsilon)^2$, rather than a quadratic, and so not readily solvable. Second, equation (28) has *no amplitude dependence*, the factors of A cancel in deriving equation (26). Moreover, this fact does not depend on the form of the gravitational potential, i.e., $\omega(q)$, but is a universal result of the constant amplitude, free

oscillator model. (Clearly, it is also approximately true for amplitude functions $A(q)$, which depend weakly on Lagrangian position q.)

Both the thickness of the rings, and the position of their birth depend on the perturbation amplitude through equation (13). After a ring's formation, while solutions to equation (13) mark the ring boundaries, there is at all times a solution to equation (28) for some q corresponding to a particle located within the interior of the ring which can be viewed as the ring center. Thus, the propagation of a ring center is independent of the (constant) amplitude, and depends only on the gravitational potential in the disk. *This is confirmed in the simulations with Hubble-like and softened point-mass potentials.*

Again it is helpful to consider some limiting cases. First, consider the central regions where $q/\varepsilon << 1$, $f_1 \approx (3\text{-}2p)/2$, $f_2 \approx -(3 + 10p + 4p^2 - 8p^3)/(2(2p + 1)^2)$. Then when $p=1$, equation (28) reduces to $\omega t \tan(\omega t) \approx -1$, with the first few solutions being $\omega t \approx 0.89\pi, 2.97\pi, 4.98\pi,...$(when $p = 3/2$, then $\omega t \tan(\omega t) \approx 5/9$, $\omega t \approx 1.05\pi,...$). Since in this limit $\omega \propto q^{(2p-3)/2}$ (from eq. [8]), the ring center propagates according to

$$q_{II} \propto t^{2/(3-2p)}, \tag{29}$$

with the subscript II recalling that this is a second derivative condition. Note also that with $\omega t \approx n\pi$ *(for* $n > 1$*)*, then $r \approx q$.

Now consider the (Keplerian) limit $q/\varepsilon >> 1$. In this limit $f_1 \approx 3/2$, $f_2 \approx -3/2$, (independent of p) and $\omega t \tan(\omega t) \approx 1/3$. The first few relevant solutions to this equation are $\omega t \approx 1.033\pi, 3.011\pi$, and 5.007π. In this limit $\omega \propto q^{-3/2}$, so equation (29) is replaced with

$$q_{II} \propto t^{2/3}. \tag{30}$$

Since the phase is nearly the same as before, $r \approx q$ again, and equation (30) implies a much slower ring propagation rate in the outer disk (see Figs. 3, 7).

This and most of the other results in this section, are also well-illustrated by Figure 7. In this figure the ring boundaries are plotted as solid ($A = 0.1$, $p=1$) and dashed ($A = 0.2$, $p=1$) curves, while the approximate ring centers are plotted as dotted curves. The procedure used to determine the ring boundaries is as follows. Recall that previously we concluded that caustic can usually occur only in the intervals $(2n-1)\pi - \pi/2 < \omega t < (2n-1)\pi + \pi/2$. (These intervals are marked on the x-axis in Fig. 7.) For any given phase within an allowed interval, equations (13) and (14) can be used to calculate q_c, the Lagrangian coordinate of the caustic particle at that phase. Then we can divide the phase by $\omega(qc)$ as derived from equation (8) to derive t. Finally, equations (14) and (6) are used to derive r_c the caustic position at time t. To plot the ring centers we approximated their phase as $\omega t \approx (2n-1)\pi$, and repeated the above procedure for the center position as a function of time. The increase in ring width with amplitude discussed above is obvious in this graph. Also the position of the ring center is independent of the disturbance amplitude. Recall that in the first ring the caustic condition is not satisfied for $A = 0.1, 0.2$, but it is in the second ring. The amplitude dependence of the caustic birthpoint is also evident in the second ring.

3. Stellar Densities within Rings

The local star density in the galactic disk is given by equation (9) up to the time of singularity formation. Even after the two caustics have formed, it is apparent from Figure 2 that the equation is still valid within the ring if it is applied piecewise to each of the three star streams discussed above. In the middle (or interior) stream r decreases with q, so the density must be computed from the absolute value of dr/dq.

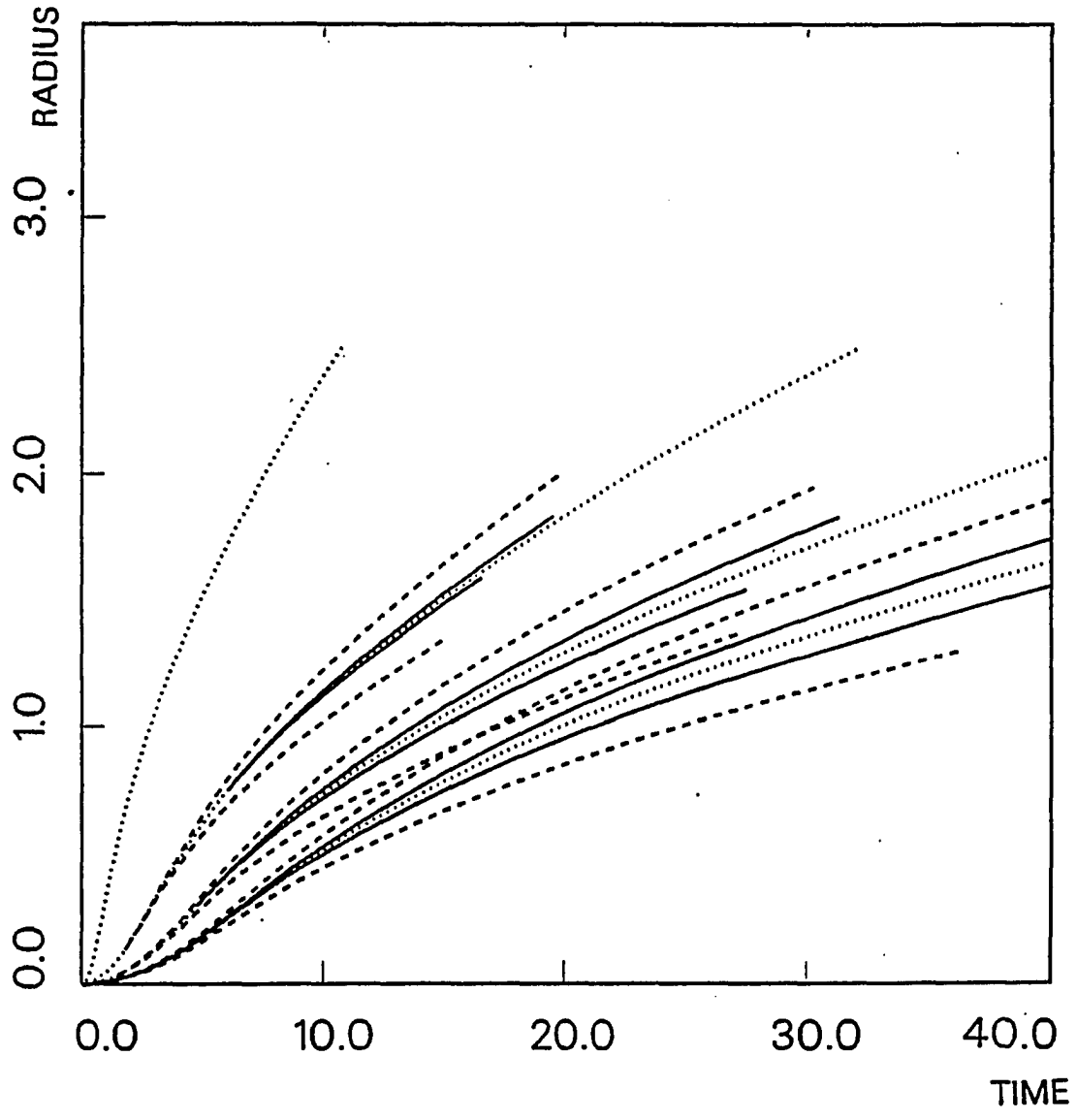

Fig. 7. - Radial propagation of the first four pairs of ring edges in the cases with perturbation amplitude $A = 0.1$ (solid curves) and $A = 0.2$ (dashed curves), and $p=1$. In both cases no caustic forms in the first ring, and the separation between the two folds is negligible in the second ring in the small amplitude case. The dotted curves mark points at the ring center as described in the text.

In fact, because the phase ωt of the ring center is always approximately equal to odd multiples of π, it is especially easy to estimate the density of this middle stream in the ring center. When $\omega t = (2n\text{-}1)\pi$ $(n = 1, 2, 3,...)$ and $r \approx q$, equations (6), (9), and (12b) yield,

$$\frac{\rho_{mid}}{\rho_o} = \left(\frac{r}{q}\left|\frac{dr}{dq}\right|\right)^{-1} = \frac{1}{\left|1 - (2n\text{-}1)\pi A f_1\right|}. \tag{31}$$

A careful examination of Figure 3 reveals that the middle stream is the densest. The density of the incoming stream does not vary rapidly, and is therefore roughly the same for ring and inter-ring, so to estimate its value it is sufficient to use the (inter-ring) phase $\omega t \approx 2(n\text{-}1)\pi$ (see Fig. 3). Then the corresponding density is

$$\frac{\rho}{\rho_o} = \frac{1}{1 + 2(n - 1)\pi A f_1}. \tag{32}$$

Similarly, the phase of the outgoing stream is roughly $\omega t \approx 2n\pi$. Thus, the ring density is approximately the sum of the three stream densities given by equations (31), (32), and (33) below.

The ring density can be contrasted with an estimate of the rarefied inter-ring density at phase $\omega t = 2\pi n$,

$$\frac{\rho_{rare}}{\rho_o} = \frac{1}{1 + 2\pi n A f_1}. \tag{33}$$

As n increases the inter-ring density continually decreases. However, this is often not observable since as we have seen the higher-order rings generally overlap each other, leaving no pure rarefaction region.

Since according to equation (12), $1.0 < f_1 < 1.5$ for $q > \varepsilon$, the

denominator in equation (31) will take its smallest value in the first ring if A is greater than about 0.2, yielding the highest density there. Higher-order rings, with larger values of n will have lower interior densities. If, on the other hand, $A << 0.1$, then the quantity in the absolute values will be positive in the first ring, approach zero in the second or later rings, and then become progressively more negative as n increases further. Thus, the second or later ring will have the maximum interior density. For example, if $A = 0.02$, then this argument suggests that the sixth ring has the maximum interior density. *Again, restricted three-body simulations confirm these predicted trends.*

Quantitative comparison is more difficult, however, for practical reasons which are also relevant to observational comparisons. To make this comparison we divide the target disk in the simulations into 50 annuli, and compute the density within each. In the low-amplitude case ($A < 0.1$), where the rings are thin, this division is sufficient to resolve the rings, but not to make a very accurate estimate of their internal density. If we divide the target disk into many more annuli, then there would be too few particles in each annulus to allow accurate density determinations. This difficulty is less severe in the large amplitude case, where rings are thicker. However, comparison is still difficult due to the overlapping of the third and later rings, as well as the weakness of the first ring.

Figure 8 shows the run of density in one case where quantitative comparison is possible. This simulation is much like that shown in Figure 5 except with a somewhat larger amplitude of $A = 0.23$ ($M_C/M_G = 0.3$), and an initial $1/r$ density profile. The density profile is shown at times of 5 and 7 units, when the second ring is moving toward the outer edge of the disk. Even with the annular averaging, the inner and outer edge caustics of the ring are evident. Apparently, the third ring's edges are also visible, although Figure 5

Fig. 8 - Density profiles at two times in the single (bulge) component case, with an initial $1/r$ density profile. The density unit is arbitrary, but the same in both graphs, while the radius is measured in terms of the initial disk radius.

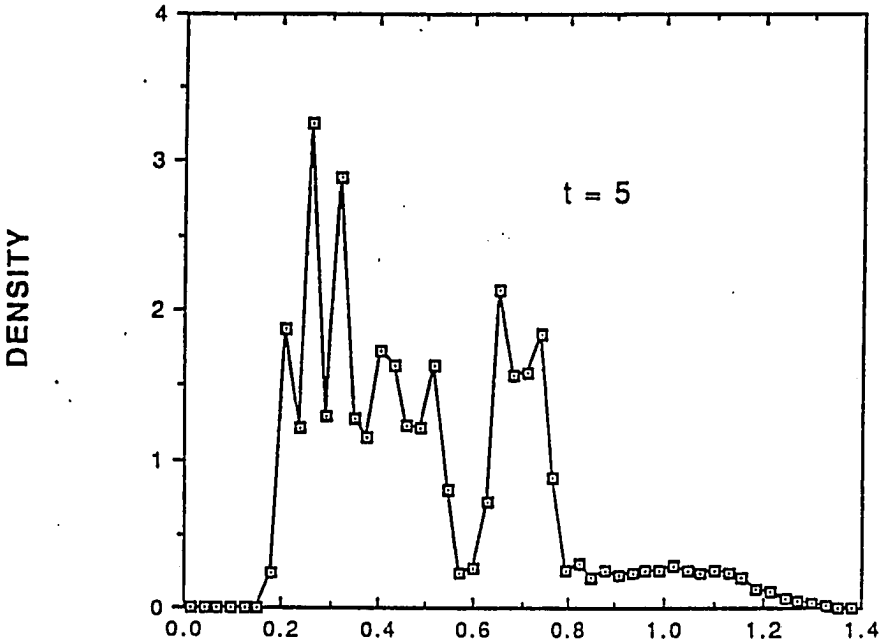
DENSITY
t = 5
RADIUS
0
1
2
3
4
0.0
0.2
0.4
0.6
0.8
1.0
1.2
1.4

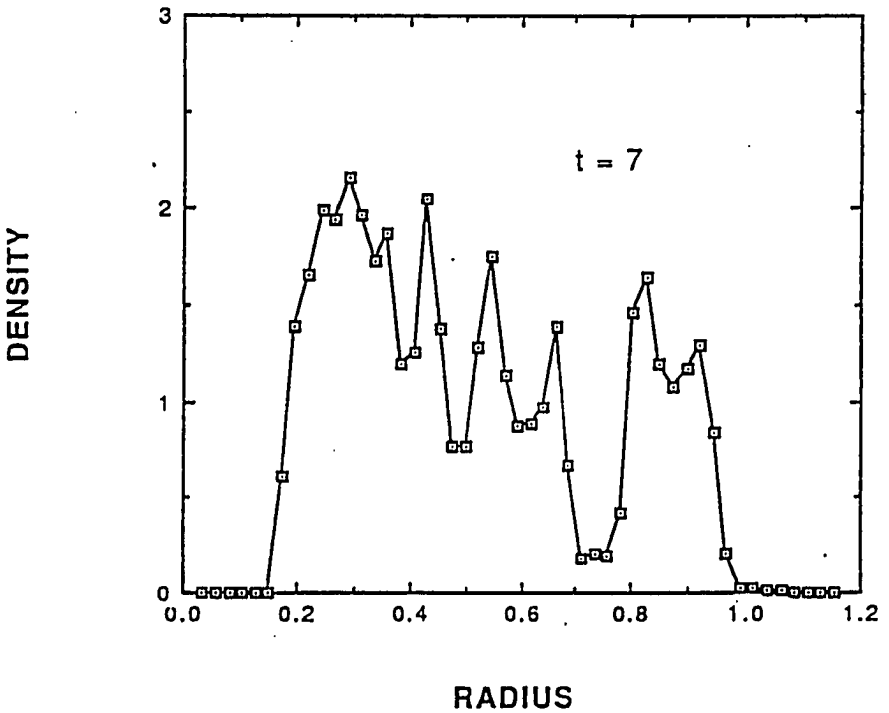
DENSITY
t = 7
RADIUS
0
1
2
3
0.0
0.2
0.4
0.6
0.8
1.0
1.2

would lead us to expect some overlap between the third and fourth rings at this time. (Note also that initially the center of the disk had no test particles, which accounts for the density drop there.) In this case equations (31)-(33) predict a density contrast of 5.0 between the interior of the second ring and the rarefied region behind it, and a factor of 1.7 between the densities of the second and third rings. (This is assuming $q >> \varepsilon$, so $f_1 \approx 1.5$.) The values derived from the numerical calculation are 6.5 for the ring-inter-ring contrast, and 1.3 for the ring-to-ring ratio at $t = 5$, and 6.1 and 1.3, respectively at $t = 7$. Thus, these density contrasts stay constant with time as predicted by the analytic model. We can roughly correct for the $1/r$ initial density profile in the simulations, compared to the flat profile analytic estimates, by multiplying by the ratio of mean ring or inter-ring positions. Then the ring-to-ring density ratio becomes 1.9, and the ring-inter-ring ratio becomes 7.4. Given the roughness of the analytic estimate, these comparisons seem quite good. Note, the small gap followed by a high peak behind the third ring probably indicates overlap between the third and fourth rings.

IV. EFFECTS OF DISK AND HALO POTENTIALS

In this section, we generalize the results of the previous section by presenting numerical simulations in which the target galaxy has a gravitational potential consisting of (rigid) bulge, disk and halo components as described in Section III(A). In particular, the inclusion of a flattened disk potential approximates the disk self-gravity. Also a modest random velocity component was given to the test particles initially to mimic disk star velocity dispersion. The analytic theory is very messy. Therefore, only a very simple semi-analytic example will be discussed, followed by the numerical results. From the outset, we expect that much of the qualitative behavior discussed above will be unchanged, for this behavior consists of the generation and propagation of the basic singularities or catastrophes that are generic to Lagrangian dynamical systems. However, even the details of the evolution of these singularities can have important ramifications for the morphologies of galaxies.

A. Effects of a Halo

A simple way to generalize the softened point-mass bulge is to add a second component, for example, that given by equations (24) and (25), to represent a massive halo. Much of the analytic work above can be straightforwardly generalized to this two-component case. Some of the differences are illustrated in Figure 9, which shows the kinematic trajectories in an example with a perturbation amplitude $A=0.1$ and a bulge potential identical to the case shown in Figure 3c, but with an additional halo of mass $M_H = 10M$, and a scale length $a = 5\varepsilon$. The time units in Figure 9 are

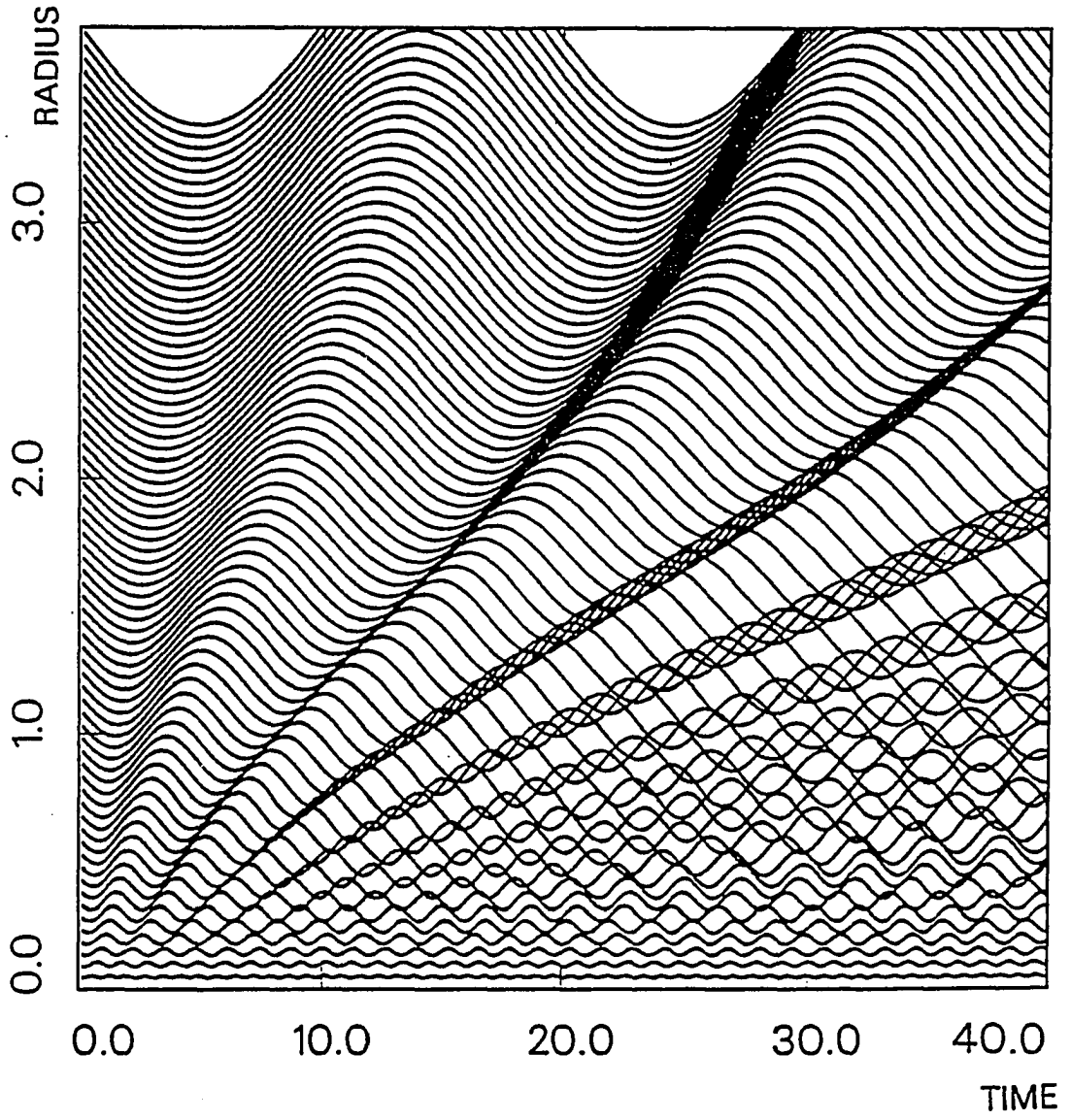

Fig. 9 - Radial trajectories as in Fig. 3, with amplitude $A = 0.1$, and a massive halo of characteristic length $a = 5\varepsilon$ (see text).

rescaled to the halo free-fall time from a radius $r=a$, which allows a better comparison to Figure 3.

First of all, we find that most of the structure within a radius $r/\varepsilon = 2$, where the bulge dominates, is very similar to the pure bulge example in Figure 3c. Secondly, ring characteristics change at radii between 2 and 4, where the halo potential becomes important. Rings propagate more rapidly, a simple consequence of increased epicyclic frequencies, which results from the large halo mass. The rings also become weaker in the outer regions, indicating a decreasing amplitude A. This phenomenon contrasts with the results of the previous section, where the amplitude A remained nearly constant with radius. Using the radial force balance condition (eq. [3]), except with the halo acceleration (eq. [25]) instead of the softened point-mass acceleration, we find that the perturbation amplitude in a pure halo potential, in the limit $q/a >> 1$, is,

$$A \approx \frac{1}{2}\frac{M_c}{M_H}\left(\frac{a}{q}\right). \tag{35}$$

where a is the halo scale-length and $M_H = 4\pi\rho_0 a^3$.

Massive halo examples suggest that galaxies with a faint ring of very large diameter, or galaxies with multiple, widely spaced rings, are likely to possess a massive, extended halo.

B. Numerical Results

The analytic work clearly indicates that an extended halo can affect ring morphology. In this section, we present several numerical simulations which confirm this conclusion, and give some indication of how it depends on the specific form of the halo potential.

The first of these simulations is shown in Figure 10, which shows snapshots of ring development in a target galaxy with bulge-disk-halo components in the ratio (0.2:1:1) by mass. The scale-lengths of the bulge, disk and halo, b, c and a, are 0.05, 0.25 and 0.8 units, respectively. The cutoff radius of the halo is 1.2 units. The companion galaxy has a mass of 10% of the total target mass, it approaches on a slightly hyperbolic orbit, and impacts perpendicular to the disk at its center. The case shown in Figure 10 is analogous to the single-component case shown in Figure 4. In fact, in comparing the two figures the overall impression is that the two cases are very similar.

On the other hand, the rings in Figure 10 are generally thinner than those in Figure 4. In Figure 10 the rings have roughly constant width as they propagate outward, in contrast to Figure 4, where rings thicken slightly. This trend is also evident in Figure 11, which shows the results of a simulation exactly like that in Figure 10, but with a 30% mass companion. With equations (6), (17), and (35) we can derive the following expression for the ring half-width in the halo potential,

$$\frac{\Delta r}{a} \approx \frac{1}{2}\frac{M_c}{M_H} \sin(\theta), \tag{36}$$

which predicts no broadening with radius (except possibly through the phase angle θ). Thus, constant width rings seem to be a property of this halo potential. Comparison of Figures 3, 4, 5, 10, and 11 suggests a few generalizations. First, if three or more stellar rings can be resolved within a disk, then the disturbance amplitude was probably small, i.e., the companion has a relatively low mass (10%). On the other hand, a relatively high mass companion generates a morphology consisting of an outer ring plus a lens (overlapping rings). A similar morphology does appear at late times in the

Fig. 10 - Head-on view of a test particle disk in a bulge-disk-halo potential following the central impact of a 10% companion. Time units are the same as in Figs. 4, 5.

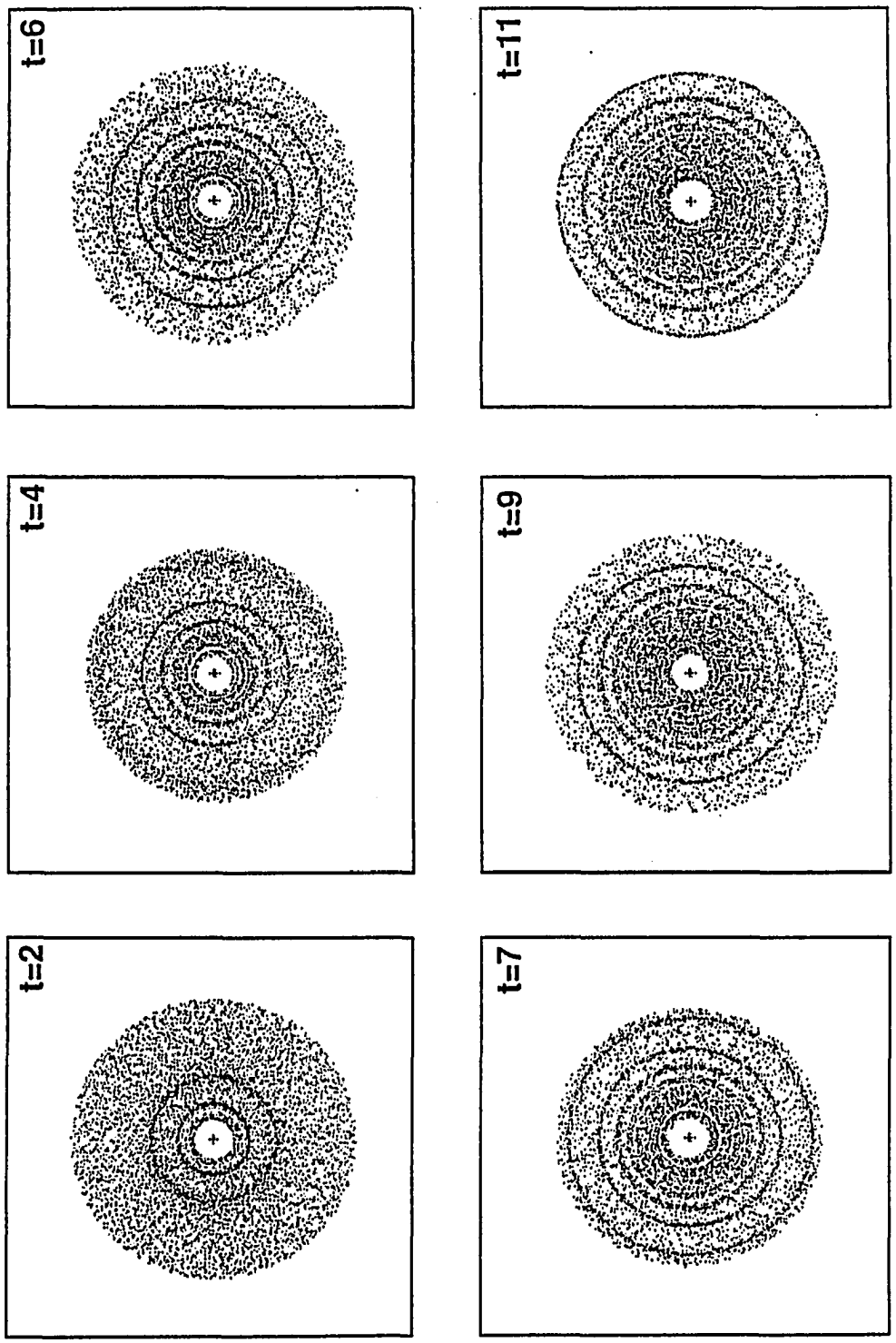
t=6
t=11
t=4
t=9
t=2
t=7

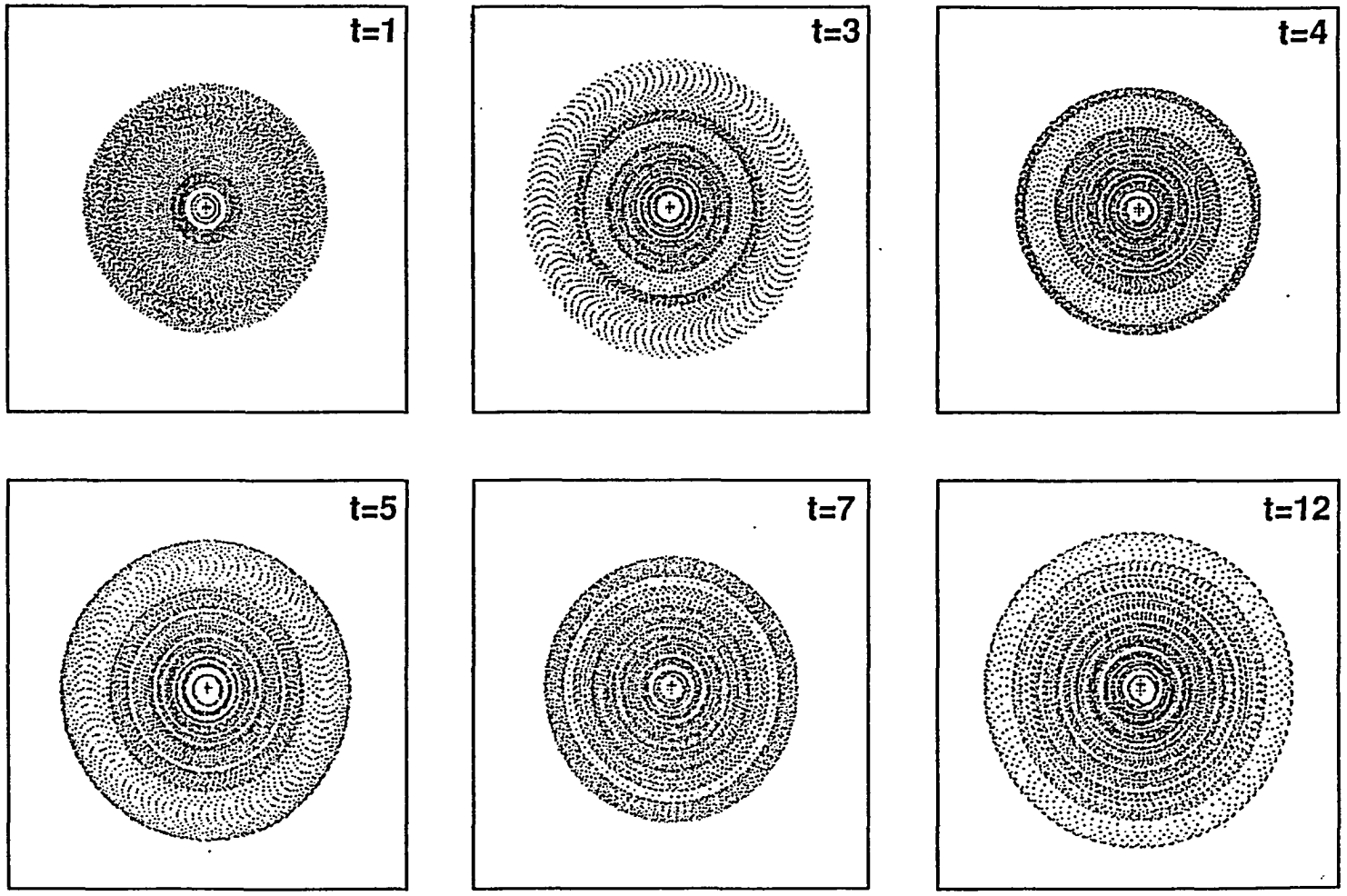

Fig. 11 - Same as Fig. 10, but with a *30%* companion.

low amplitude case. These conclusions seem relatively independent of the form of the potential. As noted above it appears that ring spacing, ring widths, and density contrasts also contain information about the potential as well as the amplitude. Obtaining this information is easier if the age of the rings and the amplitude can be estimated independently from the size of the companion and its distance from the ring.

C. Test Particle Orbits

It is interesting to examine the orbits of test particles in the bulge-disk-halo potential, as an extension of the discussion of Section III(C), which dealt with orbits in the single-component potential. This, in turn, provides a better measure of the approximation's relevance to real galaxies. Figures 12a and 12b show the radial and vertical motions of a test particle relative to its unperturbed radial position in the multiple-component potential. In both cases the particle was initially located at the outer edge of the disk ($q/a = 1.25$). The particles in Figures 12a and 12b are taken from the simulations shown in Figures 10, and 11, respectively.

Like the single-component case shown in Figure 6, the radial oscillations in both Figures 12a and 12b are quite sinusoidal at all times after the impact at $t = 0$, in agreement with the epicyclic approximation. The oscillation period is found to be about 3.3 time units. In the outer disk the bulge and disk potentials can be approximated as point masses, and then replacing the first term on the right-hand-side of equation (8) with $G(M_B + M_D)/q^3$, we derive an analytic estimate of $P = 3.4$ time units.

The vertical oscillations also have a generally sinusoidal form, but of lower amplitude than the radial ones. Moreover, the vertical oscillations appear to be modulated on a timescale of several periods, especially in the

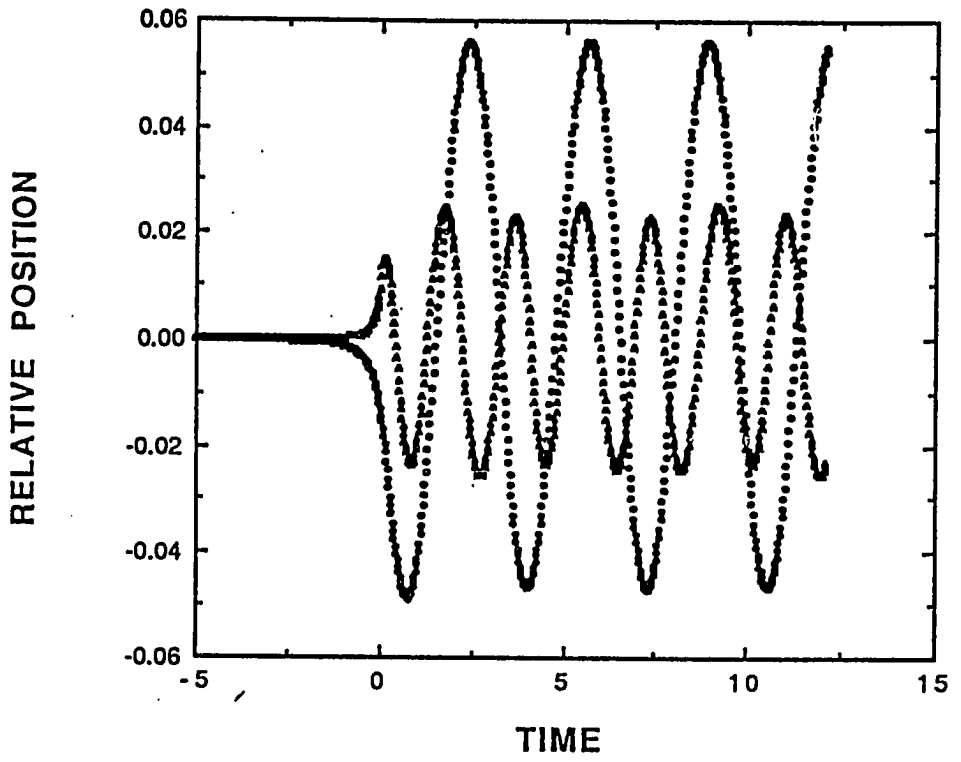

Fig. 12a - Epicyclic oscillations of a test particle initially located at the outer edge of the disk after a collision with a 10% mass companion The larger amplitude oscillation corresponds to the radial motion within the disk, and the smaller amplitude oscillation corresponds to the motion perpendicular to the disk.

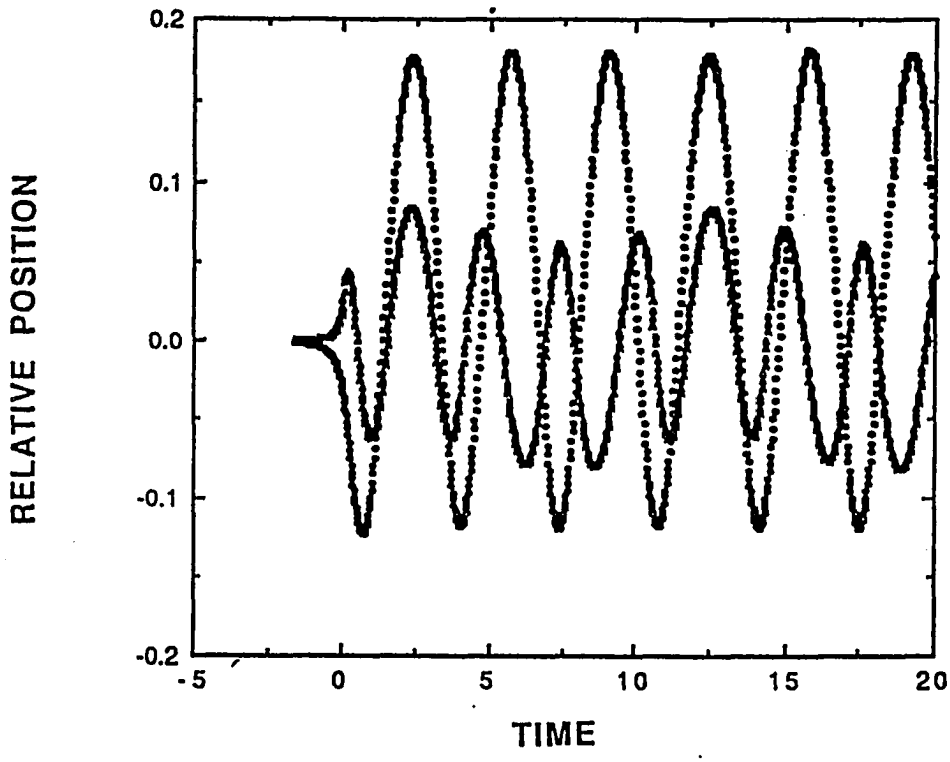

Fig. 12b - Same as Fig.12a, but with a 30% mass companion.

case shown in Figure 12b. In this case the periods of the vertical and radial oscillations appear to be in a 4:3 resonance, and this is probably the cause of the beating behavior. (The vertical oscillations feel the radial motions through the change in the vertical component of the gravitational force as a function of radius.)

The mean amplitudes of the radial oscillations in Figure 12, and other calculations not shown, are seen to scale roughly as M_C/M_G, as expected from equation (35) for constant q/a. We can rederive equation (35) including point mass approximations for the bulge and disk contributions in the limit $q/a >> 1$, to get,

$$A_{BDH} = \frac{1}{2}\frac{M_c}{M_H}\left(\frac{a}{q}\right)\left[1 - \frac{\frac{1}{2}\frac{M_c}{M_H}\left(\frac{M_B + M_D}{M_H} - \frac{\pi}{2} + \frac{1}{2}\frac{M_c}{M_H}\right)}{\frac{q}{a} + \frac{1}{2}\left(\frac{M_B + M_D}{M_H} - \frac{\pi}{2}\right)}\right] . \quad (37)$$

For the examples shown in Figures 12a and 12b equation (37) predicts $A = 0.05, 0.18$, respectively, in good agreement with the figure.

V. OBSERVATIONAL COMPARISONS

A. Previous Observations of Ring Structure

The theory above predicts ring widths, ring positions and relative overdensities in rings as a function of time, form of the target galaxy potential, and collisional amplitude. Assuming that the stellar ring caustics are not promptly smoothed away, there are however several practical difficulties that complicate the comparison of theory and observation. The first is distance, there are few nearby cylindrically symmetric rings. The most well-known ring galaxies have diameters of less than 2 arcminutes (see Arp 1966, Arp and Madore 1987, and Theys and Spiegel 1976), making high-resolution studies difficult. The second "difficulty" is the vigorous star formation in rings (see, e.g., Theys and Spiegel 1976, Appleton and Struck-Marcell 1987a, Jeske 1986, and Majewski 1988). In catalog photos, rings often show a knotty structure. Detailed studies reveal that the knots are young star associations, see e.g., Thompson and Theys' (1978) study of VII Zw 466, Few, Madore and Arp's (1982) study of the Lindsey-Shapley ring, and Joy *et al.*'s (1989) study of the Cartwheel. This is a difficulty in the present context because it means that most of the observational work done to date concerns primarily the young stars and the gas they have formed from. The compressible gas dynamics in rings will be very different than the stellar dynamics (Struck-Marcell and Appleton 1987).

The best way to study the surface density distribution of the old stellar population is with near-infrared photometry, since most of these stars' energy output is emitted in this waveband. To date relatively little work of

this kind has been published, but see Majewski and Herald 1988, Majewski 1988, and Joy *et al.* 1989. Majewski and Herald did find that rings were "more extended" in the infrared than in the optical. However, Joy *et al.* found that in at least one quadrant of the outer ring of the Cartwheel galaxy, there is little or no infrared emission! Neutral hydrogen disks typically extend to larger radii than optical disks in late-type galaxies, and this is also the case in the Cartwheel, according to unpublished VLA data of Higdon (1989, private communication, Astronomy Department, University of Texas). In the Cartwheel, the ring wave may have already propagated out of the stellar disk, and the visible bright ring may consist entirely of young stars and gas. This is a sobering result in view of the fact that the Cartwheel has become something of a standard ring galaxy since Toomre (1978) first compared his models to it.

A third problem is the presence of stellar bars, which may affect the waves resulting from an otherwise symmetric collision. For example, Taylor and Atherton's (1984) interferometry study of the Vela ring, which has a prominant bar, shows that its kinematics are not compatible with those of a simple rotating, expanding ring. (Moreover, the interferometric observations are detecting the numerous HII regions, not the old stellar population.)

B. Future Observations

Several workers have undertaken new observations, including near-infrared CCD surface photometry of rings. Specifically, J. L. Higdon has recently obtained data on the Arp 178 system, including the ring galaxy companion (1989, private communication, Astronomy Department, University of Texas). Appleton and his collaborators have also obtained near-infrared data on several ring-like systems at the UKIRT facility (1989,

private communication, Department of Physics, Iowa State University). Other systems that we would suggest as possible tests of the caustics theory include, AM 2159-330, AM 0126-680, and AM 0544-393. These systems appear relatively early-type, do not possess a prominant bar, and are sufficiently extended to permit relatively high-resolution observations.

The theory above may also apply to some of the Hoag-type galaxies recently discussed by Schweizer *et al.* (1987, also see Struck-Marcell 1990), Although Schweizer *et al.* favor an accretion event as the origin of the ring in Hoag's object itself, the galaxies in this class appear very similar to the numerical models presented above. Thus, some of them may be collision remnants.

This example does raise an important point about the comparison of ring theory and observations - there may be more than one way to produce symmetric rings. Accreted material may settle into a symmetric ring, although multiple concentric rings would not be expected in this case. It is also not clear why accretion rings should have sharp caustic edges (although the ring edges do appear relatively sharp in Hoag's object). It is also possible that non-central collisions could generate symmetric rings. However, a variety of such collisions have been investigated numerically, and most show readily detectable asymmetries (see Toomre 1978, Schweizer 1986, Hernquist and Quinn 1988, Huang and Stewart 1988, Wallin and Struck-Marcell 1988, and Appleton and James 1989).

Besides surface photometry, spectra to obtain velocity information across rings would also be very useful. Unfortunately, the picture presented by the stellar velocities in regions of multiple star streams may be complicated. This is a relatively minor problem in the case of narrow rings, like that in Figure 3c, where the stars are moving roughly parallel in all three streams. In broad rings, like those in Figures 3a and 3b, there will be a

significant range of positive and negative velocities within a (spatially resolved) ring. If the velocity width is large, and its profile not symmetric, it will be difficult to observe the net radial velocity of the broad ring. To date, most of the analyses of spectra of rings, reported in the literature, focuses on the HII region emission. It appears that high quality absorption line spectra of the old stars would be difficult to obtain.

VI. CONCLUSIONS

In the preceding sections we have seen that cylindrically symmetric stellar ring waves in galaxy disks can evolve in a variety of ways, depending on the amplitude of the perturbation and the potential of the target galaxy. Rings can thicken as they propagate outward (Section III), remain at a nearly constant width (Section IV[B]), or be pinched off at large radii (Section IV[A]). Multiple, closely spaced rings can result from a low-amplitude collision (Fig. 3c), while an outer ring can appear well separated from overlapping inner rings, or an apparent lens structure in halo-dominated potentials (Figs. 9 and 11). (The latter appear relatively common among rings in galaxy catalogs, which may be an argument for the existence of halos in those cases.)

There is great variety among the observed ring galaxies, for example, in the Arp-Madore catalog. The fact that numerical simulations can replicate this variety of form can be considered another success of the Lynds and Toomre collisional model for rings.

Despite the variety of form, however, there is a great deal of simplicity in the rings. Firstly, all of the (single-encounter) rings consist of paired fold caustics, i.e., an inner and outer edge, with a high-density interior. Secondly, the simple (quasi-)impulsive, kinematic oscillation equations (Section II) seem to provide a remarkably accurate model of the numerical simulations. Moreover, simple analytic approximations to these equations allow very good estimates of oscillation periods and amplitudes (even in multiple component potentials), the evolution of ring widths, and ring birth and propagation characteristics. Stellar densities inside and between rings can

also be estimated with somewhat less accuracy. The success of the kinematic model implies that it may be an efficient tool for interpreting observations. The good agreement found between the kinematic model and the restricted three-body simulations provides an additional indication that despite the approximated nature of the kinematic model, the basic ring phenomenon is indeed kinematic. At the same time, it will be necessary to compare the model to fully self-consistent N-body simulations to check the validity of the approximations used in both the restricted three-body method and the kinematic model. Preliminary comparisons reported above provide some assurances of the relevance of the two presented methods to real ring galaxies.

Other complications remain as well, including: the gas dynamics, star formation in rings (see Appleton and Struck-Marcell 1987a, b, and Struck-Marcell and Appleton 1987), and especially gas-star interactions. It will require a good deal more numerical and observational work to understand the processes at work in these areas.

VII. REFERENCES

Alladin, S.M. 1965, *Ap.J.* **141**, 768.

Appleton, P.N. and Struck-Marcell, C. 1987a, *Ap.J* . **312**, 566.

Appleton, P.N. and Struck-Marcell, C. 1987b, *Ap. J.* **318**, 103.

Appleton, P.N. and James, R. A. 1989, preprint.

Arnold, V.I. 1972, *Functional Anal. Appl.* **6**, 254.

Arnold, V.I. 1976, *Comm. Pure Applied Math.* **29**, 557.

Arnold, V.I. 1980, *Mathematical Methods of Classical Mechanics* (New York: Springer-Verlag), Appendix 12.

Arnold, V.I. 1984, *Catastrophe Theory* (New York: Springer-Verlag).

_____ 1986, *Catastrophe Theory*, 2nd English edition (New York: Springer-Verlag).

Arnold, V.I., Gusein-Zade, S.M.,and Varchenko, A.N 1985, *Singularities of Differentiable Maps*, vol. I (Boston: Birkhauser).

Arnold, V.I., Shandarin, S.F. and Zeldovich, Ya. B. 1982, *Geophys. Ap. Fluid Dynamics* **20**, 111 (ASZ).

Arp, H. C. 1966, *Atlas of Peculiar Galaxies* (Pasadena: California Institute of Technology).

Arp, H. C., and Madore, B. F. 1987, *A Catalog of Southern Peculiar Galaxies and Associations* (Cambridge: University Press).

Binney, J. and Tremaine, S. 1987, *Galactic Dynamics* (Princeton: Princeton University Press), p. 447-450.

Chandrasekhar, S. 1943, *Ap. J.*, **97**, 255.

Chatterjee, T.K. 1987, *Astrophys. Space Sci.* **132**, 177.

Few, J. M. A., Madore, B. F., and Arp, H. C. 1982, *M.N.R.A.S.* **199**, 633.

Golubitsky, M., and Schaeffer, D.G. 1985, *Singularities and Groups in Bifurcation Theory*, Vol. I. (New York: Springer-Verlag).

Hernquist, L. and Quinn, P. 1987, *Ap. J.* **312**, 1.

_____ 1988, *Ap. J.* **331**, 682.

Huang, S-N., and Stewart, P. 1988, *Astr. Ap.* **197**, 14.

Jeske, N. A. 1986, Ph.D. thesis, University of California, Berkeley.

Joy, M., Tollestrup, E. V., Harvey, P. M., McGregor, P., and Hyland, A. R. 1989, *B.A.A.S.* **20**, 1000.

Lotan, P. and Struck-Marcell, C. 1990, submitted to Ap. J.

Lynds, R., and Toomre, A. 1976, *Ap.J.* **209**, 382.

Majewski, S. R. 1988, in *Towards Understanding Galaxies at High Redshift*, eds. R. Kron and A. Renzini (Dordrecht: Reidel).

Majewski, S. R., and Herald, M. 1988, *B.A.A.S.* **19**, 1032.

Majthay, A. 1985, *Foundations of Catastrophe Theory* (Boston: Pitman).

Ostriker, J.P. and Peebles, P.J. 1973, *Ap. J.* **186**, 467.

Poston, T., and Stewart, I.N. 1978, *Catastrophe Theory and Its Applications* (Boston: Pitman).

Quinn, P. J. 1984, *Ap. J.* **274**, 596.

Saslaw, W.C. 1985, *Gravitational Physics of Stellar and Galactic Systems* (Cambridge: Cambridge University Press), Ch. 62.

Schweizer, F. 1986, *Science* **231**, 227.

Schweizer, F., Ford, W. K. Jr., Jedrzejewski, R., and Giovanelli, R 1987, *Ap. J.* **320**, 454.

Struck-Marcell, C. 1990, *A. J.*, **99**, 71.

Struck-Marcell, C. and Appleton, P.N. 1987, *Ap.J.* **323**, 480 (paper II).

Taylor, K. and Atherton, P. D. 1984, *M.N.R.A.S.*, **208**, 601.

Theys, J.C. and Spiegel, E.A. 1976, *Ap. J.* **208**, 650.

Thompson, L. A., and Theys, J. C. 1978, *Ap. J.* **224**, 796.

Toomre, A. 1977, in *The Evolution of Galaxies and Stellar Populations*, eds. B.M. Tinsley and R.B. Larson (New Haven: Yale University Observatory), p. 401.

Toomre, A. 1978, in *IAU Symposium no. 79, The Large-Scale Structure of the Universe*, ed. M.S. Longair and J. Einasto (Dordrecht: Reidel), p. 109.

Tremaine, S. 1981, in *The Structure and Evolution of Normal Galaxies*, eds. S.M. Fall and D. Lynden-Bell (Cambridge: Cambridge University Press) p. 67.

Villumsen, J. V. 1985, *Ap. J.* 290, 75.

Wallin, J. F. and Struck-Marcell, C. 1988, *A. J.*, **96**, 1850.

White, S.D.M. 1982, in *The Morphology and Dynamics of Galaxies*, eds. Martinet, L. and Mayor, M. (Sauverny: Geneva Observatory), p. 289.

EFFECTS OF SATELLITE MULTIPLE PASSAGES AND MERGER ON A RING GALAXY

ABSTRACT

A physical classification of collisional ring galaxies based on the presence of an apparent companion as well as the morphology and kinematics of the target disk is proposed. This classification can possibly be identified with the empirical classification to O-type and P-type ring galaxies of Few and Madore. The classification is achieved by including the effect of dynamical friction (DF) in the collisional ring galaxy picture of Theys and Speigel and Lynds and Toomre, who interpret these objects as the product of a nearly head-on collision between a disk galaxy and an arbitrary galaxy. In our classification, one class of ring galaxies possesses separate detached companions because DF is too weak to have captured the collider. A second class lacks apparent companions since the latter has either merged with the target galaxy or been disrupted. A transition class consists of ring glaxies with detached companions in the process of merger. The significance of mergers in ring galaxies, evident in our simulations, has been largely overlooked in the past, despite the wide recognition based on various investigations that head-on collisions of two galaxies at low relative velocities are highly likely to result in a merger.

We present results of numerical simulations for disk galaxies undergoing collisions in which dynamical friction is included. The star component is modelled by a restricted three-body code which invokes realistic bulge, disk, and halo potentials. The disk gas component is described by a set of cloud fluid hydrodynamic equations. The simulations show that when DF leads to the capture of the companion into a damped oscillatory orbit before ultimately merging or disrupting, the process of ring formation

persists and is even enhanced. Each passage of the companion generates a new set of rings with interesting interplay between them. The multiple passages and merger generate various features in the target stellar disk which are different from single collision rings in their morphology and kinematics, including knotty structures, straight arms, and combinations of broad and thin rings separated by highly rarefied regions. A crucial point is that the ringing is found to last 10^8 -10^9 years after the companion settles to the center of the target galaxy and is essentially merged. This implies that a merged ring galaxy might very well appear like other collisional ring galaxies, even though it lacks an apparent distinct companion. A simple kinematic model for ring formation, adjusted for the special case of multiple collisions, reproduces some of the features found in the restricted three-body simulations and provides insight into the morphology and kinematics of multiple collision disks. Observational support for the present generalized collision picture is presented including comparison with specific objects from the Arp and Arp-Madore (AM) catalogs and some Hoag-type galaxies.

I. INTRODUCTION

Searches for the mechanism(s) responsible for ring galaxy production date back at least to Burbidge and Burbidge (1959) who suggested that these objects may be "the aftermath of a close collision between an elliptical and a spiral" or "the formation of a new galaxy in the wake of another system". Vorontsov-Velyaminov (1960) regarded ring galaxies as a sub-type of spiral galaxies, whereas Sersic (1970) proposed that explosive processes in a galaxy may result in ejection of material in an annular structure. Since ring galaxies are usually not strong radio or X-ray sources, the last interpretation can be ruled out. Freeman and deVaucouleurs (1974) proposed that ring galaxies may be generated in the collision of an intergalactic cloud with a spiral galaxy. However the abundance of such clouds as estimated by Lo and Sargent (1979) is evidently too low to account for all known ring galaxies, though a portion of ring galaxies, in particular folded rings such as Arp 144, may have originated in this fashion.

The widely accepted collisional mechanism was put forward independently by Theys and Speigel (1976) and Lynds and Toomre (1976). In this picture an intruding galaxy (of mass greater than 1% the target mass) penetrates the disk galaxy nearly head-on (within about the inner 15% of the disk radius, and tilted no more than 45 degrees to the disk rotation axis) and causes a temporary increase in the inward gravitational pull on the disk constituents. As the intruder emerges from the other side of the disk its extra gravitational pull gradually diminishes and the disk bounces outward in an attempt to restore centrifugal balance. The particles then overshoot their original equilibrium radius and start to radially oscillate about it

(superimposed on their rotational motion) with a longer oscillation period and a larger amplitude for stars or clouds with larger initial radii. The net effect of all particles engaging in differential oscillatory motion is a series of density waves propagating from the disk center out to its edge.

The collision scenario has gained much popularity, in particular because many ring galaxies possess physically close companions lying near their minor axis, as expected of a companion situated on a disk symmetry axis seen in projection. In most cases where a companion is present, it travels with a velocity relative to the target ring galaxy which is typical of binary galaxies or small groups. Many rings were observed to have outward radial velocities compatible with the picture of an outwardly propagating density wave (Jeske 1986). High star formation rates are found in ring galaxies, which are globally 2-6 times the rates of more normal galaxies, but as much as 50-100 times higher in the high density regions of the rings (Appleton and Struck-Marcell 1987a). This is to be expected since the high density associated with the outwardly propagating shock wave in the target disk gas results in extremely enhanced star formation (Appleton and Struck-Marcell 1987b; Jeske 1986; Struck-Marcell and Appleton 1987). Lastly, occurrence of observed ring galaxies, particularly in dense clusters, is reasonably compatible with theoretical calculations for the frequency of interactions between a disk galaxy and another galaxy under conditions required for ring formation (Thompson 1977; Chatterjee 1987; Athanassoula and Bosma 1985; Arp and Madore 1987; Dostal and Metlov 1978, 1979). All in all, the collision scenario fares well when tested against observations.

Collisional theories however have often been questioned in cases where one or more of the constituents appears to be missing. For example, Theys and Speigel (1976) discuss the absence of a clearly identifiable companion to the ring II Zw 28, and speculate that "the thickened portion of the ring hides a

companion projected onto the ring". Few and Madore (1986) find that of a sample of 69 ring galaxies about one half do have a statistically significant excess of companions (P-type), whereas the other half lacks such an excess (O-type). Consequently, they raise the possiblity that a mechanism other than a galaxy-galaxy central collision might be responsible for O-types. In another sample of ring galaxies, Jeske (1986) finds that at least 5 out of 30 ring galaxies lack physical companions, and in a survey of ring galaxies near rich clusters conducted by Thompson (1977) 4 out of 14 rings had no companions (the remaining 10 rings had a total of 24 companions, most of which are probably unrelated to the ring formation).

In this paper we generalize the standard collision theory of ring galaxy formation by including the DF between the target galaxy and the intruder. The motivation for considering the effects of merger on ring galaxies is quite strong, in particular since ring galaxies arise from the most central collisions experienced by disk galaxies. Sastry (1972) and Sastry and Alladin (1977) find in numerical estimates, that head-on collisions between two galaxies will lead to tidal capture if the two galaxies are centrally concentrated (polytropes of index n=4) and collide at relative velocities smaller than 600 km s^{-1}, or to disruption if one is homogeneous and the other is centrally concentrated in a collision with a relative velocity smaller than 500 km s^{-1}. They also find that if the colliding galaxies differ in mass by an order of magnitude, but are of the same dimension, the disruption probability is considerably increased. White (1978), in N-body simulations, finds that in an interpenetrating collisions of two galaxies in bound or parabolic orbits, merger is expected to occur within one initial orbital period. Miller and Smith (1980) find in almost all of their N-body experiments that close encounters, even at high (>500 km s^{-1}) relative speeds lead to mergers. Since relative velocities between ring galaxies and their intruding companions are typical of binary

galaxies or small groups (roughly 200 - 400 km s^{-1}), and thus even lower than relative speeds considered in the above referenced investigations, ring galaxies are thus excellent candidates for mergers. The possible existence of massive dark halos around disk galaxies and ring galaxies in particular, would contribute significantly to the merger probability.

In our work we consider the following questions: (1) can capture of an initially unbound companion occur due to DF on a time scale comparable to the density wave (ring) propagation time? (2) does ring structure persist after multiple passages and merger ? (3) are multiple-passage rings different in a recognizable way relative to single-passage rings ? The answers to these questions could clarify the origin of ring galaxies without apparent companions and their relation to ring galaxies with companions and their formation mechanisms.

To answer these questions we have performed the following calculations. We model separately the response of the gas component and the star component to multiple, nearly perpendicular, passages of the companion. The disk star component is investigated by employing a restricted three-body code where both the companion's and the test particles' motions are governed by realistic bulge, disk, and halo gravitational potentials. A description of our model and the results are given in Section III.

The present restricted three-body code, rather than a full N-body code, has the obvious advantage of computational time economy, and thus the possibility of exploring a greater region of the huge parameter space. Furthermore, it appears that as far as the effects on the target disk, the restricted three-body method is adequate for calculating the satellite motion. Specifically, by comparing similar simulations which only differ in the details of the oscillatory motion of the companion, we find that the response of the target disk is insensitive to the exact sinking rate of the companion. In

particular, we find that the approximate gravitational feedback of the distorted target galaxy on the motion of the companion, as approximated by Chandrasekhar's (1943) DF formula (eq. [1]), is sufficient for investigating the effects of multiple collisions on the morphology and kinematics of ring galaxies. (However, it is probably insufficient if one is interested in the satellite sinking rate proper.) On the other hand, effects of self-gravity on the disk itself following multiple collisions are potentially very important. Nevertheless, in our simulations the inclusion of a "fattened" disk component (defined in Section III) provides a realistic *effective field* acting on each of the disk constituents. This makes for a significant improvement over the more widely used simulations which included spherical potentials only. Yet, the effects of distortions in the disk, such as ring structure and thickening or warping of the disk, on the effective gravitational field, as well as two-particle gravitational interactions are not considered in our treatment. Therefore, follow-up calculations with a self-gravitating, self-consistent N-body code with realistic values of velocity dispersions of the stellar component would be desirable. The response of the gas component to multiple passages is modelled by solving a set of cloud fluid hydrodynamic equations. The model and the results are presented in Section V.

A simple kinematic model for the ring formation mechanism is presented for the special case of multiple collision in Section IV. A detailed study of various properties of *single-pass* symmetric ring galaxies from numerical simulation and analytic calculation based on the Toomre kinematic model (Lynds and Toomre 1976; Toomre 1978), was carried out by Struck-Marcell and Lotan (1990, hereafter SML), and for asymmetric collisions by Struck-Marcell (1990). We find that the SML kinematic model, when extended to include multiple collisions, reproduces and explains the main features found in our restricted three-body simulations, in particular ring

broadening and thinning.

In Section VI we discuss the relevance of merged ring galaxies to various observational features of ring galaxies, and conclude that merger is a plausible explanation for the absence of companions in a portion of ring galaxies. In Section VII we list several other theories which might explain the absence of companions in some ring galaxies, and conclude that these theories may offer an explanation for a portion of ring galaxies with no excess of companions, but not for all of them. Conclusions are summarized in Section VIII.

II. EFFECTS OF DYNAMICAL FRICTION ON THE COLLIDING COMPANION

The mechanism of DF has been considered in many applications since it was first introduced by Chandrasekhar in 1943 (See, e.g., Tremaine (1981) on galaxy mergers; Tremaine (1976) in a discussion of the orbits of the Magellanic clouds; Kashlinsky (1987) on the evolution of the luminosity function in clusters of galaxies; Casertano, Phinney and Villumsen (1987) on orbit circulization; Byrd, Saarinen and Valtonen (1986) on dynamical friction on a satellite of a disk galaxy.)

The DF force on a particle of mass m_s moving with a velocity $\mathbf{v} = v\hat{\mathbf{v}}$ through an infinite uniform background of stars with mass density ρ and a Gaussian velocity distribution with dispersion σ, is described by Chandrasekhar (1943) as

$$dv/dt = -4\pi G^2 m_s \rho v^{-2} [erf(x) - x\, erf'(x)] (\ln \Lambda) \hat{\mathbf{v}} . \qquad (1)$$

The quantity x is defined by $x = v/(\sigma\sqrt{2})$, $\Lambda = P_{max}/P_{min}$, and P_{max} and P_{min} denote the maximum and minimum values of the "impact parameters". For low speeds v of the massive body, DF is linear in v, whereas for large values it decays as $1/v^2$. Interestingly, the peak of the force occurs for $v/\sigma = \sqrt{2}$ which is roughly the value of realistic collision velocities of binary galaxies. For instance, a typical velocity dispersion of the halo is about 150 km/s, whereas a typical relative velocity of field galaxies is around 250 km/s. The ratio of the two is rather close to $\sqrt{2}$, implying that for head-on collisions DF may act close to its maximum strength and possibly play a significant role

in binding the colliders. Indeed in our simulations we find that in a head-on collision, capture of the companion into a bound orbit is easily obtained for realistic collision parameters. In such cases the companion passes through the target disk several times, typically two or three, before essentially merging with it. In fact, the merging rate in our simulations is an underestimate since only DF due to the halo is considered. DF due to the bulge and disk stars, as well as tidal interactions with the target galaxy may contribute significantly to the merging rate, or to possible disruption of the companion. These mechanisms are not included in this work, but are definitely worthy of inquiry in order to obtain more realistic merging rates and disruption probabilities. Figure 1a (fine line) is a plot of the position versus time of an initially marginally unbound companion, which is subject to the gravitational attraction of the target galaxy as well as to DF due to the target halo (taken from model B of our restricted three-body simulations, described in Section III[D] below). Until $t=17$ the companion's damped oscillatory motion reaches beyond the scale of this graph. Therefore, only those parts of the motion within 0.5 length units above or below the disk are plotted. For $17 < t < 22$ the damped motion is already confined within the scale of this graph, and for later times it basically overlaps the z=0 axis. This figure demonstrates the high sinking rate of the satellite after the first collision. In addition, the bold line in this figure which describes the z-motion (z is the polar axis of the target disk) of a test particle in the target disk, shows the immediate response of the particle to the motion of the satellite. (See Section III[B] on the heating in the z-direction of the test particle disk.)

III. RESPONSE OF THE STELLAR DISK

A. The Model

The stellar component is simulated in our work by a restricted three-body code in three dimensions. The target galaxy potential consists of three components: bulge, disk and halo. The companion galaxy is simulated as a single bulge-like component. The potentials due to all components are time independent during an entire simulation.

The bulge is characterized by a mass density distribution (which will be termed "Hubble -like" profile) of the form

$$\rho(r) = (bM/\pi^2)/(r^2 + b^2)^2 \ , \qquad (2)$$

where M is the total mass of the bulge and b is its characteristic length. The corresponding gravitational acceleration is

$$g = [2GM/(\pi r^2)] \{ (r/b)/[1+ (r/b)^2] - tan^{-1}(r/b) \} \ , \qquad (3)$$

where G is the gravitational constant. This density distribution is intermediate between the modified Hubble profile (which goes as $(r^2+b^2)^{-3/2}$) and the Plummer density profile (which goes as $(r^2+b^2)^{-5/2}$). It has the advantage that it does not decrease as rapidly for large r as does the Plummer potential (Mihalas and Binney 1981, Section 4.4.3), yet its total mass is finite by contrast to the modified Hubble profile. In all cases the companion galaxy is also simulated as a single Hubble-like profile (eq.[2]).

The second component is a three-dimensional disk with an exponential

density distribution in both the radial and z directions. Our choice was made in accordance with several observational works (Freeman 1970; Kent 1984; Wevers 1984; Wevers, van der Kruit and Allen 1986) which indicate that the radial intensity profile in disk galaxies is well fitted by an exponential function. The z dependence of disk galaxies has been fitted by the function $sech^2(z/z_0)$ (van der Kruit and Searle 1981a,b; 1982) for a sample of galaxies, and by an exponential in the z direction by Wainscoat, Freeman and Hyland (1989) for another sample of galaxies, as well as our Galaxy (Gilmore and Reid 1983; Pritchet 1983). For our restricted three-body code, our choice was a density distribution exponential in both directions, which we term a "fattened disk potential". In fact, "fattening" the disk is of great importance in our simulations, since we have found that a strictly planar disk potential (due to a mass density distribution of the form $\rho(r) = [M_D/(2\pi c^3)]e^{-(r/c)}$) gives rise to anomalous behavior of particles residing in the near vicinity of the disk plane, due to the discontinuity at the plane of the attractive force generated by a strictly planar disk. The fattened potential, by contrast, generates a continuous force which diminishes to zero as one approaches the disk plane. The "fattened disk" is described by the expression

$$\rho(r)= [M_D/(4\pi c^2 d)]e^{-[(r/c) + (|z|/d)]} \qquad (4)$$

where M_D is the total disk mass, c and d are the radial and vertical scale lengths, respectively, and (r,ϕ,z) are the cylindrical coordinates of a field point. For convenience we introduce dimensionless coordinates (R,Z) and constant ξ defined by $R=r/c$, $Z=z/c$, and $\xi = d/c$, respectively. In our calculations we typically chose $\xi = 0.07$, in agreement with the Bahcall and Soneira (1980) model of our Galaxy. It can be shown (for example, see Lotan and Luban 1990) that the gravitational field (henceforth the "disk field") due

to the mass distribution described by equation (4) has two nonzero components, given by

$$E_z = (GM/c^2) \int_0^\infty dx\, xJ_0(Rx)[e^{-Z/\xi} - e^{-Zx}]\, (1+x^2)^{-3/2}\, (\xi^2 x^2 - 1)^{-1}, \quad (5a)$$

$$E_r = (GM/c^2) \int_0^\infty dx\, xJ_1(Rx)[\xi e^{-Z/\xi} - e^{-Zx}]\, (1+x^2)^{-3/2}\, (\xi^2 x^2 - 1)^{-1} \quad (5b)$$

where J_0 and J_1 are Bessel functions of the first kind.

The evaluation of the field components at each time step for the 10,000 test particles in our restricted three-body simulations is computationally extremely time consuming. Therefore, we chose to evaluate the components of the disk field for the points of a two-dimensional square mesh within a domain D defined by $|Z| < 10,\ 0 < R < 20$. By symmetry, $E_z(R,-Z) = -E_z(R,Z)$ and $E_r(R,-Z) = E_r(R,Z)$, so that it is sufficient to consider positive values of Z only. The resulting values of E_z and E_r are stored in two rectangular arrays. Linear interpolation using the entries of these arrays provides values of the field components for any point interior to the domain D. For points exterior to the domain D we used asymptotic expansions of equation (5) derived in Lotan and Luban (1990). The latter procedure was necessary only for the intruder which travels far from the disk plane, and therefore outside of the domain D.

Accurate and efficient numerical evaluation of the integrals in equations (5a) and (5b) by conventional methods for the regime $Z/R < 0.005$ is extremely difficult, due to the slow decay of the Bessel functions for large argument. Indeed, in our simulations the orbits of the test particles remained nearly at all times in the vicinity of the disk plane, so that an accurate treatment for this regime is crucial. This problem was overcome by using a technique, briefly described in Appendix B, which provides values of these

integrals to high accuracy. Our technique is built on use of the Levin-T series acceleration method (Levin 1973, Lotan and Luban 1990).

Inclusion of a disk potential is a *necessity* in our simulations. Since multiple collisions obviously give rise to significant heating in the direction perpendicular to the disk plane (see subsection C[2] below), only the large restoring force exerted by a flat disk tends to prevent unrealistic exaggeration of this behavior.

The third component of the target galaxy in our simulations is a nearly isothermal halo of mass density distribution

$$\rho(r) = \rho_o / [1 + (r/a)^2] \quad , \qquad (6)$$

where ρ_o is the central density and a is a characteristic length. We will also use the quantity σ defined by $\sigma = (2\pi G\, \rho(0) a^3)^{1/2}$ with units of velocity, and R the cut-off radius of the halo, beyond which the mass density abruptly drops to zero. The corresponding gravitational acceleration is

$$g(r) = (-4\pi G \rho_o a^3 / r^2)\, [(r/a) - \tan^{-1}(r/a)] \quad . \qquad (7)$$

In our restricted three-body code the centers of mass of the target and intruder are moving in response to their mutual gravity. The origin of the frame of reference used in the simulations is chosen to be the geometrical center of the main galaxy, and therefore a fictitious acceleration term correcting for the non-inertial frame reference is added to the accelerations of all bodies and particles. The target galaxy is surrounded by up to 10,000 test particles representing the stars in the fashion described below. Each test particle's motion is governed solely by the bulge, disk and halo potentials of the target, and the Hubble-like potential of the companion galaxy. The mutual

gravitational attraction between test particles (stars) is neglected. The target and companion, unlike the point-like test particles, are extended. Since the companion may also be roughly of the same size and/or mass as the target bulge, the gravitational potential between the two is calculated as that between two interpenetrating rigid clouds of "Hubble-like" mass distributions. If r is the distance between the centers of the bulge and companion "Hubble-like" clouds, M_B and M_C are their respective masses, and b_B and b_C are their respective characteristic lengths, then the mutual gravitational potential energy is

$$U(r) = [(2GM_BM_C/(\pi r)]\ tan^{-1}[r/(b_B+b_C)] \quad . \qquad (8)$$

The derivation of equation (8) is given in Appendix A.

In the calculation of the energy of interaction between either the target disk or halo with the "Hubble-like" companion, the latter is assumed point-like since indeed it is likely to be significantly smaller in size than either of the former.

The target test particles are initially spread in planar, equally spaced annuli, each containing the same number of particles. This translates into an 1/r density distribution. (Some simulations used an exponential distribution instead.) All particles are assigned circular velocities consistent with centrifugal balance within the target galaxy potential, with the addition of a small amount of random velocity component. The amount of random velocity was chosen to be less than realistic velocity dispersions of old population stars in order to partially compensate for the lack of self-gravity in the simulations. Self-gravity would obviously tend to enhance the ring structure through the mutual gravitational attraction of the ring constituents. By contrast, higher velocity dispersions would tend to dissolve any structure.

The calculation is carried out using the following dimensionless units. The outer radius of the test particle disk is chosen as one length unit, and the unit mass is arbitrary. Thus a velocity unit corresponds to the circular velocity of a test particle orbiting a "Hubble-like" bulge of one unit mass, at the edge of the test particle disk. Time units are derived as the ratio of length and velocity units, and the time of closest approach is defined as time zero. A simulation is typically started at $t = -5$ time units. Free parameters involved in the simulations are: Target to companion mass ratio; inclination, impact parameter and relative velocity at closest approach; mass, characteristic length and velocity dispersion of each individual component (target bulge, halo, and companion). The equations of motion of all test particles and the companion are solved using a fourth order Runge-Kutta method. As indicated in Section II the companion equation of motion includes a term describing the DF force applied to it by the target halo. The DF force generated by the disk stars is neglected since in a nearly perpendicular collision the companion will travel a very short distance through the thin disk. Tidal forces between the target bulge and the companion are also ignored, although they could play an important role in sinking rates in very central collisions, in particular if the target is an early type galaxy with a large bulge. A fixed time step is invoked throughout an entire simulation, except in cases where DF is included, a smaller time step is used for the companion only, assuring accurate integration even when DF and the resulting acceleration are large.

Most of the simulations were performed in pairs. One simulation included the DF deceleration term (eq. [1]) in the companion equation of motion, whereas the other simulation left it out. Since we use relative velocities between target and companion in the first collision which are parabolic or moderately hyperbolic, the simulations without DF never result

in capture, while simulations with DF may result in either capture or escape, depending on the various parameters used.

B. Simulation Results

1. Broad Rings and Other Morphological Features

The main features that emerge from the simulations are as follows. Up to the time of the second collision in the simulation with DF, the evolution of the test particle disk in a pair of simulations (one with and the other without DF) is almost identical. Shortly thereafter a new set of rings starts propagating outward in the case with multiple collisions. The most obvious effect is that rings due to successive passages are broader than first collision rings, and often the rarefaction between them is more pronounced. The width of these broad rings is typically one quarter (but up to 40% as in model E(b) at $t=10.4$ for instance) of the disk radius, which is a factor of 2 or more broader than single collisions rings. Also, the appearance of the test particle disk after multiple collisions varies greatly with time. Broad rings alternate narrow rings (an interpretation of this result is provided by a kinematic model presented in Section IV), the disk smooths out and structure reappears at later stages, etc. By contrast, much less variation is found in the structures formed in the test particle disk following a single collision.

Even if the first collision is quite symmetric, subsequent collisions may become increasingly asymmetric. As a result, structure formed due to later collisions will grow increasingly asymmetric. Indeed we find that "later" rings may be connected by inner bridges, a ring might appear knotty (Figure 3iii case C[b]), or straight segments may form (Figure 3iii case D[b]), as opposed to the normally rounded structures of single-collision rings.

2. Heating of the Disk in the *z*-Direction

The development of the test particle disk in the direction perpendicular to the disk plane is obviously affected by multiple collisions. Each collision contributes to heating and thus thickening of the disk in this direction. As a result, a disk which undergoes multiple collisions and merger will become significantly thicker than a single collision disk. This effect in turn also contributes to the broadening of rings in the radial direction (other broadening mechanisms are detailed in Section IV below), because particles which were close together within a certain ring gradually drift away and occupy different heights above and below the original disk plane. Being situated in different positions, the particles are subjected to different gravitational forces and start moving somewhat incoherently. As a result their distance from the disk axis of rotation is different, and the whole ring becomes broader.

Figures 1a and 1b demonstrate the significant amount of heating generated by multiple collisions. Both figures describe the motion of a test particle disk in a restricted three-body simulation (model B, see next subsection for a complete description of this model). Figure 1a (bold line) describes the z motion versus time, from the start of the run at $t=-5$ until $t=50$ (well after merger), for a particle which was initially at a radial distance in the disk plane of 0.8. Until the time of the first collision at $t=0$ the test particle moves within the disk plane and thus has no z-motion whatsoever. Immediately thereafter the particle starts oscillating in this direction with a moderate amplitude. However, after the second collision at $t=12.9$ the oscillation amplitude grows dramatically (approximately 4 to 5 times larger than its value prior to the second collision). Comparison with the motion of the companion, described by the thin line on the same graph, shows the immediate response of the test particle to the oscillations of the

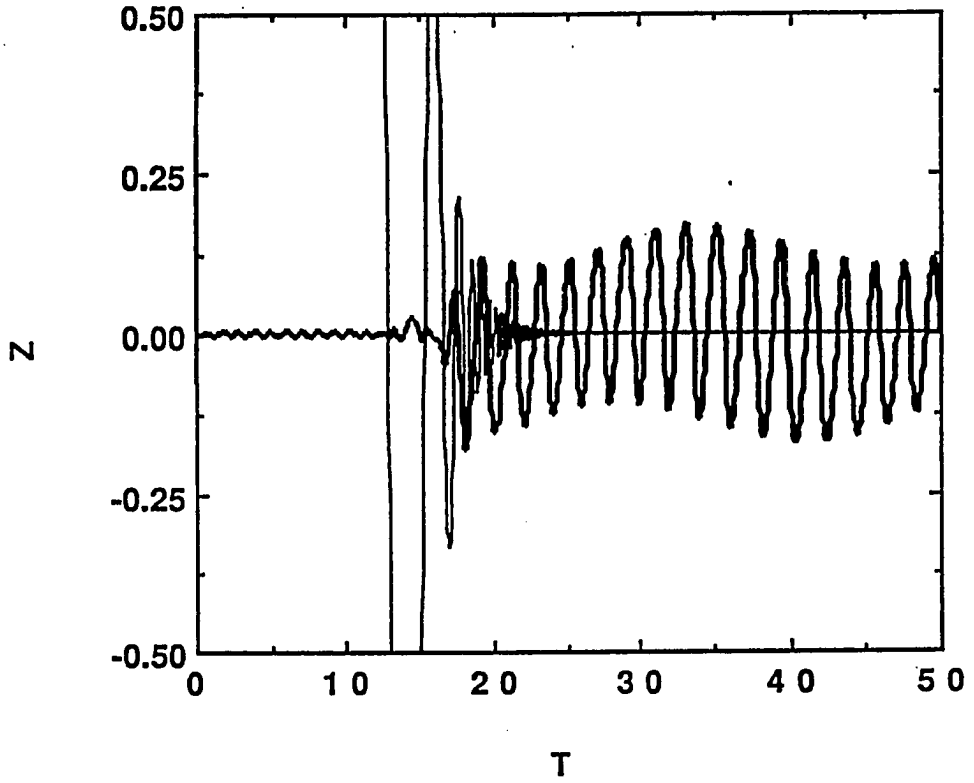

Fig. 1a - z-motion vs. time of the companion (fine line), and of a test particle (bold line) in a restricted three-body simulation (model B). See section III(B) for interpretation.

companion, and how each additional collision excites the growth of amplitude of the particle's motion.

A different way of looking at the z-heating is provided by a plot of the z position versus the radial position at different times for a disk test particle. Figure 1b is such an r-z plot with different time periods represented by different symbols (see figure caption). From this figure we see that the heating process is somewhat gradual and the last oscillations of the companions still shake the disk particles in the z-direction. By contrast, as will be shown in Section IV below, the radial motion is barely affected by those final small oscillations of the companion. This result can be understood, since for the test particles which are fairly close to the disk plane at all times, even small oscillations of the companion above and below the disk, amount to a significant perturbation to the perpendicular force acting on them. By contrast, the final oscillations of the companion in the vicinity of the target center are small relative to the radial distance of a typical particle and thus have little effect on it.

Figure 1c is an edge-on view of an entire test particle disk following head-on collisions and merger. The thickness of the test disk demonstrates the significant amount of heating in the z-direction. A single head-on collision (case (a)) results in a much more modest (by a factor of 10 approximately) disk thickening than does the multiple-collision disk (case [b]). (Both figures are taken from model B[b] at $t= 10$. See subsection [C] below for a complete description.)

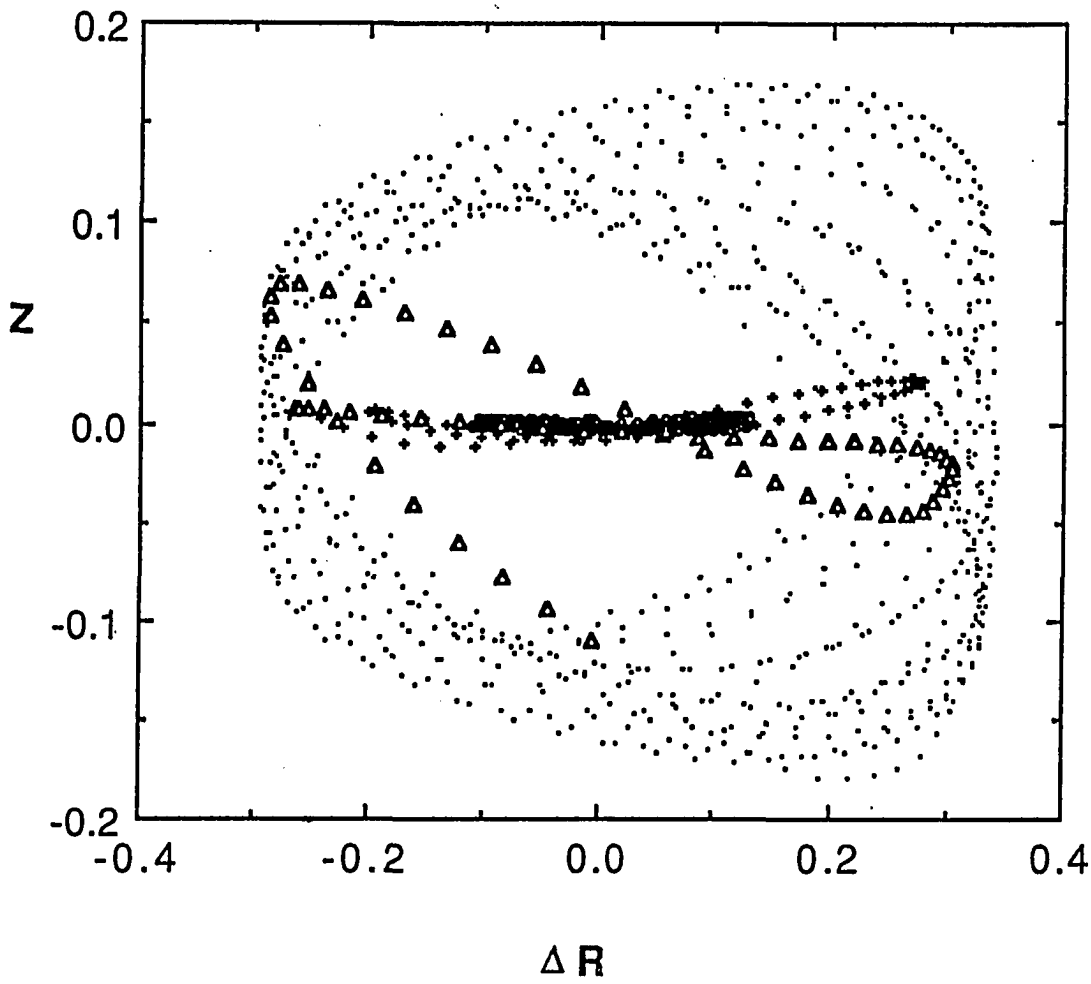

Fig. 1b - Plot of z vs. the radial epicyclic displacement defined by $\Delta r(t) = r(t) - r_{initial}$ of a test particle in a restricted three-body simulation (model B) : (o), prior to second collision (t<13); (+), between second and third collisions (13<t<15.5); (▵), between third collision and merger as defined in the text (15.5<t<18); (.), (t>18).

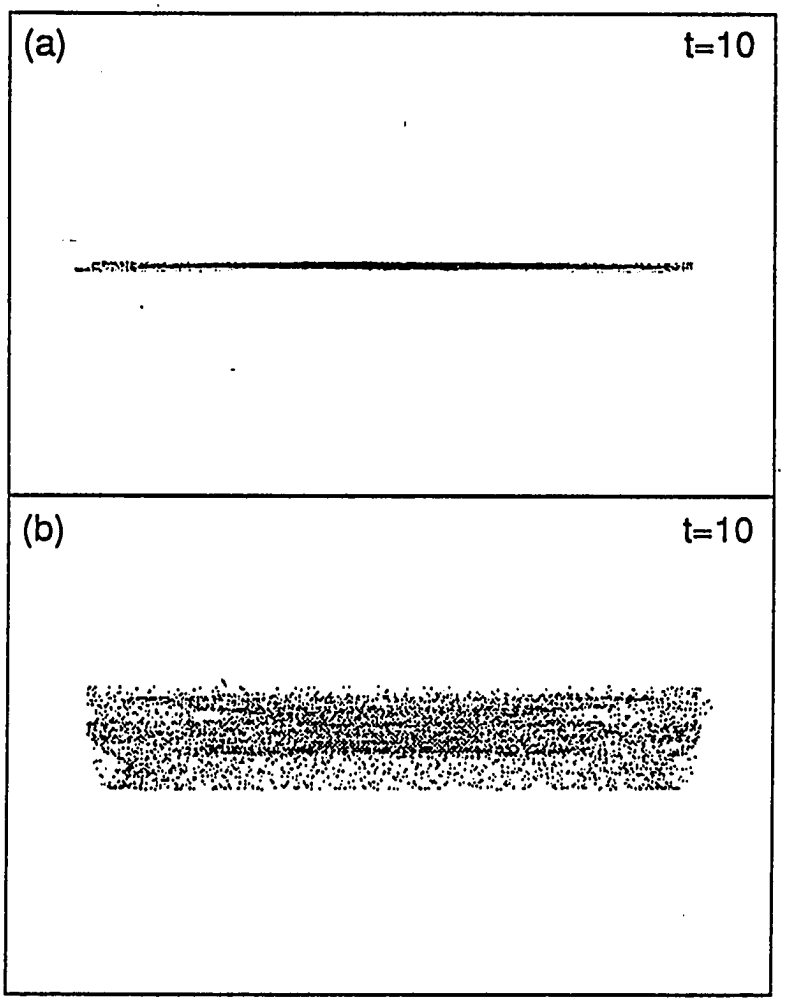

Fig. 1c - Edge-on view of the entire test particle disk at *t=10* following (a) a single passage (b) multiple passages of the companion (taken from model B).

C. Kinematics

Figure 2a is a plot of radial velocities in the disk plane versus the radial distance in the disk of all the test particles in a restricted three-body simulation for a single collision. (The data are taken from model B[a] described in the next subsection.) Figure 2b is similar except it describes a disk following multiple collisions and merger (model B[b]). Figure 2a is representive of radial velocities of ring waves, and its interpretation as interpenetrating star streams is quite obvious. Typically, the first couple of rings following a head-on collision consist of three streams, while later rings usually overlap so that more streams are involved (see SML). The loops, each of which represents one ring, are roughly of the same size, namely the radial velocities, radial velocity dispersions and their radial thicknesses are similar. The multiple collision and merger case (Fig. 2b) is very different. Some loops are much wider than those in the single collision case (Fig. 2a), while others are much smaller and are superimposed on the larger loops. The wide loops are a manifestation of broad rings mentioned in subsection (A) above. They spread over some 30% of the disk radius and evidently have much larger velocity dispersions than single collision rings. The smaller loops superimposed on the large ones represent narrow rings with small velocity dispersions, which overlap the broad rings. An interpretation of this phenomenon is again provided by the kinematic model described in Section IV (Figs. 4b and 4c of the kinematic model show the combination of broad and narrow rings, and their possible overlap). In summary, multiple collision rings have larger velocity dispersion in broad rings and smaller velocity dispersions in narrow rings, relative to single collision rings. In Section VI(D) below we deal with the observational implications of this result.

Fig. 2a - Radial velocity vs. radius of 10,000 test particles following a single passage (taken from model B(b) at $t=10$).

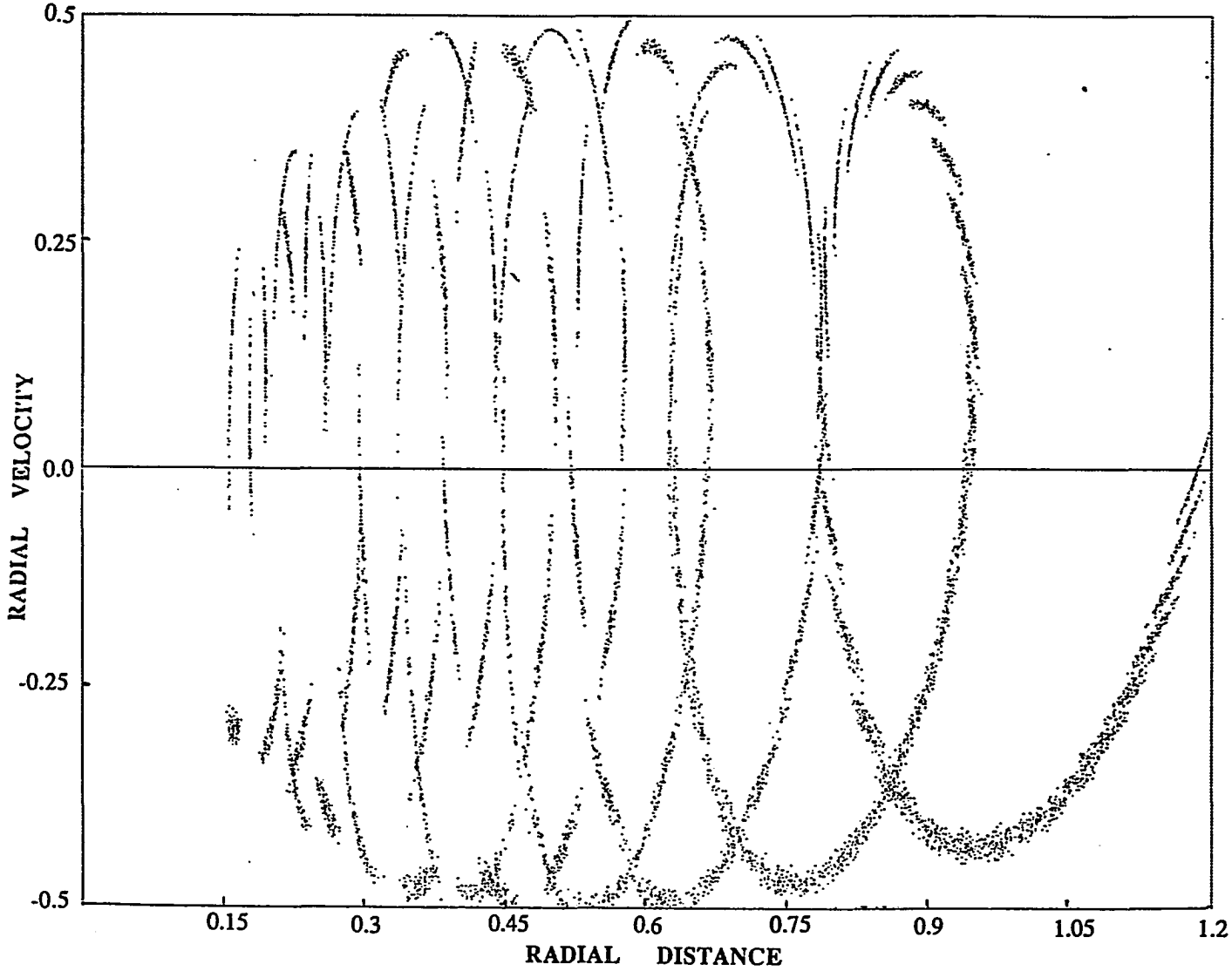
0.5
0.25
0.0
-0.25
-0.5
RADIAL VELOCITY
0.15
0.3
0.45
0.6
0.75
0.9
1.05
1.2
RADIAL DISTANCE

Figure 2b - Same as figure 2a, but following multiple passages of the companion.

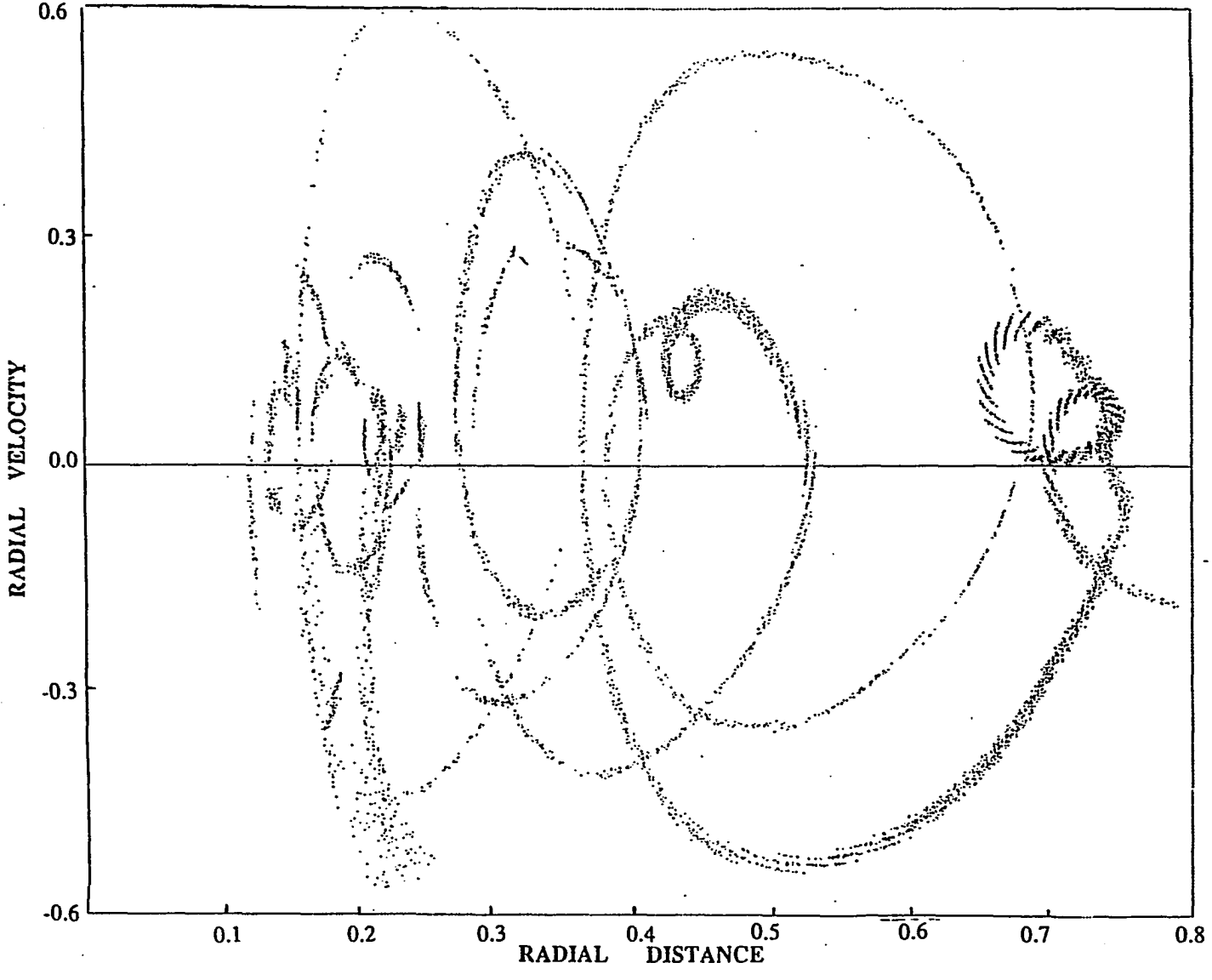
0.6
0.3
0.0
-0.3
-0.6
RADIAL VELOCITY
0.1
0.2
0.3
0.4
0.5
0.6
0.7
0.8
RADIAL DISTANCE

D. Description of Individual Simulations

In this section, we will briefly describe selected simulation pairs which are representative of the rest of the simulations which we have conducted. The parameters for each simulation are given in Table 1. This table contains the following columns. The first column is the model letter code. The second, third and fourth columns give the parameters of the bulge, disk, and halo components respectively, using the same symbols as those in the text. The fifth column contains the target to companion mass ratio. The last two columns list the distance (R_{min}) and the inclination (*INCL*) angle at closest approach. Note that in all the simulations presented here, closest approach occurs when the companion crosses the disk plane. Each row represents a pair of simulations with (case b) and without (case a) DF, except for model D which is an oblique collision with DF, and model F which is an off-center collision without DF. The orbit of the companion in each model is summarized in Table 2. In the column titled "maximum separation" we list the maximum distance achieved after the first penetration and before the second one with the corresponding time, the times and impact parameters of the second and third collisions, and the approximate time of merger. (Merger is taken to occur once the center of the companion is permanently confined within a distance of the disk potential scale length - typically 0.25 length units - from the target center.) The time of the first collision is defined as $t=0$ and the corresponding impact parameter (denoted R_{min}) is given in Table 1. All quantities included in Tables 1 and 2 are measured in the dimensional units described above.

Figure 3 consists of selected snapshots of the test particle disk for the various models. In all cases the disk is viewed pole-on. The model letter

TABLE 1

Parameters of Restricted Three-Body Simulations

Model	Bulge		Disk		Halo				Companion		Mass	R_{min}	INCL
	M	b	M	a	M	R	γ	σ	m_c	b_c	Ratio		
A	1	0.1	1	0.25	9.4	6	0.9	1	0.5	0.08	22	0.01	90
B	1	0.3	1	0.3	3.9	2	1.2	1.6	1.18	0.3	5	0.2	90
C	1	0.2	1	0.25	0.62	1	0.6	0.9	0.53	0.16	5	0.2	90
D	1	0.2	1	0.25	0.62	1	0.6	0.9	0.53	0.16	5	0.2	70
E	1	0.3	2	0.3	0.94	1	1.5	2	1.31	0.3	3	0.02	90
F	1	0.3	0.5	0.25	0.94	1	1.5	2	0.5	0.1	4	0.25	90

TABLE 2

Orbit of Companion in Restricted Three-Body Simulations

Model	Maximum Separation		Second Crossing		Third Crossing		Merger
	Time	Distance	Time	Distance	Time	Distance	Time
A	4.4	4.98	9.1	0.03	12.6	0.028	15.5
B	1.6	2.29	3.5	0.00007	5.1	0.00021	6.4
C	2.0	1.97	4.3	0.094	5.5	0.23	5.3
D	2.3	2.1	5.3	0.6	5.7	0.1	6.4
E	3.1	3.2	6.1	0.004	8.3	0.07	11.0
F [a]	...	...	...	...	...	...	...

[a]This model does not include DF and therefore no multiple collisions take place.

accompanied by either the notation (a) for the single collision case, or (b) for the multiple collision case, appears in the upper left hand corner of each frame. The time is listed in the upper right hand corner.

Model A

(shown in Figure 3i)

This is a case of a low mass companion (mass ratio is 22), and a target galaxy which is halo dominated. Until $t=9.25$ - shortly after the second collision - the cases with and without DF are practically identical. The first noticeable difference at that point is that due to the additional inward gravitational pull introduced by the second collision in case (b), the entire test particle disk shrinks in size, and later bounces back. Around $t=11$ the test disk in case (a) appears to smooth out and the ringing is essentially over. However in case (b), roughly at that time new structure emerges, notably a set of broad rings. Around $t=12$ the outer ring spreads over some 30% of the radius (if the low-density outer part is ignored). For certain periods of time ($t=12.75$ for instance) the test disk seems almost relaxed and structureless. Later on, however, structure reappears in the form of broad rings ($t=14.25$, 15.5) and lenses ($t=15$). Clearly, structure is retained well after merger at $t\approx15.5$. Such a galaxy would appear as a ring galaxy *without* an apparent companion. Starting at $t=16.5$, well after merger, asymmetric structure forms due to the asymmetries of the last collisions. From $t=22$ the test disk is practically smoothed out.

This pair of simulations demonstrates that: (1) the ringing phenomenon continues well after merger. Therefore it is possible for a ring galaxy to possess no apparent companion and yet originate in the "classical" head-on collision. (2) a merged ring galaxy may possess broad rings, relative to single

Fig. 3i - Pole-on view of the test particle disk for model A described in section III(D). The upper-case letter in the upper left hand corner of each frame identifies the model, and it is followed by either (a) for the single collision case, or (b) for the multiple collision case. The time is listed in the upper right hand corner of each frame.

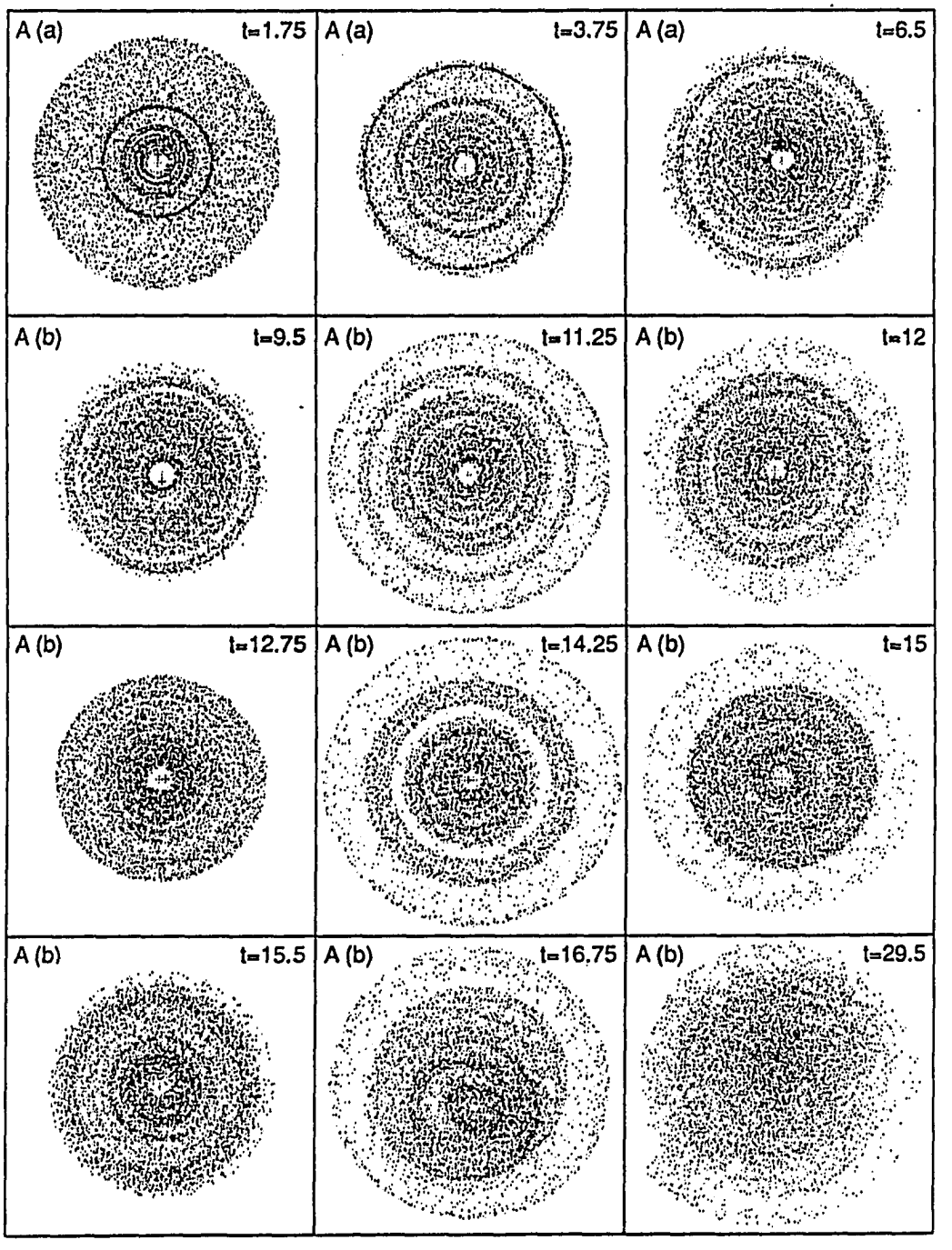
A (a) t=1.75
A (a) t=3.75
A (a) t=6.5
A (b) t=9.5
A (b) t=11.25
A (b) t=12
A (b) t=12.75
A (b) t=14.25
A (b) t=15
A (b) t=15.5
A (b) t=16.75
A (b) t=29.5

collision rings, during certain phases of its evolution.

Model B

(shown in Figure 3ii)

In this model the companion is of moderate size (target to companion mass ratio is 5). Many characteristics of this model are common to the previous model A. Shortly after the second collision in case (b), the test disk shrinks, and it appears that what are separate ringlets in case (a) (at $t=4$), merge to become one thick ring in case (b). This broad ring later separates again into several ringlets as it propagates outward, some of them broad and some narrow ($t=4.8$ in case [b]). While in case (a) the appearance of the test disk is essentially the same at all times (while ringing lasts), the test disk in case (b) varies greatly with time from almost smooth disk, to prominent ring structure with pronounced rarefaction in between rings. Sometimes the rings are extremely broad ($t=6.2$ for instance), while at other times, at $t=7.4$ for instance, they are very narrow. The kinematic model presented in Section IV provides an explanation for this behavior.

In fact, the outer narrow faint ring and the inner broad stronger ring at $t=7.4$ resemble similar features in the following bull's-eye galaxies (all on pg. 6.10 in AM): AM 0544-393 (described by AM as "bull's-eye + elliptical outer ring"), AM 0126-680 (similar description), AM 2159-330 and AM 0656-745 (the last one has a bar which our simulations do not have). The picture at $t=7.4$ is a pole-on view of the test particle disk, an oblique view would obviously result in the outer circular ring appearing elliptical.

From this simulation (and others) we again conclude that a merged ring galaxy might take altogether different shapes at different phases of its evolution. As noted earlier, the ring structure is maintained long after the

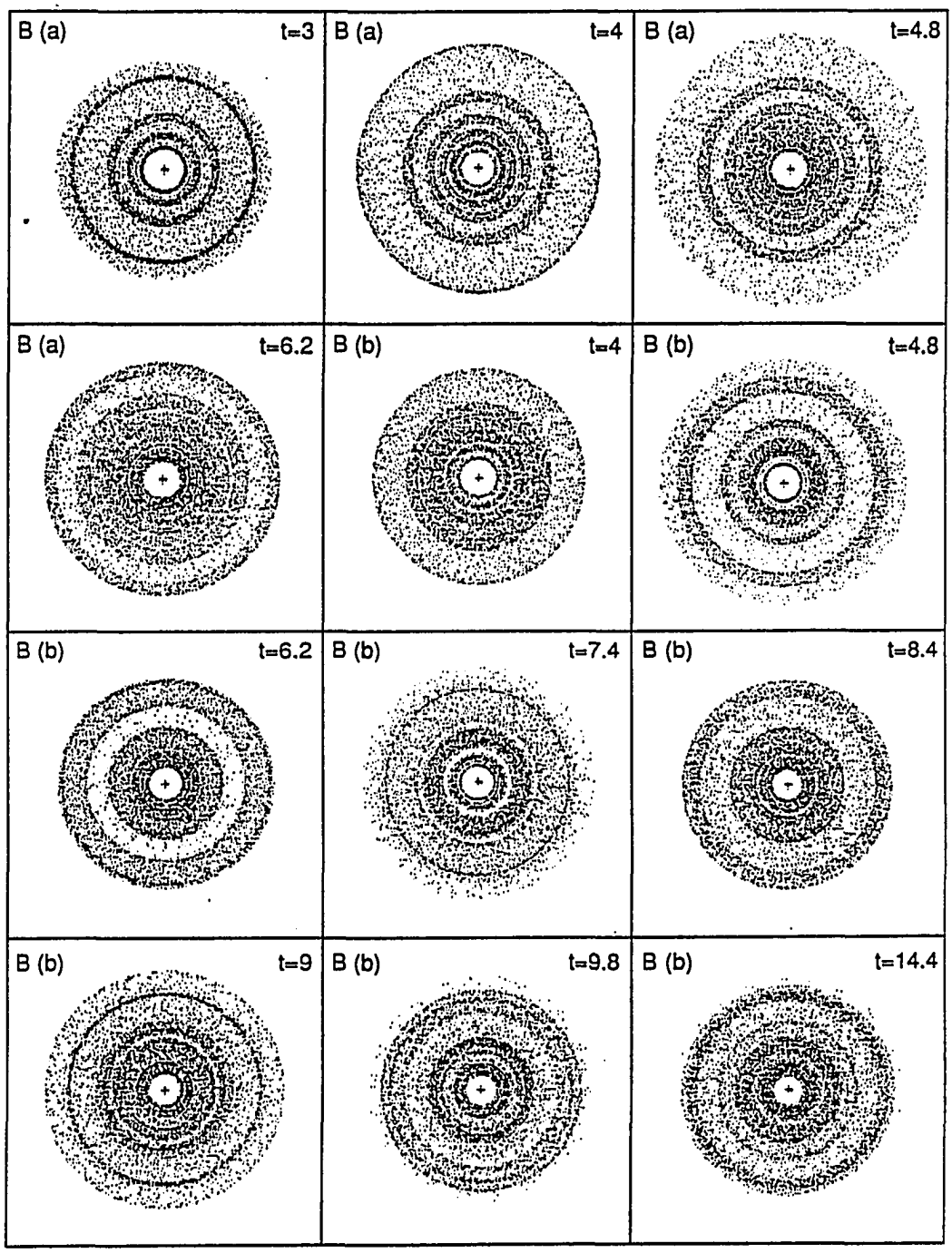

Fig. 3ii - Same as Fig. 3i, but for model B.

companion is practically merged, allowing the ring galaxy to have no apparent companion.

Model C

(shown in Figure 3iii)

In this simulation the target galaxy is dominated by a disk and a bulge, and possesses only a small mass halo. The collision in this case is moderately off-center (impact parameter is about the same as the bulge and disk characteristic lengths). This asymmetry is quite obviously reflected in the shape of the propagating rings virtually from $t=0$. The width of any given ring varies with azimuthal angle (see the outer ring at $t=3.8$, for instance). The test disk appears as outer and inner rings connected by "spokes". There appears to be some similarity between the test disk at $t=5.8$ and $t=6$ and the galaxy AM 2026-424 (AM pg. 6.7) which is described by AM as "ring with companion in ring". The "spokes" in this AM galaxy and in our model at $t=6$, appear to have similar shape and lie at the same relative positions. In addition the faint tail in the simulation may be identified with a trace of a tail in the south-west side of this galaxy. As described by AM, the companion is within the ring. If this is not just a projection effect, but rather the companion is indeed physically close to the ring center, it is possible that this companion is in the process of merger and has possibly collided with the target more than once. The time $t=6$ in our model pertains to shortly after the third collision. It would be extremely interesting to measure the relative velocity between the ring and the companion in AM 2026-424, and determine whether the two are gravitationally bound. This could provide a test of the scenario of an eventual merger in this system.

The structure of this somewhat off-center collision becomes even more

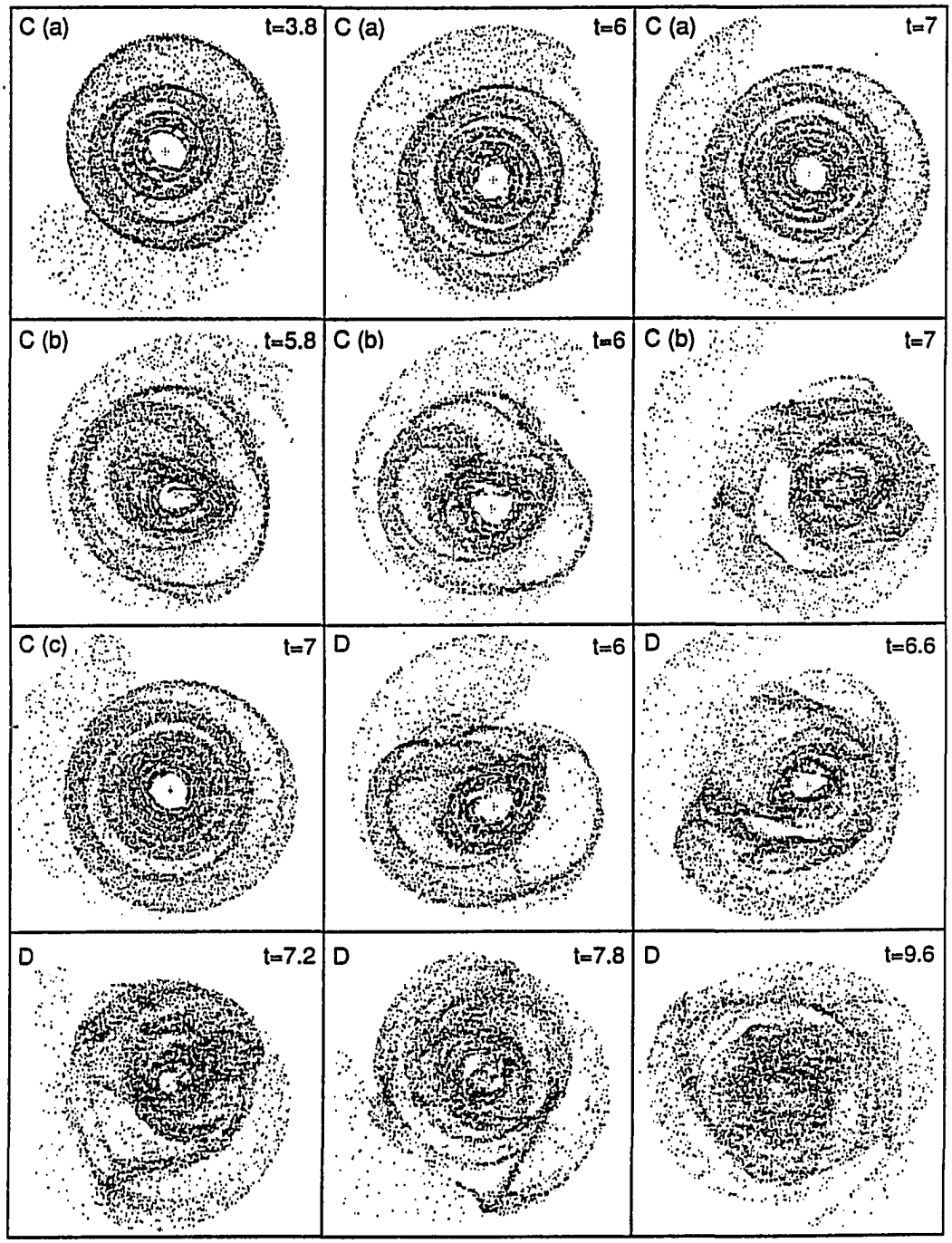

Fig. 3iii - Same as Fig. 3i, but for models C and D.

fascinating after merger has taken place at $t \approx 5.3$. Starting at $t=7$ the outer rings appears quite knotty, a structure which is completely nonexistent in the single collision case, but is prevalent in real ring galaxies. The multiple collisions in this case are off-center to the degree that quite asymmetric structure results, instead of broadened rings. As in previous models, the galaxy takes different shapes at different stages of its evolution. In fact, in many stages such a galaxy would not be classified as a ring galaxy, but rather as some other type of irregular disturbed galaxy (but without an apparent companion!).

Model C(c) is an oblique (inclination of 50^{o} from the target axis of rotation) single collision which is otherwise identical to model C(a). A snapshot at $t=7$ is given in Figure 3iii. The nearly identical appearance of the two configurations demonstrates the mild effect of inclination in ring forming collisions (as long as the inclination angle is less that 45^{o} of the symmetry axis). The impact parameter is a much more sensitive parameter. However, in multiple collisions, the sensitivity to the inclination angle is dramatically greater, since each additional oblique collision adds up to the overall asymmetry of the disturbance. This effect is demonstrated in the following model.

Model D

(shown in Figure 3iii)

This model differs from model C(b) in the obliqueness of the collision only. Yet, the development of the test particle disk until $t=5$ is almost identical in the two models. In fact, starting at $t=6$ model D appears no longer ring-like, but rather as sections of rings connected in various ways. Around $t=7.2$ a perfectly straight feature appears which does not exist in the

perpendicular model C. An interesting example of a straight structure is found in AM 1939-515 (AM pg. 10.13), described by AM as having "disturbed arms + 6 companions", and Arp 28 described as having "straight heavy arm". However, further work is required in order to establish a common origin between the above galaxies, and this model. At later times, the structure becomes quite irregular, although an outer ring can still be identified at *t=9.6*.

Model E

(shown in Figure 3iv)

This case involves a bulge and halo of comparable mass, a heavier disk, and a massive companion (1/3 the target mass). The second passage in case (b) occurs shortly before the ringing due to the first collision is over. Around *t=6.8*, the disks in both cases are almost completely smoothed out. Shortly thereafter, at *t=7*, structure reappears in the disk in case (b) in the form of broad rings propagating outward. At *t=10.4* a ring of nonuniform width, stretches over some 40% of the radius (if the probably undetectable faint outer ring is ignored). At various times the structure becomes quite asymmetric, due to the growing asymmetry of the last passages. At *t=11.6* there appears an outer spiral arm which originates at one point on the ring, where it forms a V-shape with that part of the ring. (A V-shape (cusp) is one of the generic two-dimensional caustic waveforms. See Struck-Marcell 1990.) The ring galaxy AM 0608-752 (AM pg. 6.4, described as "off-set nucleus (rings + companions)") seems to have a spiral arm originating from the east side of the ring. This arm winds some 180° whereas that in the simulation winds more than 360°. It is possible that a deeper exposure of this galaxy would reveal a longer arm. The ring galaxies AM 0227-484 and AM 2134-471 (both on pg. 6.4 in AM) possibly possess similar structures as well.

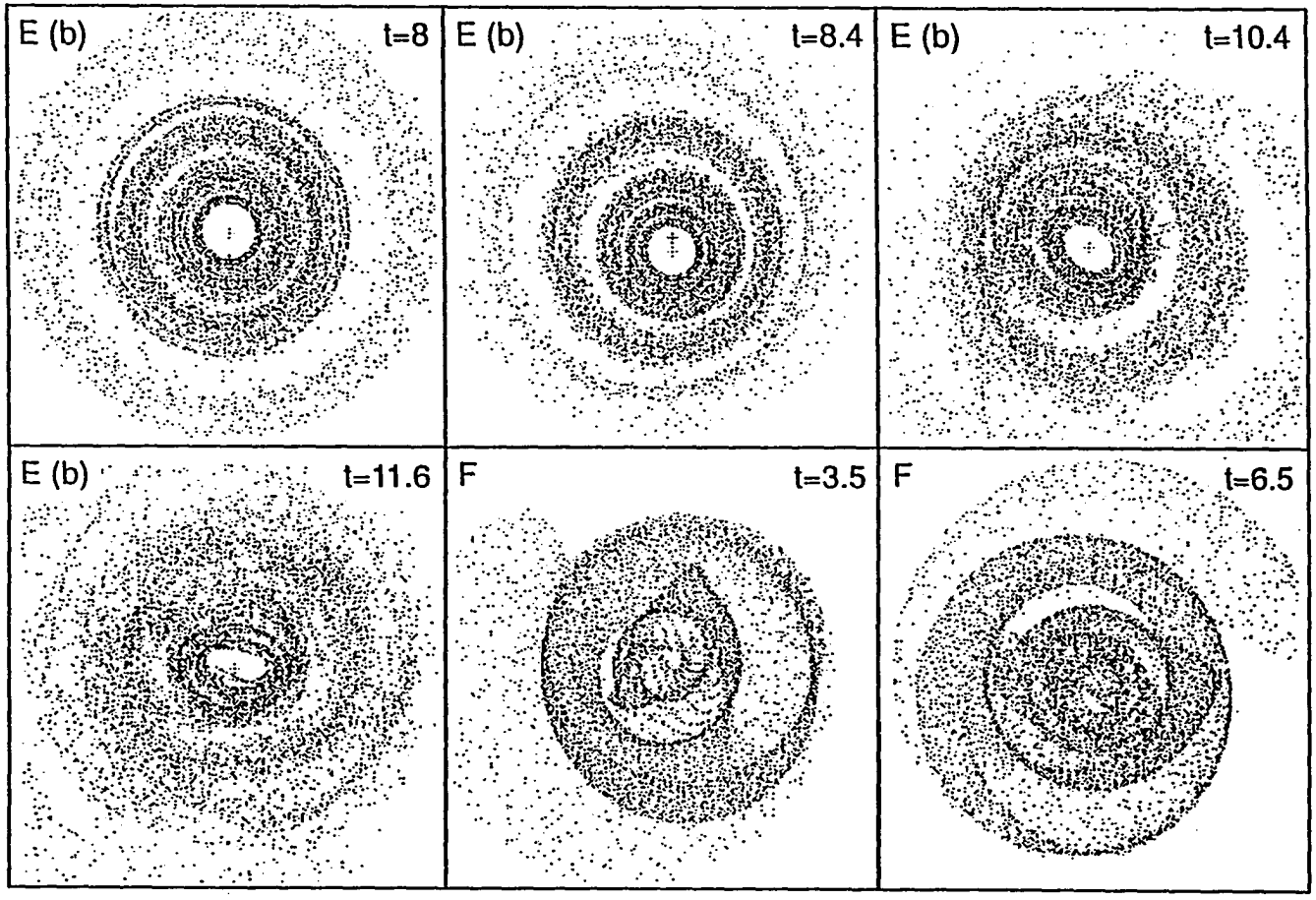

Fig. 3iv - Same as Fig. 3i, but for models E and F.

Model F

(shown in Figure 3iv)

This model is different from all the previous ones. DF is not included here, and the collision is quite off-center. This model is interesting in the context of this paper since the off-centeredness of the collision results in broad rings as well. The rings are asymmetric and typically broad on one side and narrow on the other. There is also an inner structure that resembles an eye ball. Arp 107 is a ring galaxy whose ring is broad on one side and narrow, almost vanishing, on the other. It also contains an inner structure and a close companion. This galaxy is a candidate for a perpendicular off-center collision similar to the one described by this model.

IV. UNDERSTANDING BROAD RINGS WITH A SIMPLE KINEMATIC MODEL

Lynds and Toomre (1976) pointed out that the basic ring phenomenon results from the kinematic epicyclic oscillations excited by an impulsive disturbance. Struck-Marcell and Lotan (1990, hereafter SML) used a version of this model to derive various characteristics of ring galaxies including oscillation periods and amplitudes, ring widths, ring birth and propagation characteristics, spacing between rings, ring and inter-ring densities, motion of individual stars in a ring and other properties, and their dependences on the perturbation amplitude and the form of the colliding galaxies' potentials. The basic feature of the kinematic model is that a star in the target disk, in response to an impulsive perturbation, will execute radial harmonic oscillation superimposed on its orbital motion. Figure 4a shows the time development of trajectories of particles which started out at different distances from the origin. Each particle's trajectory is described by $r=q-Aqsin(\omega t)$ where q is the particle's initial position (namely, distance from the center of the planar disk), r is the position vs. time, A and ω are the amplitude and the frequency, respectively, of the epicyclic oscillatory motion in the radial direction, and t is the time. The units in this graph are as follows. Distance is measured in units of the softening length of a softened point mass potential. The time unit is the free-fall time from a distance of one softening length of this potential. The amplitude A of the radial harmonic oscillation is approximately proportional to the star's initial radius and depends on the companion to target mass ratio. The oscillation frequency ω is roughly proportional to $q^{-3/2}$, and also depends on the structure of the

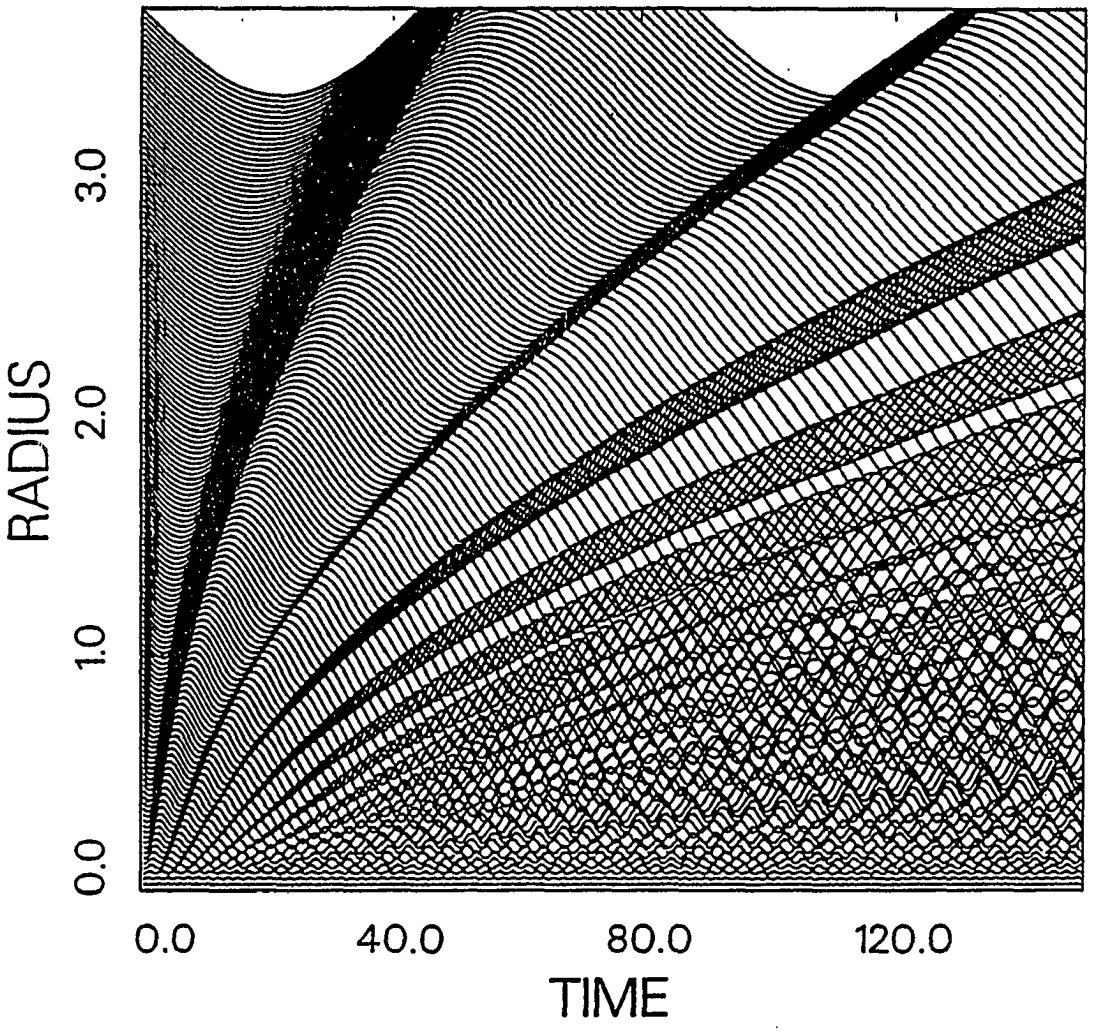

Fig. 4a. - Radius -time plots of the stellar trajectories $r(q,t)$ in the SML kinematic model, calculated according to eq. (9) for a single collision case. The target to companion mass ratio is 20.

target galaxy (see SML for details). The net effect of the stars' differential motion is the propagation of a series of high density waves from the disk center out to its edge.

The expression in SML for ring widths shows that each ring becomes broader as it propagates out, with its width being proportional to the distance from the origin. Also, the ring width increases progressively from one ring to the next (these results are also potential dependent. See Section II[D] in SML). As a result, later rings overlap, and the whole structure becomes irregular.

In order to roughly imitate multiple collisions we introduced into the kinematic formalism a second disturbance some time after the first one, which consists of an inward velocity impulse equal to that in the first impulse. Figure 4b shows one such calculation where the target to companion mass ratio is 20. Until $t=50$ this figure was produced in exactly the same way as Figure 4a. At $t=50$ a second disturbance occurs, and the particle trajectories are adjusted accordingly. In Figure 4a progressive broadening from one ring to the next takes place, as well as broadening of each ring as it propagates outward. By contrast, after the second hit shown in Figure 4b, each ring's thickness varies *with time* from extremely narrow to fairly broad. As a result the appearance of the entire target disk will greatly vary with time, with various combinations of broad and narrow rings. In the one-hit case (Fig. 4a) the ring propagation velocity is monotonic. For instance, in SML we find that for a softened point potential the propagation velocity is proportional to t^2 for small radii, and to $t^{2/3}$ for large radii, with t denoting the time. Other potentials, including an isothermal halo potential give other dependences. By contrast, after the second hit in the two-hit case, the propagation velocity varies from fast in regions where the ring is broad,

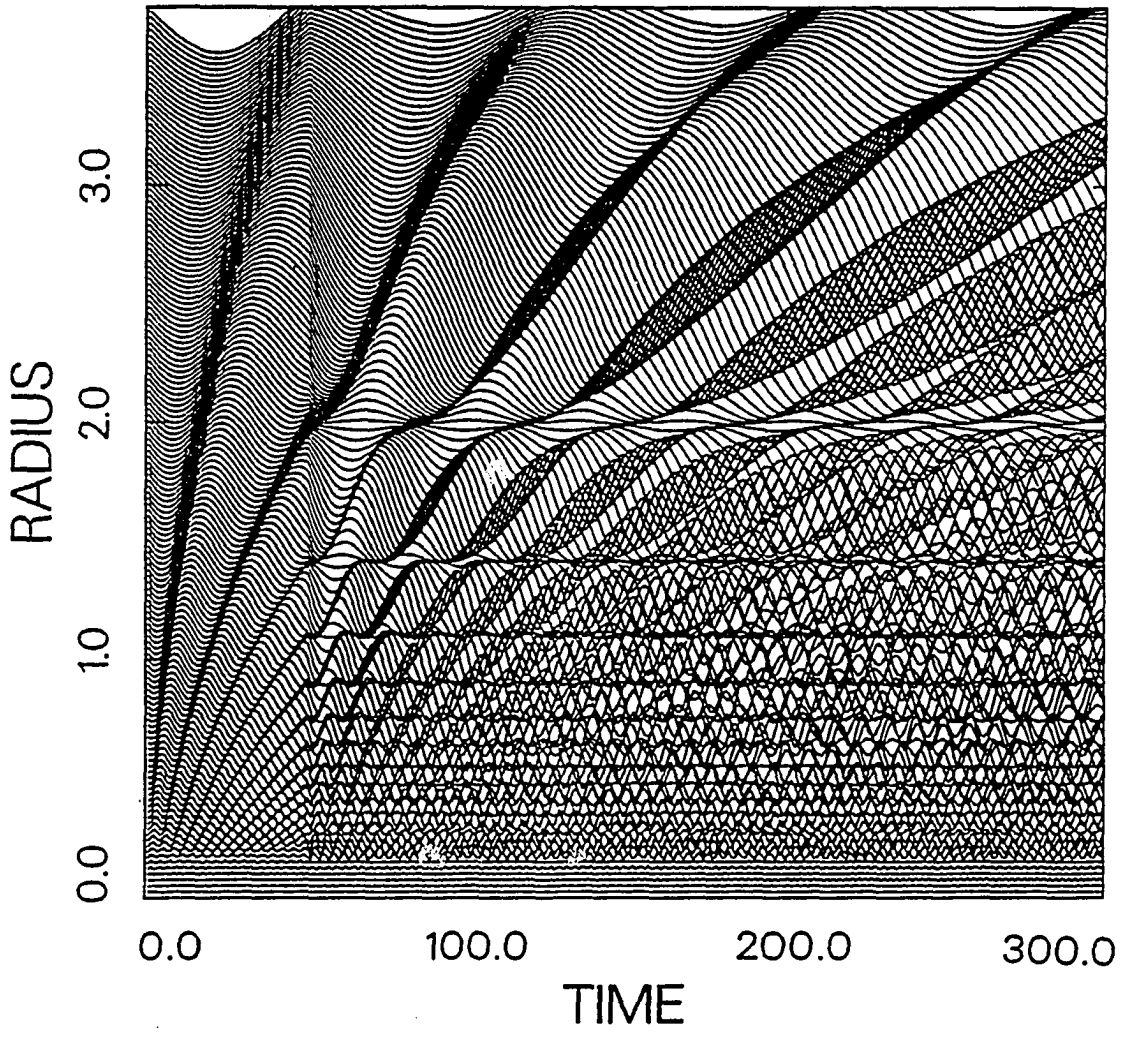

Fig. 4b - Same as Fig. 4a except for a multiple collision case.

to slow (or even zero velocity, namely the ring is stationary) in regions where the ring is narrow. Such behavior was indeed found in our restricted three-body simulations where multiple collisions took place. Model B (see description in Section III above) is one example. The broadening of rings by a factor of 2-3 due to a second disturbance is common to the kinematic model and the restricted three-body simulations.

Figure 4c is similar to 4b except that both hits are twice as strong. (Target to companion mass ratio is 10.) As a result the overlap of rings sets in earlier. (This behavior is true in the one-hit case as well. See SML.) In fact, in this case the flat thin portions of successive rings connect to create what appears as a long lasting stationary ring. This is one example of a simulated collisional ring of zero propagation velocity, as well as zero velocity for the matter contained in the ring.

A closer look at some individual particle trajectories in the kinematic model (Fig. 4d) offers a simple explanation for this behavior. This graph is identical to Figure 4b except that only several trajectories are printed. Particles, which at the time of the second impulse at $t=50$ were moving inward in the radial direction, in the course of their radial epicyclic motion, were given an extra pull inward, which enhanced their epicyclic oscillatory motion amplitude. (The epicyclic frequency which depends on the target potential will thus remain nearly unaffected, except for a possible phase shift.) On the other hand, particles which were on their way out are decelerated and their amplitude may decrease. The eight trajectories shown in Figure 4d range from an almost completely horizontal (first and fourth trajectories from bottom) with no epicyclic motion, to increased amplitude (second trajectory from top).

Trajectories for individual particles were also obtained from the

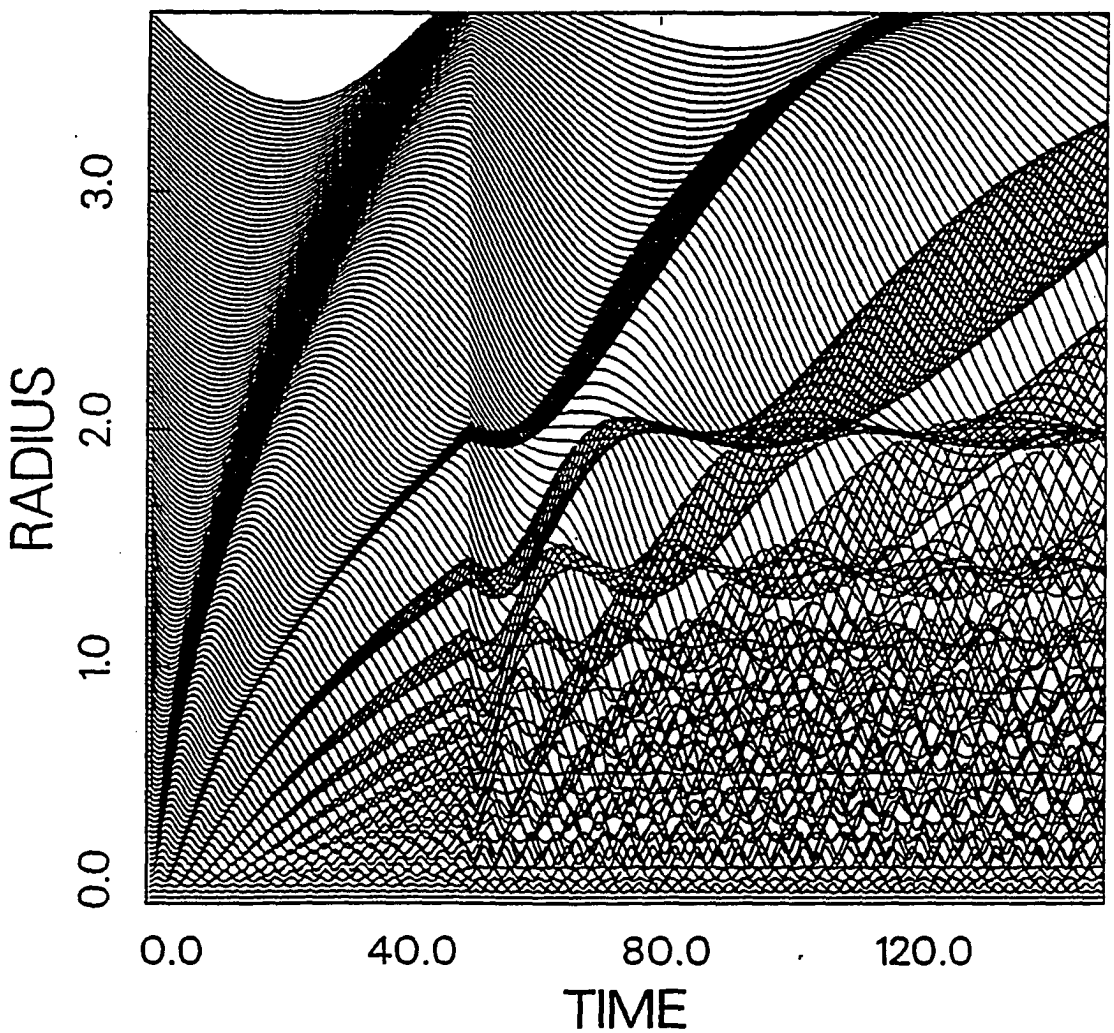

Fig. 4c - Same as Fig. 4b except mass ratio is 10.

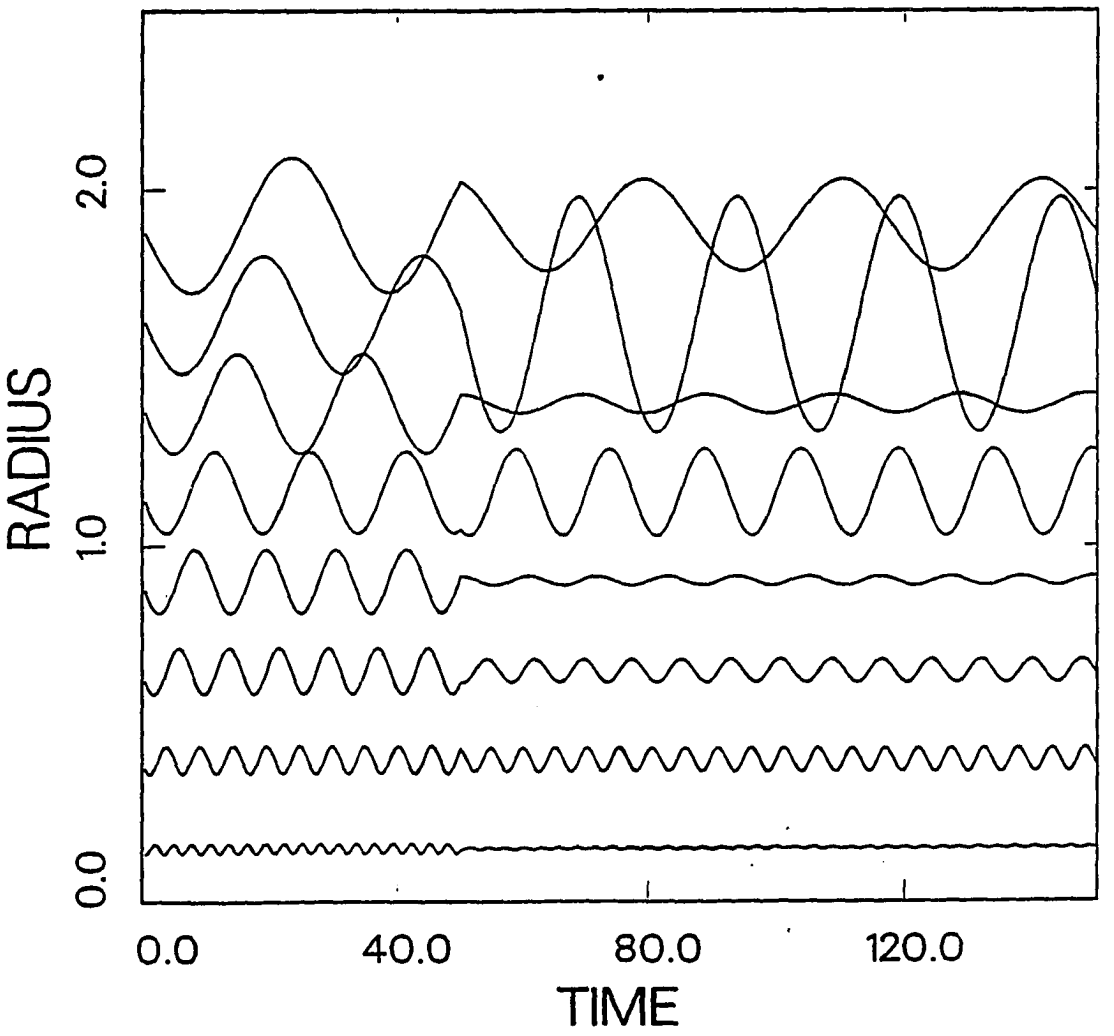

Fig. 4d - Same as Fig. 4c except only selected eight trajectories are presented.

restricted three-body code using the parameters of model B. The units are the same as those used in all our restricted three-body simulations (see Section III[A]). In Figure 4e, a particle which initially rotated at a distance of 0.8 length units suffers an increase in amplitude after the second hit (and merger), whereas a particle which was initially at a distance of 0.61 (Fig. 4f) experiences a decrease in its amplitude. (The nearly flat radial motion seen in the one dimensional kinematic model cannot be achieved in the three-dimensional simulations since the motions perpendicular to the disk interfere with the orbital and radial motion, and upset the fine tuning required for such cancellation of epicyclic motion.) In conclusion, narrow rings come about from orbit crowding of particles with damped amplitudes, whereas broad rings result from orbit crowding of oscillators with enhanced amplitude .

In addition to the velocity impulse as the companion passes interior to the orbital radius of a disk star, an equally important effect is the contraction of the average (guiding center) orbital radius of the star, due to the additional mass of the merged companion. Depending on the phase in the epicyclic cycle of any particular star, this change in the guiding center radius in a prompt merger, can itself result in either a damping of the epicyclic motion, or amplification by up to a factor of about two. For example, if the merger and contraction of the guiding center radius occur while a given star is at radial apoapse, then its radial amplitude will obviously be increased. Alternately, if the star was at periapse, it will experience a decrease of its radial amplitude. Figure 4g, taken from the kinematic model, shows the trajectories of two particles which have experienced two hits as well as contraction of their guiding centers. The behavior of those trajectories is qualitatively similar to the test particles' trajectories obtained from the restricted three-body simulations shown in Figures 4e and 4f.

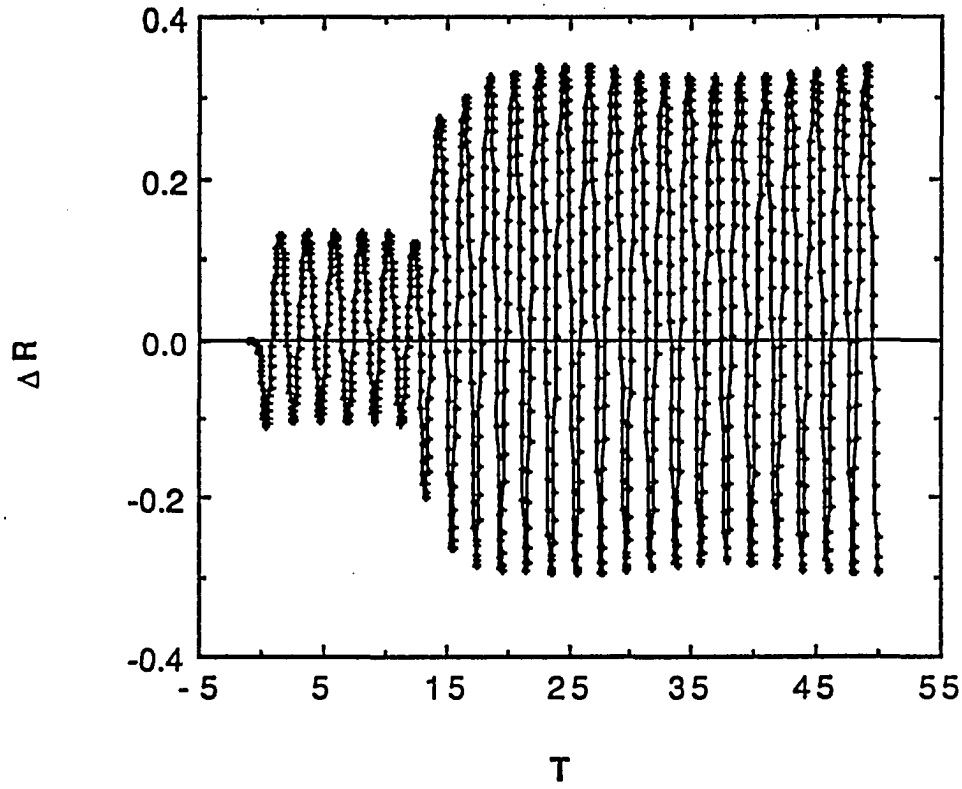

Fig. 4e - Radial epicyclic displacement defined by $\Delta r(t) = r(t) - r_{initial}$ vs. time, of a test particle in a restricted three-body simulation (model B) following multiple collisions and merger. The particle had a pre-collision orbital radius of 0.8 length units.

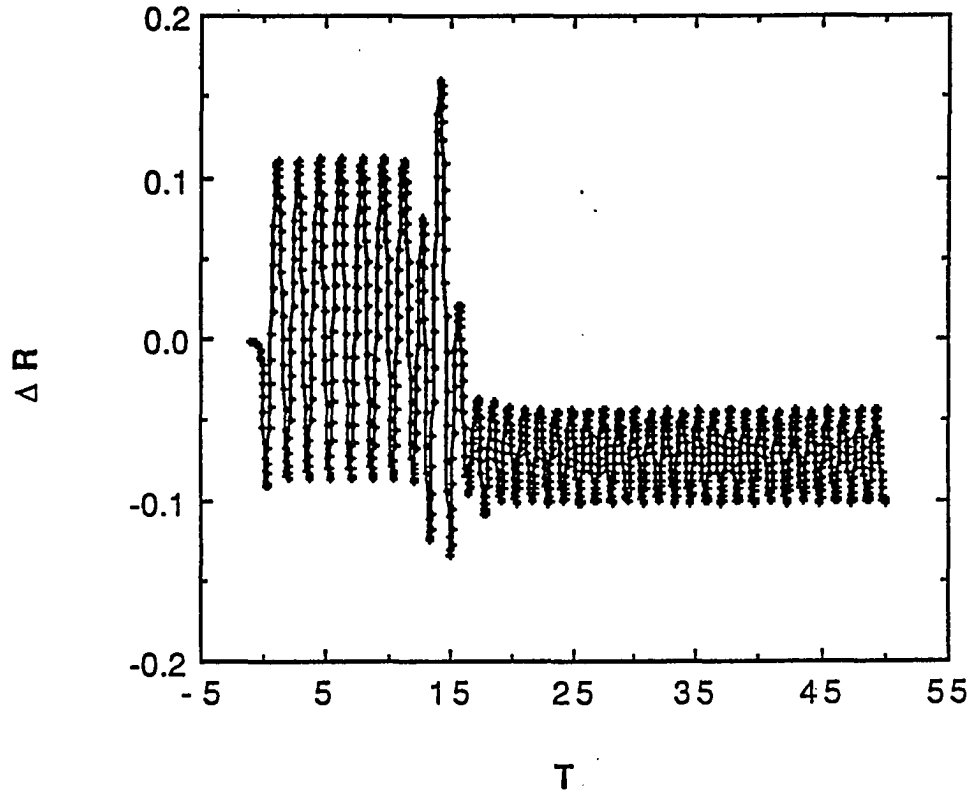

Fig. 4f - Same as Fig. 4e except particle was at r=0.61 prior to the collision.

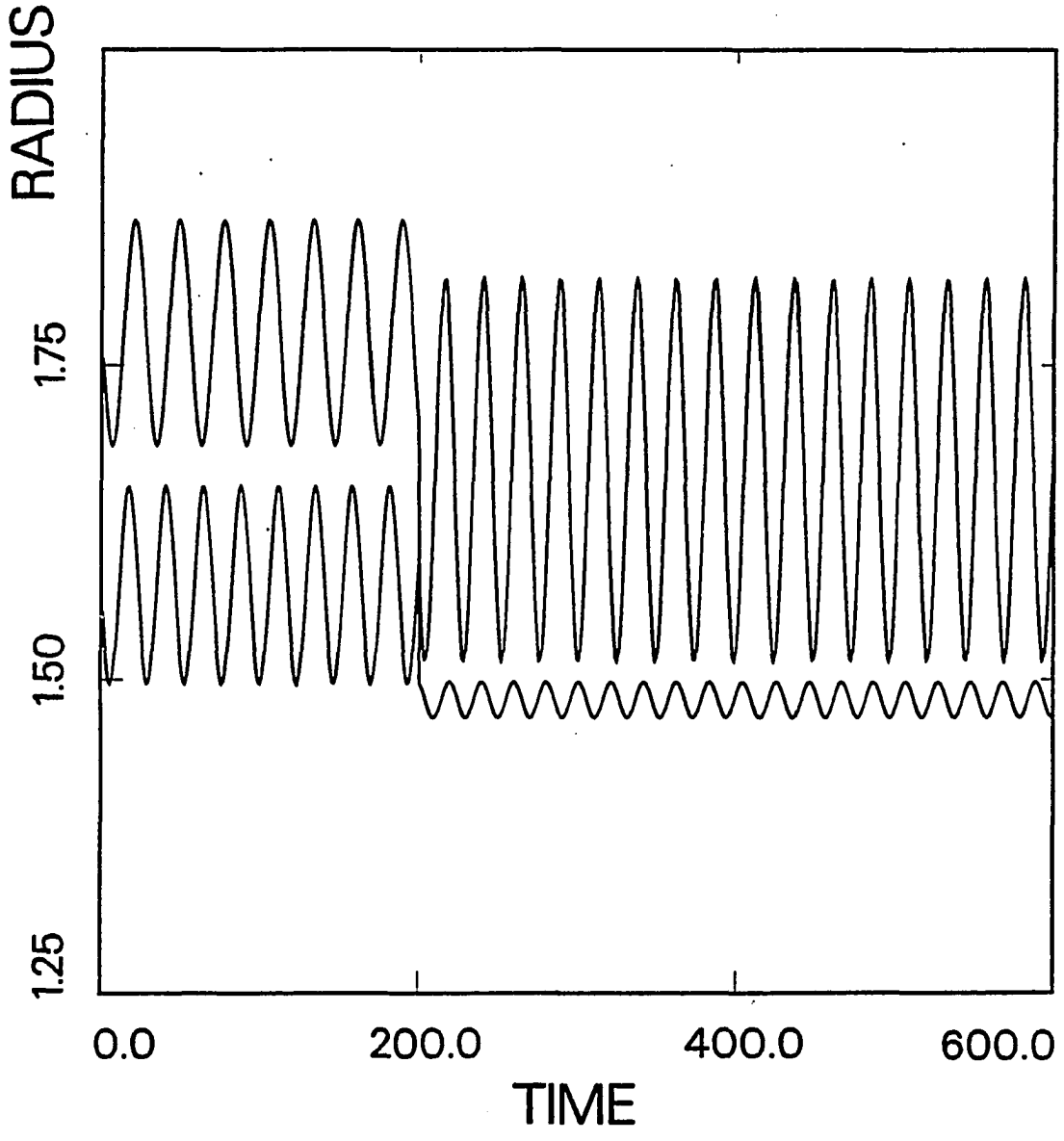

Fig. 4g - Two stellar trajectories $r(q,t)$, calculated according to eq. (9) of the kinematic model, for two particles which have experienced two hits and contraction of their guiding centers.

Despite the approximate nature of the kinematic model, in particular for multiple collisions, it is still able to reproduce certain behaviors found in the restricted three-body simulations. Specifically, the kinematic model helps us understand the bifurcation between stars whose radial epicyclic motion will be damped, and those that are amplified in a second encounter, as well as the resulting phenomenon of broadening and thinning of rings.

V. RESPONSE OF GAS DISK

A. The Model

The effect of a head-on collision, and in particular multiple collisions, on the gas component of a disk is explored using a cloud fluid hydrodynamic model in one spatial and one temporal dimension (for a complete description see Scalo and Struck-Marcell 1984, Struck-Marcell and Scalo 1984,1987). The cloud fluid model, known as the isothermal Oort model, assumes the inter-stellar medium (ISM) consists of clouds, and its behavior can be described by some local "kinetic physics". In this model the evolution of the ISM is governed by two competing mechanisms: cloud-cloud collisions and internal star formation (Field and Saslaw 1965). Cloud collision may lead to either coalesence or shredding. As a mass of a cloud exceeds a certain threshold it is assumed to contract gravitationally, fragment and form new stars. The massive stars then break up their parent cloud through winds, supernova activity and expanding HII regions. Small clouds are formed, accelerated and the cycle is closed. These processes are incorporated into a hydrodynamic formalism by taking velocity moments of the original kinetic equation. Application of this model to ring galaxies, undergoing a head-on collision with a smaller mass companion, show (Appleton and Struck-Marcell 1987b, Struck-Marcell and Appleton 1987) that a set of density waves form and propagate through the target gas disk. The leading edge of the wave is accompanied by a strong enhancement of star formation, whereas large regions inside the leading edge suffer severe suppression of star formation. The large infall velocities behind the primary ring give rise to an even stronger and more compressed second ring which often undergoes a

strong burst of star formation. The set of equations, the method for their solution and the results in the single collision case (no DF) are described in detail in the references above. In this paper we will only concentrate on the results of cases with multiple collisions due to DF, and compare them to the single collision cases.

B. Results of Hydrodynamic Calculations

Since the hydrodynamical code we use is one-dimensional, the collisions investigated are strictly head-on. In the calculations for the target gas component, the gravitational attraction of the companion on the fluid elements is included by using the free-fall solution for the companion with the DF deceleration term (eq. [1]) included. The cases of interest are those where the capture and return of the companion due to DF occur while rings from a previous passage(s) are still present in the disk.

Figure 5 shows selected snapshots of density versus position in the target disk. The four snapshots in column (a) refer to the single-collision case, and the eight snapshots in the two columns (b) refer to the multiple collision case. The time is listed in the upper right hand corner of each frame. The notation in the graphs is as follows: Numbers denote the sequential number of rings formed as a result of one specific passage, primes denote the passage number (no prime for the first passage, one prime for the second passage, etc. Thus 2" denotes the second ring generated by the third passage). Units in these graphs are as follows: Length=softening length of the target galaxy potential, e.g., 1.2-6 kpc. Time= collision time for clouds, 4-20x10^6 years. Density is given in units of its initial unperturbed value. The time of the first collision is defined as $t=0$.

Figure 5 is typical of most of the calculations, so it will be reviewed in detail. The target to companion mass ratio is 15 and the cloud fluid

Fig. 5 - Gas density vs. radial distance in the disk following a companion-target collision (mass ratio 1:15) . The four snapshots in column (a) refer to the single-collision case, and the eight snapshots in the two columns (b) refer to the multiple collision case. The time is listed in the upper right hand corner of each frame. Units and labelling are explained in the text.

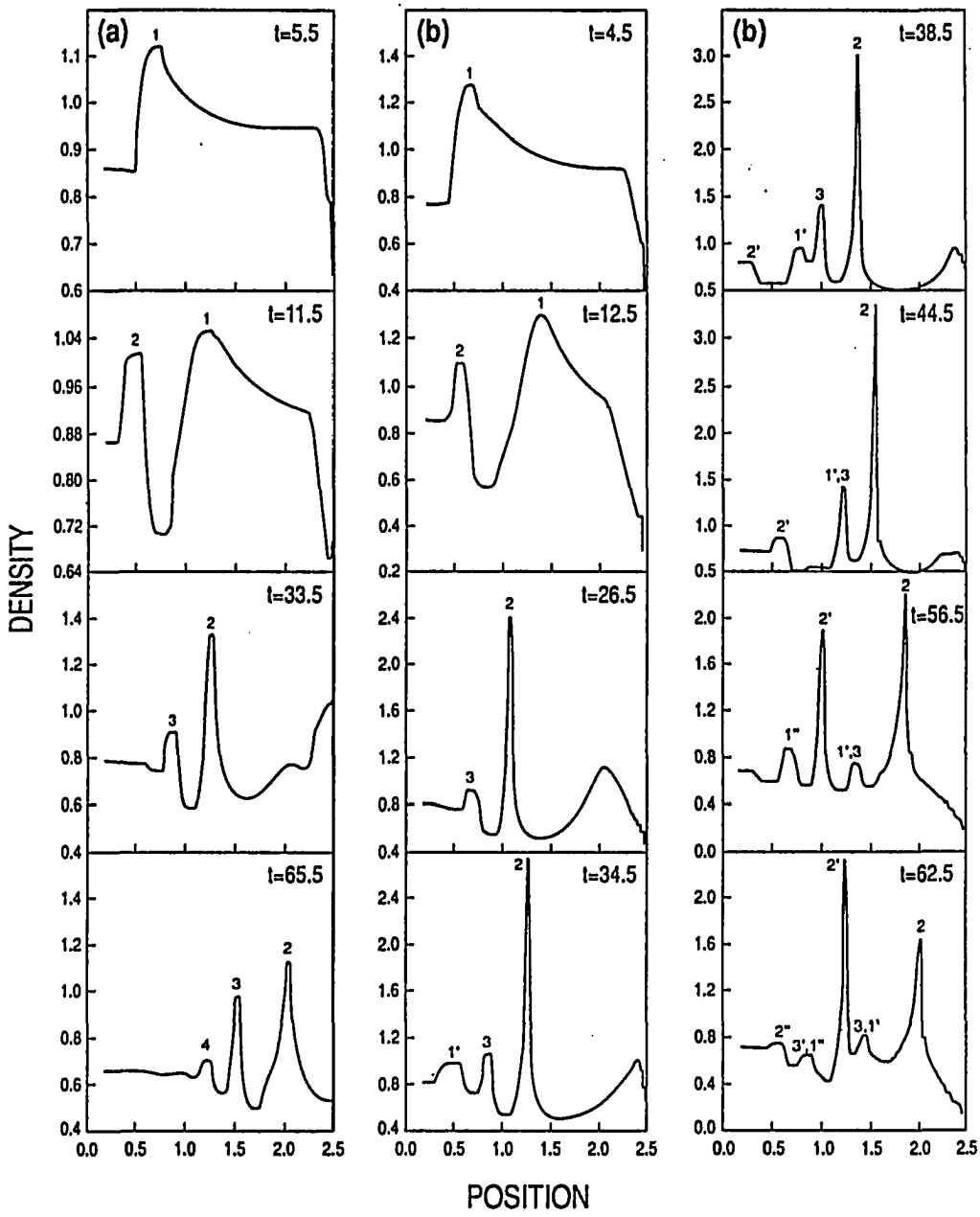
(a)
t=5.5
t=11.5
t=33.5
t=65.5
(b)
t=4.5
t=12.5
t=26.5
t=34.5
(b)
t=38.5
t=44.5
t=56.5
t=62.5
DENSITY
POSITION

parameters are the same as in Appleton and Struck-Marcell (1987b). The pre-collision mass density was chosen constant with radius throughout the target disk. In both cases the companion is situated at a distance of 32 length units above the disk when the calculation is started. In case (b) the companion comes to a halt at $t=15.5$ at a distance of 33 length units below the target disk. It then collides for the second time at $t=32$. The third collision occurs at $t=51$ after the companion receeded to a distance of 20 from the target. Later on the companion is slowed down significantly and is essentially merged.

Until the second collision in case (b) takes place, the shape, spacing, relative strength and evolution of the first couple of rings in cases with and without DF are basically alike. However since DF results in the deceleration of the companion and thus a slower collision, the interaction time is longer and consequently the rings are stronger. For the calculation presented in Figure 5 both the density and star formation indicator (see Appleton and Struck-Marcell (1987b) for a precise definition) are stronger in case (a) than in case (b) by 20-30%. Once the companion punches through the gas disk for the second time in case (b), differences with case (a) begin to emerge. In the single collision case the broad primary ring is followed by a sharper and stronger second ring and several more weak rings. Once these have propagated out of the disk, the ringing is essentially over. The main effect of multiple collisions is that each passage results in a new set of rings with interesting interplay between them. Figure 5 (case [b]) demonstrates how rings generated in successive passages may merge to create a single ring, or may gradually disappear. In particular, rings 3 and 1' converge (Fig. 5 [case (b) at $t=38.5$ and $t=44.5$) and later almost disappear. Also, as pointed out by Appleton and Struck-Marcell (1987b) the second ring is particularly

sharp and strong relative to the primary (first) ring. When DF leads to multiple collisions, typically the second ring of each passage dominates. This phenomenon is clearly seen at *t=56.5* and *t=62.5* in Figure 5 (case [b]). This implies that a ring galaxy with two rings could result from two distinct collisions with a captured companion, where each ring is the second dominant ring. The last few snapshots of case (b) show the development of the rings generated in the third collision.

In other calculations various parameters were varied including the companion to target mass ratio, the relative velocity at closest approach, the timing of the second collision, and various hydrodynamical parameters. Varying the parameters gives rise to different details in the interplay between successive sets of rings, but the main features seen in Figure 5 (case [b]) are common, namely merging of rings from successive passages, disappearance of rings, and dominance of second rings.

The differences in detail between single and multiple collision cases are interesting in their own right. However, the main conclusion is that for realistic collision parameters, rings will be propagating in the target gas disk well after DF has lead to the merger of target and intruder galaxies, as in the stellar disk.

C. Comparison of Response Between Stellar and Gas Disk

Pressure effects which exist in the gas component, but play no role in the stellar component, give rise to differences in their respective responses to single or multiple collisions. Despite the fact that epicyclic oscillations are the basic feature of the ringing phenomenon in both stellar and gas disks, only the stellar component can accommodate interpenetrating streams. The broadening effect found in the restricted three-body simulations in the multiple collision case, which involves even greater interpenetration of

streams than in single collisions is thus not possible in the gaseous component. On the other hand, in the hydrodynamic calculations the second ring (of each passage of the companion) is compressed as a result of the large infall velocities behind the primary ring. This feature is unique to the gas since in the stellar component the high velocity streams behind the primary ring will penetrate the material interior to it.

VI. COMPARISON WITH OBSERVATIONS

A. Frequency of Occurrence

The absence of companions for a non-negligible fraction of known ring galaxies is observationally well established. Some important examples are reviewed in Section I above. In this section, we argue that various characteristics of many ring galaxies are not inconsistent with the present merger scenario for ring galaxies with no apparent companion.

The merger idea is compatible with the observed relative velocities between ring galaxies and their companions. From observation, these velocities are typical of binary galaxies or small groups (Theys and Speigel 1976; Davies and Morton 1982 for the Cartwheel galaxy; Dennefeld, Lausten and Materne 1979 for the Vela ring galaxy; Jeske 1986, and others). In fact, the ring-companion systems VII Zw 466 and Arp 147 are probably gravitationally bound (Theys and Speigel 1976). Those systems which are marginally unbound or already bound are likely to become a merger.

The possibility that many ring galaxies and their companions make up a gravitationally bound pair has also been proposed in order to reconcile the observed frequency of ring galaxies in the field, with theoretical calculations of their expected occurence, assuming a disk-galaxy collision being the production mechanism. Chatterjee (1987) concludes that "the frequency of ... ring galaxies is $\approx$0.01% of spirals, compatible with the observational result, provided the frequency determination is conducted with respect to dense regions (in terms of population of galaxies)". However "stray hyperbolic encounters, taking place in sparse regions containing field galaxies, are too scarce by few orders of magnitude to explain the formation of ring galaxies

(in particular, and interacting galaxies in general). Hence, most of these interacting pairs must already have been bound doubles.... In fact, this supports the contention that in many cases a galaxy and its nearest neighbor will form a bound pair (see Tremaine, 1981)". Therefore, if a significant fraction of ring galaxies and their companions make up bound pairs, they are only likely to suffer multiple encounters and merger, and become ring galaxies with no apparent companions.

B. Bull's Eyes as Thick Rings

Our simulations show that rings in the test particle disk formed by multiple collisions, are generally broader, with more pronounced rarefaction between them, than single collisions rings. In fact, other mechanisms such as a heavy intruder ($\approx \geq 0.2$) (SML) or an off-center collision (Struck-Marcell 1990) contribute to ring broadening. In our simulations we find that broadening mechanisms can enhance the thickness of a ring by up to a factor of two roughly. A higher mass companion is also more likely to be captured (since the DF deceleration - eq.[1] - is proportional to the intruder mass). Schweizer *et al.* (1987) characterize Hoag-type galaxies as having "(1) central bodies that are neither obviously barred nor obviously inclined disks, and (2) detached outer rings that contain a significant fraction of the total luminosity". In their article they report that the ring thickness in Hoag's object is approximately one half of the disk radius. In our model E (Figure 3iv) the ring width is about 40% of the disk radius. (Note that despite the similar appearance, the inner structure in our simulation is a disk portion, and must not be confused with the core of Hoag's object which is a true spheroidal component.) Such a scenario for Hoag's object would imply that its bulge is the merger remnant of the companion and the original target nucleus. This could explain Schweizer *et al.*'s observation

that the ring and bulge share the same velocity and thus "form one single object". These authors point out that better data are needed to determine decisively whether the core of Hoag's object is a bulge or an elliptical, although their optical measurements "seem to favor a normal bulge in rotation". The possibility that Hoag's object is a merged ring galaxy would appear more likely though, if the core were shown to be an elliptical rather than a bulge.

Arp and Madore catalog (1987) includes several bull's-eye galaxies (see list in Section III [D] for model B) which are characterized by an inner thick bright ring and an outer faint ring. Such feature can be found in some of our three-body simulations, in particular model A(b) at $t=14.25$, and model E(b) at $t=8$.

C. Few-Madore Classes

Few and Madore (1986) find that a sample of 69 ring galaxies can easily be divided into two categories on the grounds of morphological differences. "P-type rings have crisp knotty structure and often a displaced nucleus, and O-type rings have a smooth structure and a centrally located nucleus". In addition they find that P-type rings have a statistically significant excess of companions, whereas O-type rings lack such an excess. In view of our simulation results we propose that many O-type rings are merger remnants of ring galaxies with their intruding companions, and thus do not have an excess of companions. In fact, O-type and P-type ring galaxies can be understood as part of a physically motivated classification presented in Table 3. In this classification, the displacement of the nucleus correlates with the off-centeredness of the collision. Smooth and knotty structures correlate with the abundance of gas in the target disk.

P-type rings would result from off-center collisions with a gas-rich late

TABLE 3

Proposed Generalization of the Few-Madore Classification

	Knotty structure	Smooth
Displaced nucleus:	P-type	"Q-type"
Central nucleus:	R-type	O-type

type disk galaxy. The small nucleus (or bulge) characteristic of late types will easily be displaced, whereas the abundance of gas results in significant star formation and thereby knotty ring structure. The companion would only travel through a small bulge or will miss the bulge altogether, would encounter little dynamical friction, and therefore is less likely to be captured. This would give rise to the excess of companions in P-type ring galaxies.

O-type rings would result from an almost central collision with an early type disk. The massive bulge would stay at the center. The paucity of gas in early-types would result in moderate star formation and thus smooth ring structure. These collisions are also more likely to lead to a capture since the companion travels through a substantial bulge thus being subject to sizable dynamical friction and tidal forces. As a result, O-type rings have little or no excess of companions.

R-type rings would be the outcome of a highly central collision with a late type disk. Similar to P-types, the abundance of gas would result in enhanced star formation and knotty structure. However, in order for the small light nucleus to remain central, the collision must be almost perfectly symmetric, making this type of ring galaxies rare.

The hypothetical Q-type rings would form in an off-center collision where the target is an early type disk galaxy. In order to displace the large bulge of such a galaxy, a very high mass companion is required. Such a strong perturbation is likely to create enormous chaos in the target disk, so that recognizable rings of this type are unlikely. This explains the nonexistence of examples of this class.

It would be very instructive to attempt determining the galaxy type of the progenitors of the Few-Madore sample of ring galaxies as was done by Jeske (1986) for his ring galaxy sample, as well as searching for possible

signs of merger in O-type rings. A statistical comparison between O-type and P-type rings regarding the ring thickness, as well as other morphological and kinematical features found in our simulations, would also clarify the origin of their differences.

D. Observational Tests

The following observational features should be searched for in comparing ring galaxies with and without companions. Infrared observations of the old stellar population should reveal broader rings on average in the class without companions (which possibly identifies with O-types) than in the class with companions (possibly P-types). However, as predicted by the simulations, multiple collisions and merger also result in ring thinning, so that narrow rings do not rule out merger. A combination of broad and narrow rings would be an even better indication of multiple collisions. In addition, broad rings are predicted to possess larger velocity dispersions than single collision rings due to the enhancement of epicyclic oscillation described in Section IV and Section III(C) above. In fact, overlapping of thin and broad rings, similar to that predicted by the kinematic model (Fig. 4c) in the merger case, may result in very unique spectral line forms.

Some ring galaxies may be in the process of merger, and may already possess some of the signatures of multiple collision rings, but still have a close companion with a radial velocity which implies that the two are possibly gravitationally bound. (For instance, VII Zw 466 and Arp 147 which according to Theys and Speigel (1976) are possibly bound.)

Ring galaxies without companions might be searched for traces of debris from a disrupted companion, in the form of low-surface brightness plumes consisting of stellar debris along the companion's path (above and below the disk).

In addition, it might be possible to determine observationally whether the nucleus in Hoag-type objects and other ring galaxies with a significant bulge, is a normal bulge component, or possibly a small elliptical which might be the "bullet" merged with the target.

VII. OTHER THEORIES FOR THE ABSENCE OF COMPANIONS IN SOME RING GALAXIES

For completeness, we should point out that other theories exist which might explain the lack of companions in some ring galaxies:

1) Some rings were formed in a fashion which does not involve a second galaxy. One possibility is that they are generic structures like bars and spiral arms (Buta 1990, and references therein). These galaxies are usually barred, and their rings are not as prominent as in collisional ring galaxies, and thus can be easily distinguished from them. Therefore, this is not a likely explanation for *prominent* ring galaxies with no apparent companions.

2) The ring formed due to an interaction with another galaxy, but the latter had enough time to travel a large distance and blend with the background. (Such a possibility was raised by Appleton and Struck-Marcell [1987b] in connection with the Cartwheel ring galaxy.) Since the companion travels roughly at the same speed as the density wave is propagating in a ring galaxy, this scenario would imply that the first ring has already propagated out of the disk, and the observed ring is in fact the second ring.

This possibility, however, offers no easy explanation for the differences between O-types and P-types of Few and Madore regarding the location of the nucleus relative to the ring. Moreover, if this were the correct explanation, we would expect that O-types which have no excess of companions would possess a knotty ring due to the enhancement of the second ring found in hydrodynamical calculations. In reality, it is the the P-types which possess knotty ring structures. In conclusion, this explanation is unlikely to solve the problem of the absence of a companion in most cases.

3) The ring formed due to the accretion of a small galaxy around a larger galaxy. This mechanism was proposed by Schweizer *et al.* (1987) as possibly responsible for the thick bright ring in Hoag's object, and by Schweizer, Whitmore and Rubin (1983) for polar rings around some S0 galaxies. As pointed out earlier, observationally determining the characteristics of the cores of such objects could help clarify their origin. Specifically, if the core is shown to be a normal bulge component accretion is the more likely mechanism, although our proposed tidal thick ring is not ruled out and a closer comparison of theory and observation is required. However, if the core is an elliptical galaxy then our proposed merger scenario may be preferred to the accretion hypothesis. In any event, O-type rings of Few and Madore, which resemble "normal" ring galaxies more than Hoag-type objects, probably cannot be explained by an accretion event.

4) The competing mechanism for ring galaxy formation proposed by Freeman and deVaucouleurs (1974) which involves a collision of a disk galaxy with an inter-galactic cloud also requires the remaining nucleus of the progenitor disk galaxy to be present in the form of a companion, and thus also does not account easily for the absence of companions in some rings. However, this possibility is not completely ruled out since disruption of the original core of the galaxy, or merger between the galaxy and the inter-galactic cloud are viable possibilities, until refuted. Yet, the low abundence of inter-galactic couds mentioned in Section I, makes it nearly impossible for this scenario to account for all ring galaxies with no apparent companions (roughly 50% of all ring galaxies according to Few and Madore).

VIII. CONCLUSIONS

In this work, we found that for realistic collision parameters DF (and tidal interactions) can lead to the merger of a ring galaxy with its companion. In such a case ring structure can persist for as long as 10^8-10^9 years after merger. Interesting differences in the details of the morphology between single- and multiple-collision rings are found in our numerical simulations for both the gas and stellar disk components. Yet, the main conclusion is that merger (or disruption of the companion) may account for collisional ring galaxies without an apparent companion. Although effects of DF and merger on ring galaxies have hardly been studied in the past, other works regarding mergers between mainly spherical galaxies (see Section I) imply that interpenetrating close encounters, such as the kind that produce ring galaxies, are very likely to lead to merger. We propose that such merged ring galaxies can account for many of the O-type ring galaxies of Few and Madore (1986), for which no statistically significant excess of companions is observed. Other characteristics of O-type and P-type rings (which do possess above average number of companions) can also be understood within our proposed picture (Section VI[C]). We further propose that some Hoag-type galaxies characterized by an unusually broad ring could possibly owe this property to the broadening effect, found in our restricted three-body simulations, that multiple central collisions have on rings in a disk galaxy. We also found that a simple kinematical model for ring formation adjusted for the multiple-collision case, is able to reproduce some of the main feature found in our restricted three-body simulations for multiple collisions, specifically broadening and thinning of rings.

As discussed in Section VII, we conclude that various mechanisms proposed in the past, can possibly account for a portion, but not all ring galaxies with no apparent companions. From our numerical simulations, and their comparison to observations, the present merger scenario appears capable of explaining a good fraction of the class of rings with no companions.

The disk self-gravity, in our simulations, is included in the form of a fattened disk potential (defined in Section III) which provides a realistic *effective field* acting on the disk's individual particles. However, effects of distortions in the disk, such as ring structure, disk thickening, and warping, as well as star-star interactions, are not included in our treatment. Thus, simulations with a fully self-consistent N-body code with realistic values of velocity dispersions of the various stellar populations would be desirable.

Observational research aimed at revealing the differences between ring galaxies with and without companions, in particular studies of ring thickness and traces of merger could shed light on the validity of the merging process in ring galaxies. Such studies could confirm the possibility that ring galaxies with no apparent companions, like other ring galaxies, have their origin in a collision between a disk galaxy and another arbitrary galaxy.

IX. APPENDIX A

In this Appendix we derive an expression for the force acting between two spherically symmetric rigid clouds as a function of the distance between their centers. By the term "rigid" we mean that the mass distribution of each cloud is fixed for all times even if they collide and interpenetrate at some stage of their motion. The force when the two clouds are at a distance r from one another can be written as

$$F = -grad\, U(r)\,, \tag{A1}$$

where $U(r)$ is the gravitational interaction energy,

$$U(r) = G\int d^3r_1 \int d^3r_2\, \rho_1(r_1)\rho_2(|r_2-r|)/|r_1-r_2| \;. \tag{A2}$$

A more convenient expression for U is obtained by noting that the integral is of the convolution form. One may thus rewrite equation (A2) as

$$Ur) = (2/\pi)\, G(1/r) \int_0^\infty dq\, \sigma_1(q)\sigma_2(q) sin(qr)/q \;, \tag{A3}$$

where $\sigma(q)$ denotes the Fourier transform of the mass density,

$$\sigma(q) \;=\; \int d^3r\, \rho(r)\, exp(iq.r) \tag{A4}$$

$$=\; (4\pi/q) \int_0^\infty dr\, r\, \rho(r)\, sin(qr) \;. \tag{A4'}$$

In the following we assume that the clouds are each described by a "Hubble-like" density distribution function (eq. [2]) where separate choices of M and b apply for each of the clouds. The advantage of this particular choice is that one obtains the following simple result

$$\sigma(q) = M e^{-qa} . \qquad \text{(A5)}$$

The evaluation of equation (A3) is then readily performed using identity (3.941) of Gradshteyn and Ryzhik (1965)

$$\int_0^\infty dq\, q^{-1} \sin(\mu q)\, e^{-\nu q} = \tan^{-1}(\mu/\nu) . \qquad \text{(A6)}$$

The final result is

$$U(r) = U(0)\,[(b_1 + b_2)/r]\tan^{-1}[r/(b_1 + b_2)] , \qquad \text{(A7)}$$

where

$$U(0) = (2/\pi)GM_1 M_2/(b_1 + b_2) . \qquad \text{(A8)}$$

Using equation (A1), the magnitude of the force exerted by one cloud on the other is

$$F(r) = [U(0)/r][(1/x)\tan^{-1}(x) - 1/(1+x^2)] , \qquad \text{(A9)}$$

where $x = r/(b_1 + b_2)$. Note that the characteristic length of the force expression is given by $b_1 + b_2$. If $x << 1$ this expression reduces to

$$F(r) \sim (2/3)[U(0)/(b_1 + b_2)]\, x. \qquad \text{(A10)}$$

Thus, as expected, for small separation distances the inter-cloud force decreases linearly to zero. In the opposite limit $(x >> 1)$, also as expected, equation A(10) reduces to the force between two point masses,

$$F(r) \sim GM_1M_2/r^2 \ . \qquad \text{(A11)}$$

X. APPENDIX B

In this Appendix, we briefly describe our method for evaluating the infinite integrals in equation (5), which provide the components of the gravitational field due to the mass distribution of equation (4). A detailed description of the method and a discussion of the accuracy achieved is given in Lotan and Luban (1990).

As stated in the text, these integrals converge very slowly for $|Z|/R < 0.005$ because of the slow decay of the Bessel functions for large values of the argument. We will here consider the integral for E_z given in equation (5a). We define the line segment S_n, (n = 2, 3, ...), as the interval, (u_{n-1}, u_n), between two successive zeros of $J_0(u)$, as well as the segment S_1 defined as the interval $(0, u_1)$. Note that the integrand in equation (5) has a single sign within any given segment S_n. The integral in equation (5), denoted by I, can be written as the infinite sum

$$I = \Sigma_n A_n \ , \qquad \text{(B1)}$$

where A_n, $(n = 1, 2, ...)$, denotes the contribution of the segment S_n. Highly accurate values of A_n can be obtained by Gaussian numerical integration. Successive values of A_n alternate in sign, and for sufficiently large n decrease monotonically in magnitude. However, the decrease is extremely slow, which rules out actually performing the sum in equation (B1). A highly accurate estimate for the infinite sum is provided by applying the Levin-T series acceleration method (Levin 1973) to the first N subintegrals A_n, where $N \approx 15$. Denoting by $I[N]$ the Levin-T estimate of

the infinite series I of equation (B1) as obtained by employing the first N terms of the series, one has $I[N] = P[N]/Q[N]$, where

$$P[N] = \Sigma_{k=1}^{N} (-1)^k k^{N-1} (I_k/A_k)/[k!(N-k)!] , \quad \text{(B2)}$$

$$Q[N] = \Sigma_{k=1}^{N} (-1)^k k^{N-1} (1/A_k)/[k!(N-k)!] , \quad \text{(B2')}$$

and $I_k = A_1 + A_2 + ... + A_k$. The estimates $I[14]$ and $I[15]$ typically agreed with each other to an accuracy of a few parts in 10^5, and the common digits can be taken to provide an estimate for the infinite series I. In the regime $|Z|/R >> 0.005$ the terms A_n decrease in magnitude sufficiently rapidly that straightforward summation of the first dozen or so terms of equation (B1) suffices to obtain accurate values of the integral.

XI. REFERENCES

Appleton, P. N., and Struck-Marcell, C. 1987a, *Ap. J.*, **312**, 566.

Appleton, P. N., and Struck-Marcell, C. 1987b, *Ap. J.*, **318**, 103.

Arp, H. C., and Madore, B. F. 1987, *A Catalog of Southern Peculiar Galaxies and Associations* (Cambridge: University Press).

Athanassoula, E. and Bosma, A. 1985, *Ann. Rev. Astron. Astrophys.* **23**, 147.

Bahcall, J. N., and Soneira, R. M. 1980, *Ap. J. Suppl.*, **44**, 73.

Burbidge, E. M., and Burbidge, G. R. 1959, *Ap. J.*, **130**, 12 and 23.

Buta, R. 1990, *Ap. J.*, **351**, 62.

Byrd G. G., Saarinen S. and Valtonen M. J. 1986, *M.N.R.A.S.*, **220**, 619.

Casertano S., Phinney E. S. and Villumsen J. V. 1987, in *Structure and Dynamics of Elliptical Galaxies*, ed. T. de Zeeuw (Boston: Reidel), p. 475.

Chandrasekhar, S. 1943, *Ap. J.* , **97**, 255.

Chatterjee, T. K. 1986, *Astrophys. Space Science*, **121**, 213.

Chatterjee, T. K. 1987, *Astrophys. Space Science*, **132**, 177.

Davies, R. L. and Morton, D.C. 1982, *M.N.R.A.S.*, **201**, 69.

Dennefeld, M., Lausten, S. and Materne, J. 1979, *Astron. Astrophys.*, **74**, 123.

Dostal, V. A. and Metlov, V.G. 1978, IAU Symposium **79**, *The Large Scale Structure of the Universe*, ed. M. S. Longair and J. Einasto, (Dordrecht: Reidel), 117.

Dostal, V. A. and Metlov, V. G. 1979, *Astronom. Zh.*, **56**, 3.

Few, J. M. and Madore, B. F. 1986, *M.N.R.A.S.*, **222**, 673.

Freeman, K. C. 1970, *Ap. J.*, **160**, 811.

Freeman, K. C. and de Vaucouleurs, G. 1974, *Ap. J.*, **194**, 569.

Gilmore, G. and Reid, N. 1983, *M.N.R.A.S.*, **202**, 1025.

Gradshteyn, I. S., and Ryzhik, I. M. 1965, *Tables of Integrals, Series, and Products* (New York: Academic).

Jeske, N. A. 1986, Ph.D. Thesis, University of California, Berkeley.

Kashlinsky, A. 1987, *Ap. J.*, **312**, 497.

Kent, S. M. 1984, *Ap. J. Suppl.*, **59**, 115.

Levin, D. 1973, *Int. J. Computer Math.*, **3**, 371.

Lo, K. Y. and Sargent, W. L. W. 1979, *Ap. J.*, **227**, 756.

Lotan, P. and Luban, M. 1990, in preparation.

Lynds, R., and Toomre, A. 1976, *Ap. J.*, **209**, 382.

Mihalas, D., and Binney, J. 1981, *Galactic Astronomy* (San Francisco: W. H. Freeman and Company)

Miller, R. H., and Smith, B. F. 1980, *Ap. J.*, **235**, 421.

Pritchet, C. 1983, *Ap. J.*, **88**, 1476.

Sastry, K. S. 1972, *Astrophys. Space Science*, **16**, 284.

Sastry, K. S., and Alladin, S. M. 1977, *Astrophys Space Science*, **46**, 285.

Scalo, J. M. and Struck-Marcell, C. J. 1984, *Ap. J.*, **276**, 60.

Schweizer, F., Ford, W. K. Jr., Jedrzejewski, R., and Giovanelli, R. 1987, *Ap.J.*, **320**, 454.

Schweizer, F., Whitmore, B. C., Rubin V.C. 1983, *A.J.*, **88**, 909.

Sersic, J. L. 1970 *Peridic Orbits, Stability, and Resonances*, ed. G.E.O. Giacaglia, D. (Dordrecht: Reidel), p. 134.

Struck-Marcell, C. 1990, *A. J.*, **99**, 71.

Struck-Marcell, C., and Appleton, P.N. 1987, *Ap. J.*, **323**, 480.

Struck-Marcell, C., and Lotan, P. 1990, *Ap. J.*, **358**, in press.

Struck-Marcell, C., and Scalo, J. M. 1984, *Ap. J.*, **277**, 132.

Struck-Marcell, C., and Scalo, J. M. 1987, *Ap. J. Suppl.*, **64**, 39.

Theys, J. C. and Speigel, E. A. 1976, *Ap. J.*, **208**, 650.

Thompson, L. A. 1977, *Ap. J.*, **211**, 684.

Toomre, A. 1978, *The Large Scale Structure of the Universe*, ed. M. S. Longair and J. Einasto (Dordrecht: Reidel), p. 109.

Tremaine, S. D. 1976, *Ap. J.*, **203**, 72.

Tremaine, S. D. 1981, *The Structure and Evolution of Normal Galaxies*, ed. S. M. Fall and D. Lynden-Bell (Cambridge: University of Cambridge) p. 67.

van der Kruit , P. C. and Searle, L. 1981a, *Astr. Ap.*, **95**, 105.

van der Kruit , P. C. and Searle, L. 1981b, *Astr. Ap.*, **95**, 116.

van der Kruit , P. C. and Searle, L. 1982, *Astr. Ap.*, **110**, 61.

Vorontsov-Velyaminov, B. A. 1960, *Soviet. Astron.* AJ, **4**, 365.

Wainscoat, R. J., Freeman, K. C., and Hyland, A. R. 1989, *Ap. J.*, **337**, 163.

Wevers, B. M. H. R. 1984, Ph. D., thesis, University of Groningen.

Wevers, B. M. H. R, van der Kruit, P. C., and Allen, R. J. 1986, *Astr. Ap. Suppl.*, **66**, 505.

White, S. D. M. 1978, *M.N.R.A.S.*, **184**, 185.

LONG-LIVED LEADING ONE-ARM SPIRAL PRODUCED IN A HEAD-ON OFF-CENTER GALAXY COLLISION

ABSTRACT

A new mechanism is presented for the production of a long-lived leading one-arm spiral based on a *nearly head-on, moderately off-center* collision. This type of collision can explain the leading one-arm known to exist in the inner parts of the Andromeda galaxy M31. Various observed features of both M31, and its dwarf satellite galaxy M32, strongly support this hypothesis. These include: (1) the radial velocity field of M31 (Byrd 1976, 1977) indicates to a high probability, that M32 intercepted the disk of M31. (2) M32 is a high surface brightness dwarf elliptical, which according to several indicators appears to be the tightly bound core of a normal elliptical galaxy, which has experienced significant tidal stripping following an interaction with a heavier companion (Faber 1973). (3) M31 possesses a flat rotation curve (Roberts and Whitehurst 1975) which indicates the existence of a massive halo. Such a massive spherical component is required for leading one-arm formation according to our simulations. In the past only *retrograde co-planar* marginally penetrating galaxy encounters have been considered for the production via collision of a leading one-arm spiral (Thomasson *et al.* 1989, Athanassoula 1978a). Furthermore, we find that for otherwise similar parameters, a nearly head-on collision usually results in a stronger more robust arm than does a retrograde co-planar encounter. Our proposed type of collision is closely related to the head-on collision known to produce ring galaxies (Theys and Speigel 1976, Lynds and Toomre 1976), and differs from it only in the degree of the off-centeredness of the collision. Nearly perpendicular collisions with impact parameter smaller than approximately 10% of the disk radius (Toomre 1977) will generally

form a ring galaxy. In our simulations we find that for impact parameters in the range 5-75% of the disk radius a single leading spiral arm will be generated. This also implies that leading one-arm spirals are expected to be several times more common than ring galaxies, if only nearly head-on collision are considered for the production mechanism. This ratio is rather compatible with observations, since ring galaxies and leading one-arm spirals comprise roughly 1% and 5% of interacting galaxies, respectively. In fact, for a sub-domain in parameter space, the collision initially produces a ring galaxy, which subsequently evolves into a disk with an outer ring and an inner leading one-arm, and finally into a grand design long-lived leading one-arm spiral, in which the arm very slowly expands. Our results are based on restricted three-body simulations.

I. INTRODUCTION

Searches for the mechanisms responsible for spiral structure in galaxy disks stretch over several decades (review articles include Toomre 1977, Lin and Lau 1979, Bertin 1980). The problem of grand design spiral pattern received special attention on both the theoretical front (Toomre 1977, Athanassoula 1984, and others) and the observational (Kormendy and Norman 1979, Elmegreen and Elmegreen 1982, 1983, 1987). Several mechanisms for sustaining spiral structure for many rotation times have been considered. The relevant one in the context of this paper is forcing from a companion galaxy. Observationally, grand design has indeed been found to often correlate with the existence of a bar or a companion galaxy. In particular, leading spiral arms have been attributed to an interaction with another galaxy. Athanassoula (1978a) showed analytically that external forcing, specifically from a companion in a co-planar retrograde orbit gives rise to a one-armed spiral morphology. Thomasson *et al.* (1989) studied co-planar retrograde collisions both theoretically and with N-body simulations, and found that a long-lived leading one-arm spiral will develop and persist provided the perturbation from the companion is large enough and the disk is surrounded by a halo of mass comparable to the disk mass or greater.

Several galaxies have been shown to contain a leading spiral arm. Both M31 (Kalnajss 1975, Athanassoula 1978b, Considère and Athanassoula 1982) and NGC4622 (see Shu 1982 and Sersic and Agüero 1972 for photographs) have a leading arm in their inner disks, and a trailing two-armed pattern in their outer disks. Generally, the frequency of leading spiral arms is low. For example, of a list of interacting galaxies (Pasha 1985) with a reliable

knowledge of their sense of rotation, only some 5% have leading spiral arms. Several explanations for this low frequency have been proposed by Thomasson *et al.* assuming a retrograde co-planar encounter is the production mechanism. These include: (1) Only a small region in parameter space can bring about this structure. (2) Lack of retrograde satellites. (3) Few spiral galaxies have massive enough halos.

In this paper, we propose a different mechanism for the production of a long-lived one-arm spiral which is based on a *nearly head-on off-center* passage of a small arbitrary galaxy through a target disk. Our investigation was carried out with the use of a restricted three-body code. We find that the formation of the leading one-arm will occur within the following reasonably large domain of parameter space. In addition to a disk component, the existence of a spherical potential in the target galaxy which comprises at least 50% of the total target galaxy mass is necessary; the collision impact parameter has to be approximately in the range 5-75% of the disk radius; companion to target mass ratio must be in the range 1/40 - 1/5; the relative velocity of the encounter must not exceed approximately 3 times the escape velocity of the companion from the target galaxy; the inclination angle, defined as the angle between the plane of the companion's orbit and the disk plane, should be in the range 50-160^{o} (but for certain impact parameters as high as 180^{o}). In addition, we find that a co-planar retrograde encounter will result in a leading one-arm spiral, provided that the impact parameter is in the range 0.8-1.5 the original disk radius. The range of leading one-arm formation, as far as the other parameters are concerned is rather similar to that of the head-on collision.

Our proposed mechanism is very likely responsible for the leading one-arm spiral residing in the inner parts of the Andromeda galaxy M31. From theoretical fits to the velocity field of M31, Byrd (1976) concluded that the

small companion M32 apparently crossed M31's disk at a maximum distance from the disk center of 16.4 kpc, and later approached the center to a minimum distance of 5.26 kpc. Faber (1973) concludes, on the basis of the amount of tidal stripping caused to M32, that the distance of closest approach must have been roughly 2.3 kpc.

Our results are based on restricted three-body simulations in which the target galaxy consists of both spherical and disk components, whose relative masses can be controlled. The companion galaxy is simulated as a single bulge-like component. The present restricted three-body code, rather than a full N-body code, has the obvious advantage of computational time economy, and thus the possibility of exploring a larger region of the huge parameter space described above. On the other hand, effects of star-star interactions following the collision are not included in our treatment. However, Thomasson *et al.* (1989), by "turning off" the star-star interactions in their full N-body code, demonstrate that self-gravity is unimportant in the theory of leading one-arm spirals, whereas in trailing arms it plays a crucial role. This finding provides a measure of confidence that restricted three-body methods are capable of reliably dealing with leading spiral arms. Yet, follow-up calculations with self-consistent N-body codes, for the parameter range considered in this work are desirable, and are part of our planned future research.

Interestingly, other types of interacting galaxies have also been shown to be produced by more than one mechanism. Ring galaxies are known to be formed in a nearly head-on central collision (Theys and Speigel 1976; Lynds and Toomre 1976). Yet, in a study of shell galaxies, Hernquist and Quinn (1988) find that a co-planar fly-by encounter gives rise to a ring structure in the test particle disk (Fig. 8 of their paper). Two-arm spiral structure can also be produced by both co-planar and head-on off-center collisions.

Obviously, various galactic structures can be produced by more than one mechanism.

In order to gain deeper understanding of the phenomenon of leading one-arm spirals, we employed a simple kinematic model (Struck-Marcell 1990) which is an elaboration of the Toomre kinematic model (1978) for ring galaxy formation. While indeed we were able to produce a leading one-arm for a certain range of parameters, the structure was rather short-lived, which appears to be a generic property of the kinematic model.

The remainder of this paper is divided as follows. A description of the numerical method and a thorough study of the parameter space, are given in Section II. In Section III we discuss the orbits of individual particles in the one-arm spiral disk, following the collision. Simulations of leading one-arm formation with the use of a simple two-dimensional kinematic model is described in Section IV. Implications to observations are discussed in Section V, and conclusions are summarized in Section VII.

II. NUMERICAL SIMULATIONS

A. The Model

Our numerical method is based on a restricted three-body code in three spatial dimensions. The target galaxy is composed of two components, a spherical component and a flattened disk. The companion galaxy is simulated as a single spherical component. The potentials of all components are taken as time independent during an entire simulation. A complete description of the numerical method employed in this project, including an explanation of the choice of units, is given in Section III of the third chapter "Effects of Satellite...". However, for this project the galactic halo is not represented by equations (6) and (7) in that section. Instead, the "Hubble-like" potential (eq. [2] in that section) is invoked here to represent either an entire galaxy, or a galactic halo component.

B. Parameter Study

Due to the large number of parameters involved, obviously we could not cover the entire parameter space, in a finite number of simulations. Also the choice of some parameters affects the range in which other parameters still produce a leading one-arm. Yet, we have executed some seventy runs, so that our estimate for the domain within which a leading arm forms is quite well defined. In the following we discuss the effects of varying each of the relevant parameters. The typical development of a test particle disk following a head-on off-center collision is shown in Figure 1. The parameters of this run (referred to as "run #1" throughout this chapter) are as follows. The target galaxy is composed solely of a "Hubble-like" spherical

Fig. 1 - Pole-on view of a disk consisting of 10^4 test particles taken from a simulation referred to as run #1 (section III[B]). The corresponding time is printed in each frame.

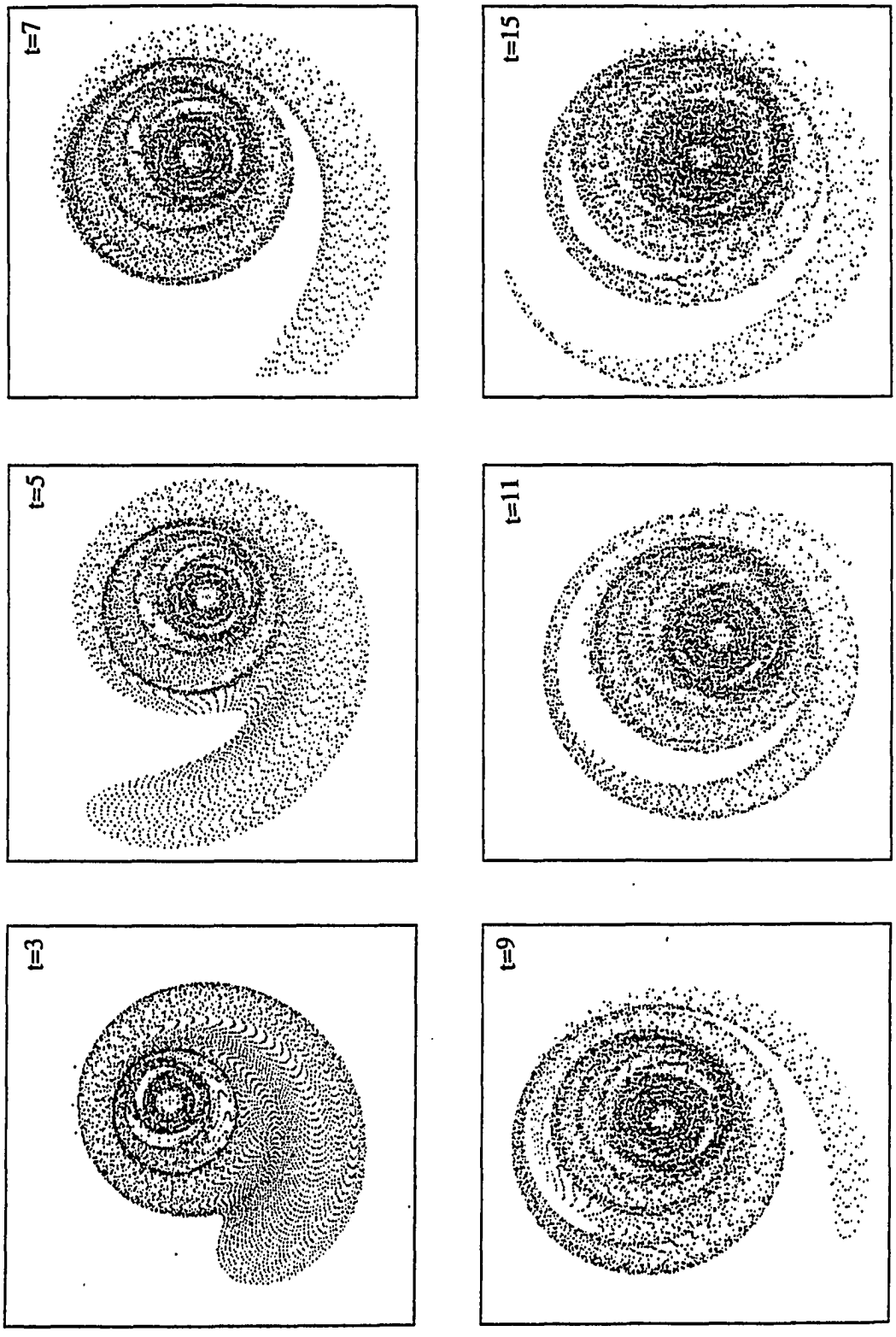
t=7
t=15
t=5
t=11
t=3
t=9

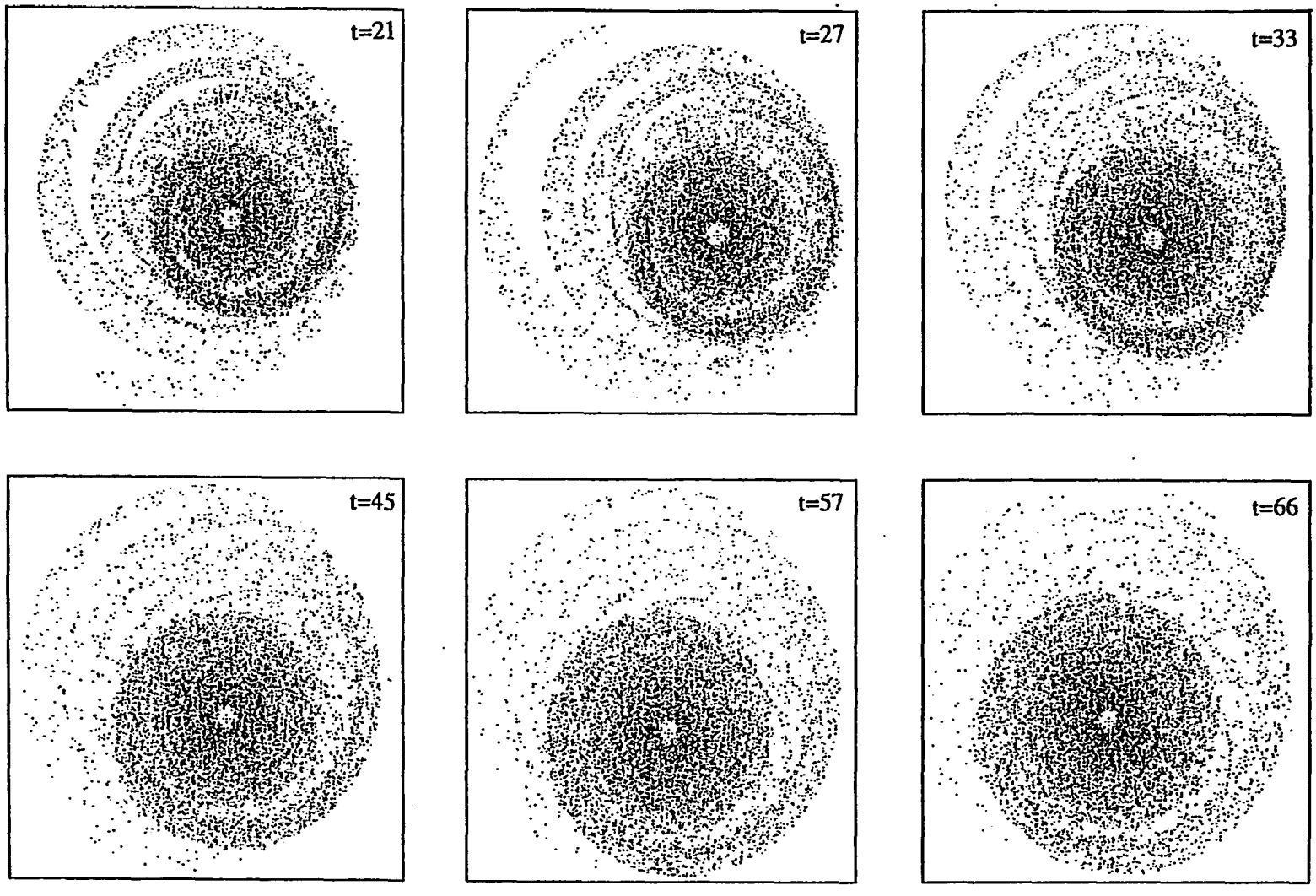

Fig.1 (continued)

component of one unit mass, which has a scale length of 0.08 units. No disk component is present in the target galaxy in this run. The companion to target mass ratio is 1/10, and the scale length of the "Hubble-like" component is 0.01. The impact parameter, relative velocity and inclination angle at closest approach are 0.16, 1.0, and 90^{o} (namely a parabolic normal collision), respectively. Until *t=6* the development of the test particle disk resembles that of a ring galaxy, although the existence of a faint tail implies that a significant asymmetry was involved in the collision. Between *t=7* and *t=9*, the disk undergoes transformation from a ring galaxy, into a leading one-arm spiral. Starting at *t=10*, an obvious leading arm structure dominates the inner disk, and the outer tail is quite tightly wound. From that time until around *t=60* (which for a reasonable choice of the dimensionless parameters, refers to a time of approximately $5x10^{9}$ years after the collision), the arm thickens and gradually expands to the outer parts of the test disk. In this simulation, as well as all other simulations described in this chapter, closest approach occurs at the instant the companion crosses the target disk plane.

1. Impact Parameter

The impact parameter was found to be one of the crucial parameters that determine whether a leading one-arm will form or not. In our simulations we find that a leading spiral arm will form if the passage of the companion through the target disk occurs roughly in the range 5-75% of the disk radius. This is a rather wide range, in particular relative to the mere inner 10% of the target disk radius required for ring galaxy formation. As indicated above, this would also imply that leading one-arm spirals are expected to be several times as frequent as ring galaxies, if only nearly head-on collisions

are considered to be the primary production mechanism. This ratio is evidently compatible with observations. Ring galaxies comprise roughly 1% of interacting galaxies, whereas leading one-arm spirals make up approximately 5% (Pasha 1985). A refinement of our estimate for the relative frequency of ring galaxies and leading one-arm spirals, should also consider other types of formation mechanisms for these types of galaxies. Yet, the rough agreement between theory and observations provides some support to the collisional scenario for both ring galaxies and leading one-arm spirals. By contrast, retrograde co-planar encounters lead to the formation of leading one-arm spirals for impact parameters in the range 0.8-1.5 the disk pre-collision radius.

Figure 2 shows selected snapshots of several simulations, each differing from run #1 in the impact parameter of the collision. The corresponding impact parameters (denoted by R_m) are written in each frame. Note that in the case $R_m=0.02$ there is barely a hint of an arm. For $R_m=0.05$ the arm is well-defined, dominates the appearance of the entire target disk, and is very long-lived. In fact, the arm is still apparent at the last time step of this simulation at $t=70$, which corresponds to approximately $5\text{x}10^9$ years. As the impact parameter is further increased to 0.62, the arm becomes somewhat narrower than the in previous case. However, for $R_m=0.75$, or larger impact parameters, the post-collision test disk appears totally structureless.

2. Inclination

For favorable impact parameters we find that the range of inclination angle i (defined as the angle between the companion orbital plane and the target disk plane) required for leading one-arm spiral production is approximately in the range 50^o-160^o (but for certain impact parameters as high as 180^o). An inclination angle in the range $0 \leq i \leq 90^o$ corresponds to a

Fig. 2 - Snapshots of several test particle disks, taken from simulations which differ from run #1 in the choice of the impact parameter (R_m). The value of the impact parameter is printed in each frame. The dimensionless time in all snapshots is $t=30$.

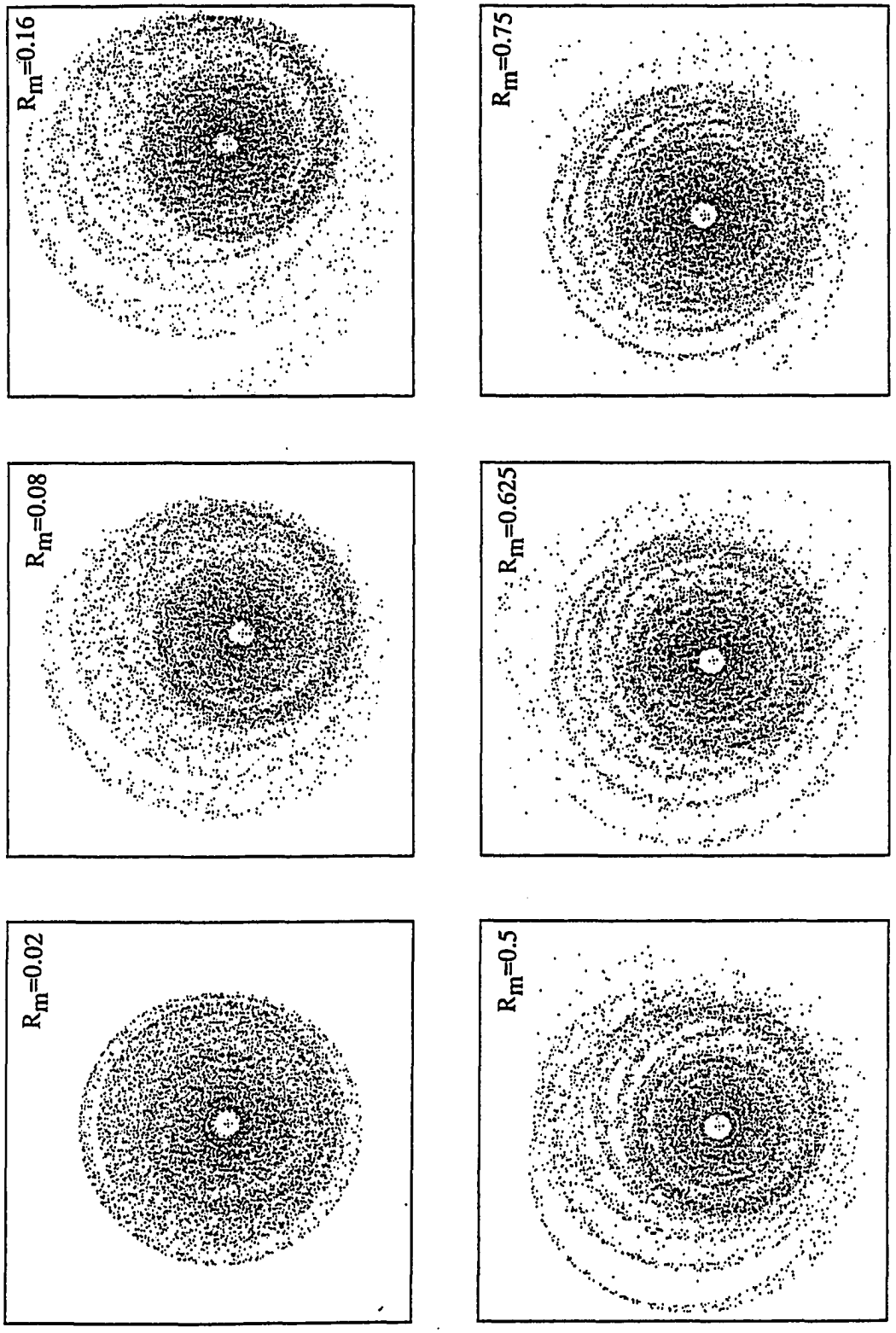
R_m=0.16
R_m=0.75
R_m=0.08
R_m=0.625
R_m=0.02
R_m=0.5

direct collision, whereas $90 \leq i \leq 180^o$ refers to a retrograde encounter. Thus, our simulations indicate that even for penetrating, nearly head-on collisions, a retrograde encounter is favorable as far as leading one-arm formation is concerned. In Figure 3 we show several snapshots taken from different runs similar to run #1 (given in Section II[B]), except for the value of the inclination angle, which is printed in each frame. For the impact parameter used in this simulation (R_m=0.16) any retrograde encounter results in the formation of a thick well-defined leading one-arm. The snapshots for the cases $i=120^o$, $i=150^o$, and $i=180^o$ (a strictly co-planar retrograde collision), demonstrate this behavior. For direct encounters the range of arm production is smaller. For $i=60^o$, a broad well-defined arm is formed. However, as the inclination angle is decreased to 30^o or a smaller inclination angle, the leading arm becomes increasingly fainter to the point of nonexistence. In fact, for a strictly direct encounter ($i=0^o$) faint interconnected rings form in the test disk instead of an arm.

3. Companion Mass

The companion mass required for the one-arm formation was found to be in the range 1/40 to 1/5 of the target mass. As the mass becomes smaller, the perturbation is simply too weak to excite the epicyclic oscillatory motion required for arm production. On the other hand, as the companion mass is increased, the epicyclic motion amplitude of the test particles grows, and the structure becomes thicker and almost structureless. This phenomenon is shared by ring galaxies as found by Struck-Marcell and Lotan (1990) using a simple kinematic model for ring formation, as well as in restricted three-body simulations of ring galaxies. In fact, if our proposed mechanism is responsible for the single leading spiral arm in M31, and assuming the

Fig. 3 - Snapshots of several test particle disks, taken from simulations which differ from run #1, in the choice of the inclination angle (i). The value of the inclination angle, is printed in each frame. The dimensionless time in all pictures is $t=18$.

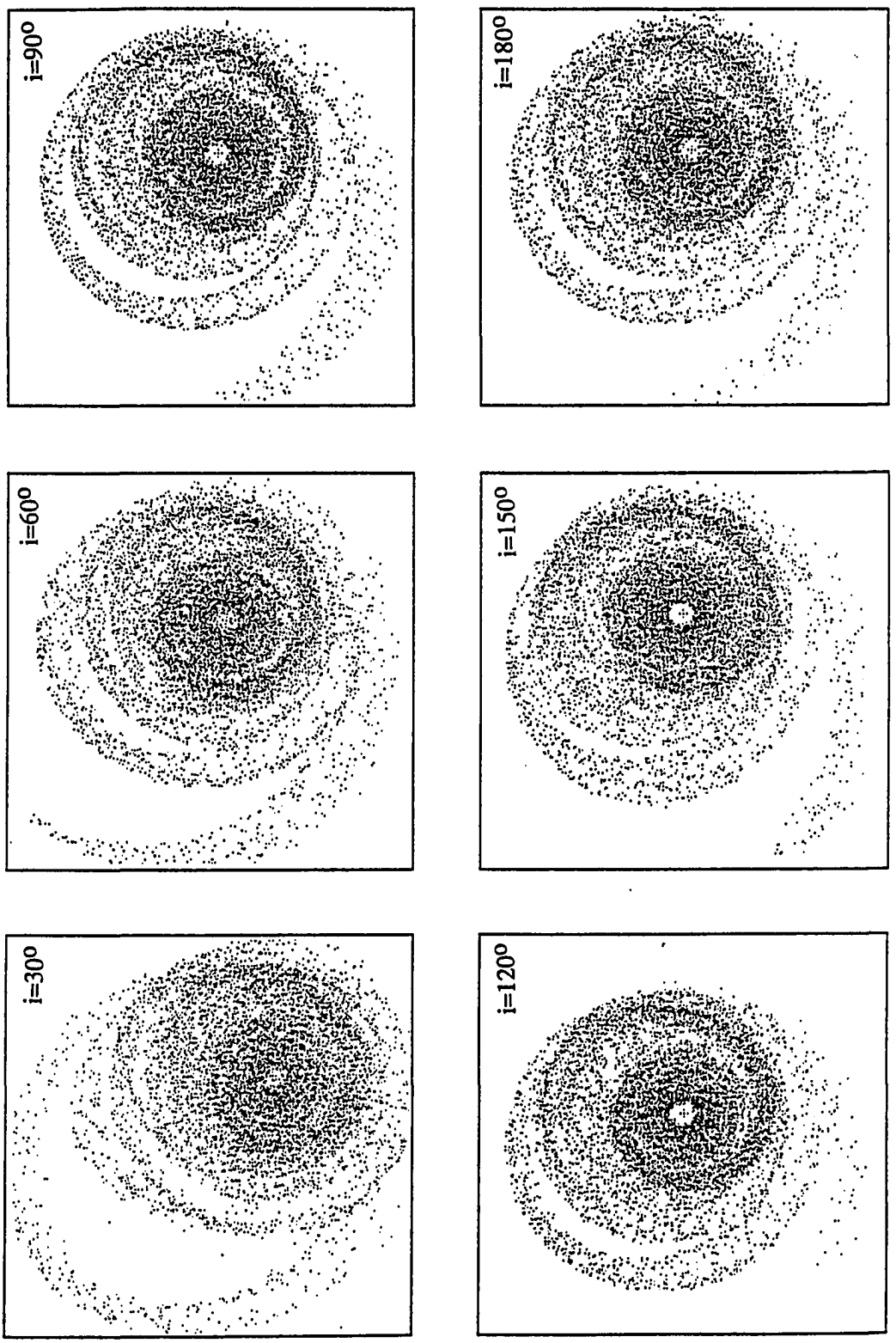
i=90°
i=180°
i=60°
i=150°
i=30°
i=120°

interloper is the small satellite galaxy M32, then the latter pre-collision mass must have exceeded 1/40 of M31's mass. However, the mass of M32 is estimated to be 1/60 the mass of M31 (Rubin and Ford 1970, Fish 1964). This discrepancy can be reconciled if M32 suffered considerable tidal stripping in the course of the encounter. Such an argument has been made by Faber (1973) and King (1962) on the basis of M32's high surface brightness, as well as the correlation between the line strength and continuum color, and its absolute magnitude.

The snapshots in Figure 4 are taken from various runs that share the parameters of run #1, except for the values of the companion mass, which are indicated in each frame. A collision with a half-mass companion does not give rise to an arm structure. As the companion mass is decreased to 1/5 the target mass, a leading one-arm forms, but it is wide and without sharp edges. In the other limit, the collision with a companion of 1/30 the target mass, an extremely faint spiral arm develops. For a mass ratio of 1/50, the post-collision test disk is essentially structureless.

4. Target Galaxy Potential

In our simulations we find that the formation of a leading one-arm requires the presence of a spherical component in the target galaxy. Furthermore, the sharpest arms are produced in cases where the target is made predominantly of a spherical mass distribution. As the amount of disk component contributing to the potential is increased, the structure becomes increasingly more dull, diffuse, and not as long-lasting. Figure 5 is taken from a simulation similar to run #1, except that a disk component of mass comparable to the spherical component mass is added to the target galaxy. The radial scale length c (see eq. [4] of Chapter III " Effects of Satellite..."

Fig. 4 - Snapshots of several test particle disks, taken from simulations which differ from run #1, in the choice of the companion to target mass ratio. The value of the corresponding ratio is printed in each frame. The dimensionless time in all pictures is $t=18$.

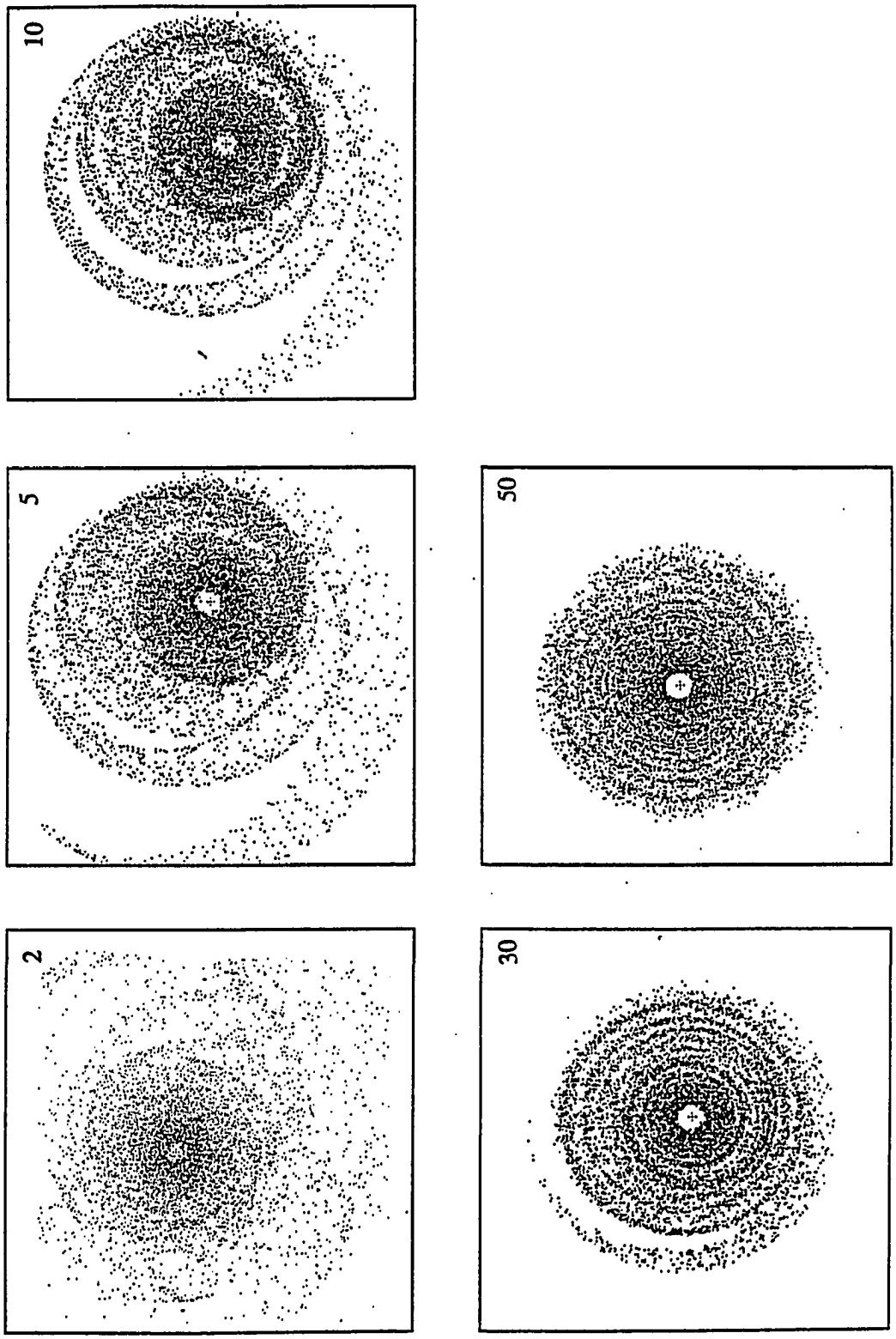
10
5
50
2
30

above) was chosen to be 0.25, which is compatible with realistic values of galactic disk components. At $t=6$ of this simulation a leading arm can already be discerned in the test disk. Subsequently, the arm thickens and expands. (See snapshots at $t=12$, and $t=15$.) From $t=20$, the structure quickly dissolves, due to mixing of the test particles. At $t=30$, the test disk is completely smoothed out.

This result is similar to the result reported by Thomasson *et al.* (1989) for co-planar non-penetrating encounters. It implies that in order for a leading one-arm to form, the pre-collision disk galaxy must possess a spherical component, most likely in the form of a dark halo, of mass equal or greater than the disk mass. A case for the existence of massive dark halos has been made from theoretical reasoning of disk stability against bar-modes by Ostriker and Peebles (1973), and observationally, from rotation curves of many spirals, including M31 in particular (Roberts and Whitehurst 1975). Observations of rotation curves of leading one-arm spirals, could indicate whether this class of galaxies indeed possesses massive dark halos. Another possibility is that the leading arm forms in the inner part of the disk where the contribution of the spherical bulge component is significant. In fact, several disk galaxies, including M31, possess single leading arms in their inner parts. (The outer parts of M31 are arranged in two trailing arms.) Observational investigation of the possible existence of a bulge component, in the region where the arm is located, could test the latter hypothesis.

Fig. 5 - The time evolution of a test particle disk, composed of a spherical "Hubble-like" component of 1 unit mass, and a scale length of 0.08 units, and a disk component of comparable mass, and a scale length of 0.25 length units. The companion mass is one-tenth the target mass, and its "Hubble-like" potential scale length is 0.02. The collision impact parameter and inclination angle are 0.16 and 90^{o}, respectively. The corresponding time is printed in each frame.

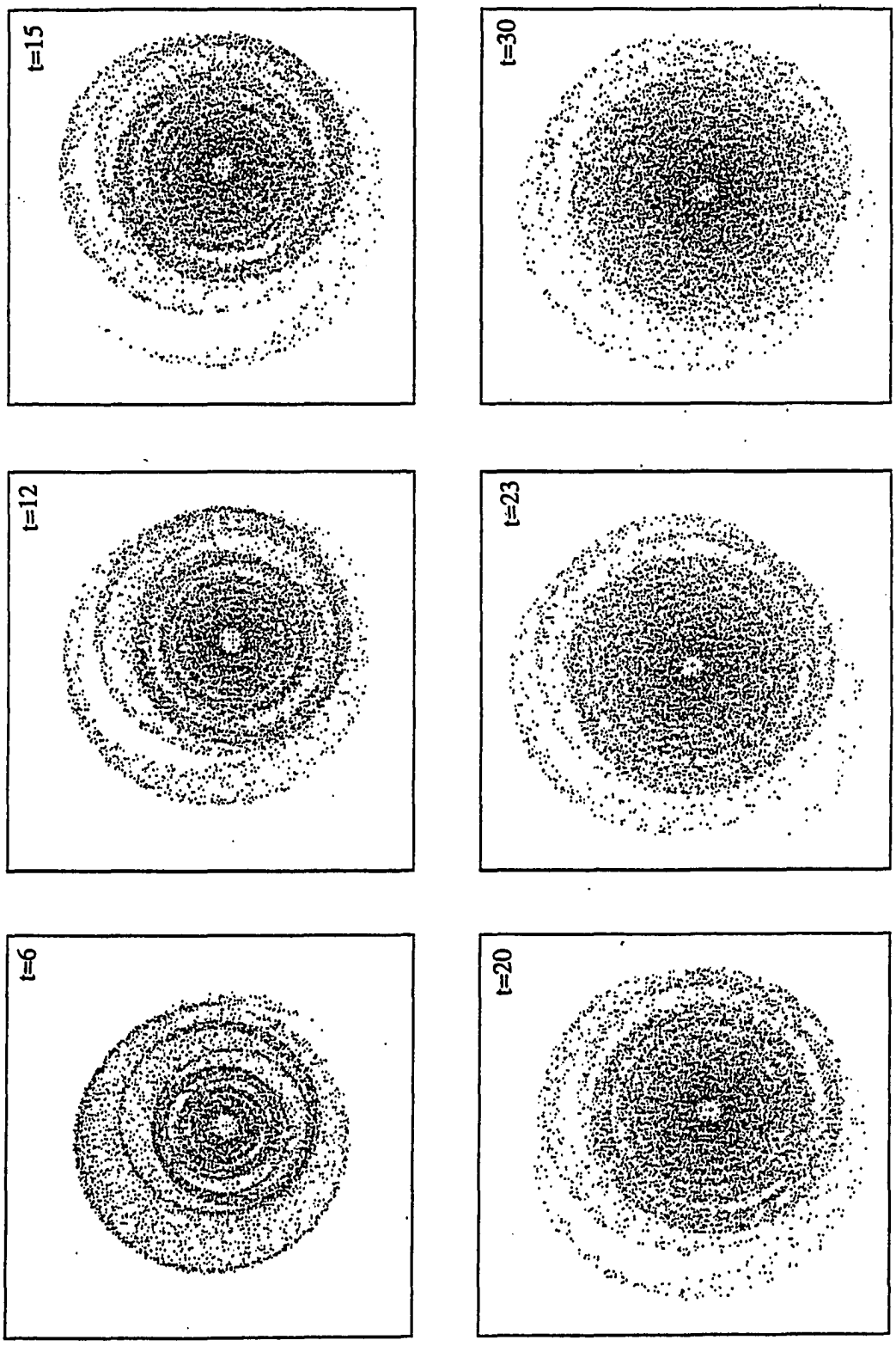
t=15
t=30
t=12
t=23
t=6
t=20

5. Relative Velocity at Closest Approach

In our simulations, we find that formation of a leading arm requires that the relative velocity at closest approach be less than 3 times the escape velocity of the companion. In addition, the relative velocity is found to affect the shape of the arm. Specifically, as v/v_{escape} increases from 1 to 2 the arm becomes narrower and sharper. This result can be understood as follows. As the relative velocity increases the interaction time decreases and the test particles respond more coherently to the disturbance. As a result the phase difference between the particles' epicyclic motions is smaller and the resulting structures are more well-defined. However, as the relative velocity keeps increasing from 2 to 3 times the escape velocity, the duration of the interaction is short enough that the particles have little time to respond to the companion's passage altogether, and the resulting structure becomes weaker. The snapshots in Figure 6, are taken from simulations similar to run #1, except for the values of the relative velocities at closest approach, which are indicated in each frame. For the $v/v_{escape} = 2$ case shown in this figure, a thick, well-defined, long-lived leading arm forms. However, as the relative velocity is increased to 3 times the escape velocity, an arm can hardly be discerned in the test disk. As the velocity is further increased to 5 times the escape velocity, no structure forms whatsoever. In fact, increasing the relative velocity of the colliders, has the same effect as decreasing the companion's mass, at least in the impulse approximation. This phenomenon is demonstrated mathematically by equation (2) in Section II of the second chapter "The Varieties of Symmetric...", which describes the abrupt change in a star's velocity following an impulsive disturbance. The same general behavior is evidently true in the restricted three-body simulations for the formation of a leading one-arm presented in this section.

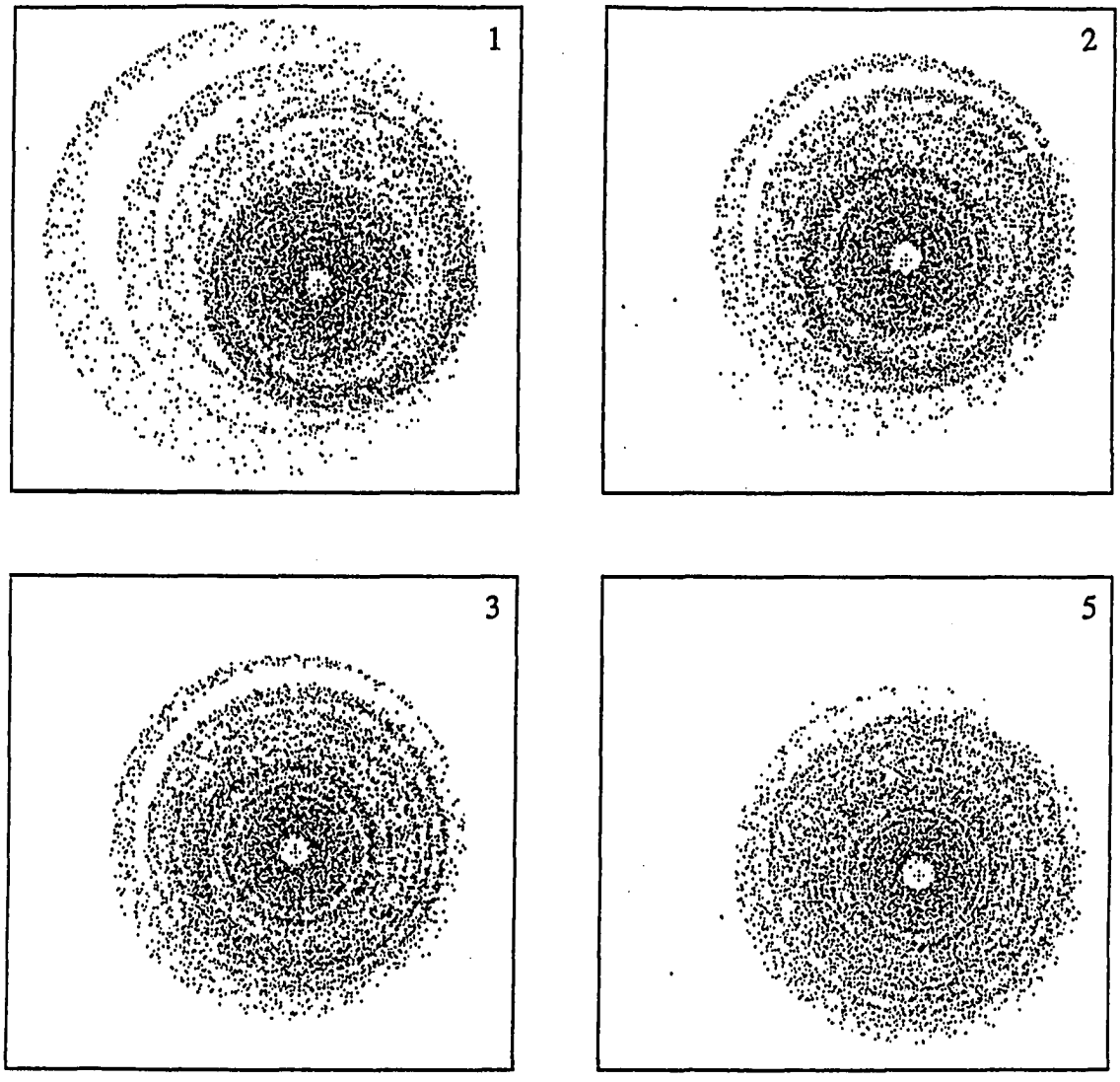

Fig. 6 - Snapshots of four test particle disks, taken from simulations which differ from run #1, in the choice of the ratio of relative velocity to escape velocity at closest approach. The value of the corresponding ratio, is printed in each frame. The dimensionless time in all four pictures is $t=24$.

6. Head-On Collision Versus Co-Planar Encounter

Several simulations of retrograde and direct co-planar encounters which we have conducted gave results very similar to those achieved by Thomasson *et al.* (1989). A comparison between our co-planar and head-on simulations yield the following results. Head-on collisions result in a leading one-arm structure for impact parameters approximately in the range 5-75% of the initial disk radius. This range may shift slightly if other parameters are varied. By contrast, co-planar encounters generally produce leading arms for impact parameters in the range 0.8-1.5 the pre-collision disk radius, namely in encounters which are mostly nonpenetrating. In addition, we find that *generally* head-on collisions with a small impact parameter, give rise to more substantial, thicker arms than do nonpenetrating co-planar encounters. In Figure 7, we show several snapshots, all taken from co-planar retrograde encounters, which differ in the value of the impact parameter, which is written in each frame. Otherwise, the structural and collisional parameters are identical to those of run #1. For impact parameters less than 0.75 the target disk radius, no structure forms due to the collision. In the range 0.8-1.4, a thin fairly faint leading one-arm develops following the collision. As the impact radius is increased beyond 1.5, arm production does not take place. The morphology of the arms produced in co-planar retrograde collisions in our restricted three-body simulations, closely resembles the structures achieved by Thomasson *et al.* who use a Miller type N-body code. This resemblance provides additional support for the validity of restricted three-body codes when applied to the problem of one-arm formation.

In comparing the arm morphology resulting from a retrograde co-planar encounter (Fig. 7) to that produced in a head-on off-center collision (Fig. 1), we find that the latter are thicker, stronger, and appear to contain

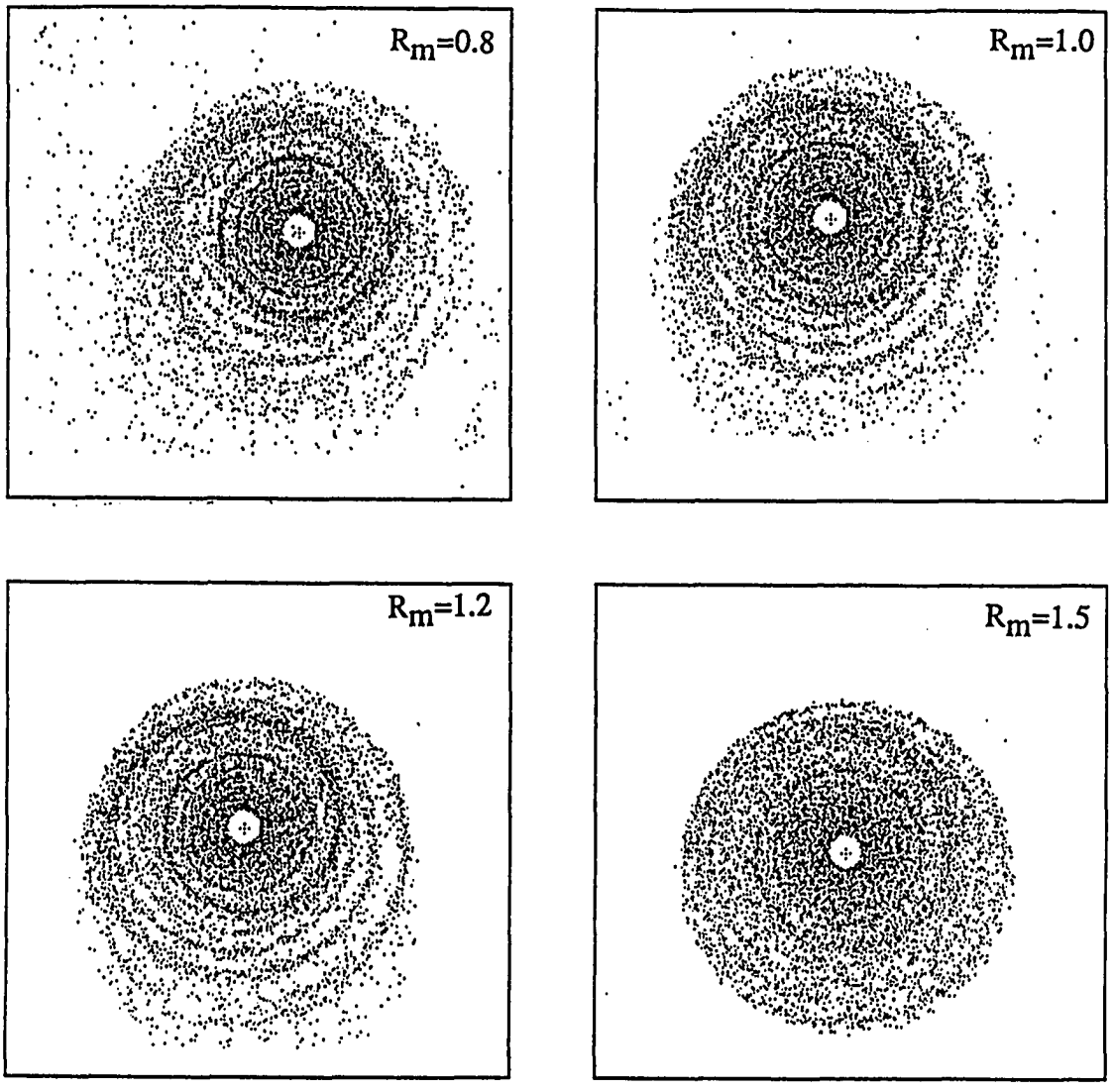

Fig. 7 - Snapshots taken from several similar simulations of retrograde co-planar encounters differing in the value of the impact parameter only. The corresponding value is indicated in each frame. The dimensionless time in all pictures is t=24.

more matter, than do the co-planar arms. This distinction could possibly provide a clue to the formation mechanism in observed one-arm spirals.

III. INDIVIDUAL PARTICLE TRAJECTORIES

Insight into the nature of the leading one-arm formation can be achieved by examination of the orbits of individual test particles. Following such trajectories in both head-on and co-planar collisions, we found the following behavior. In both types, much like in the ring galaxy case, the collision excites radial epicyclic oscillations of the test particles within the disk plane. A plot of the radial epicyclic displacement defined by $\Delta r(t) = r(t) - r_{initial}$, of a test particle in run #1, following a head-on collision is shown in Figure 8. The pre-collision radius of the particle is $r=1$. Little radial motion takes place prior to the collision (defined at $t=0$). Following the collision, the particle is engaged in a sinusoidal motion, with a frequency and amplitude which remain constant at all times. The equivalent plot for the retrograde co-planar collision is seen in Figure 9. This figure has the same main features as Figure 8, except that immediately following the collision, the particle is pulled outward, by contrast to the head-on collision in which the particle was initially pulled inward. This difference is a simple consequence of the fact that, in the co-planar case the companion's distance from the disk axis of rotation is greater than the radial distance of the particle. In the head-on case, the companion is at all times interior to the initial radius of the particle. In Figure 10, we show the projection of the test particle's trajectory onto the disk plane (the X-Y plane). This motion appears to follow a precessing ellipse which does not close on itself, at least for the period of time plotted in the figure. In Figure 11, the equivalent co-planar collision is plotted. This type of motion was also found by Thomasson *et al.* (1989) for the retrograde co-planar case. One obvious difference exists between the motion of a test

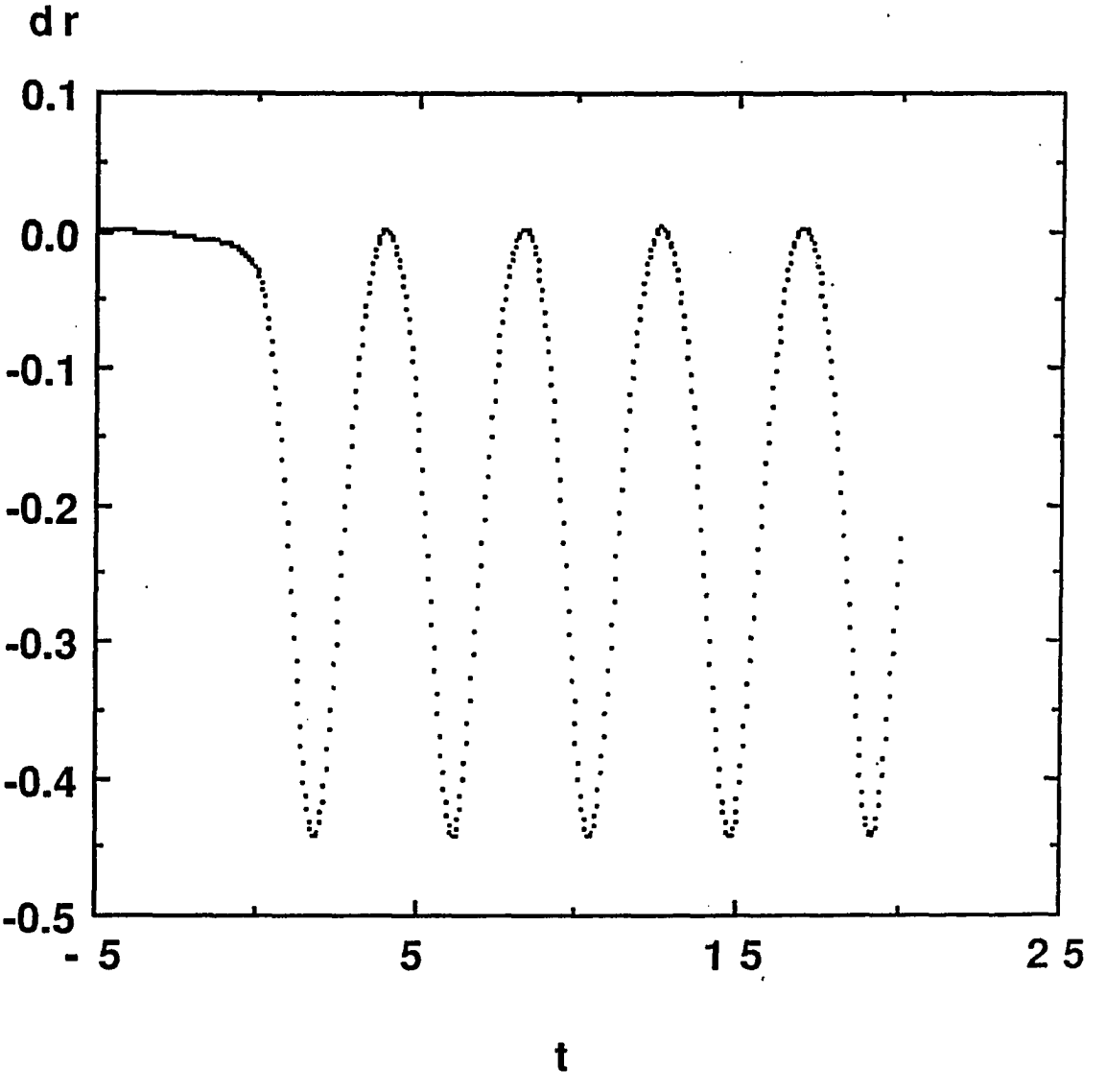

Fig. 8 - A plot of the radial epicyclic displacement defined by $\Delta r(t) = r(t) - r_{initial}$, of a test particle in run #1, following a head-on collision. The pre-collision radius of the particle was $r=1$.

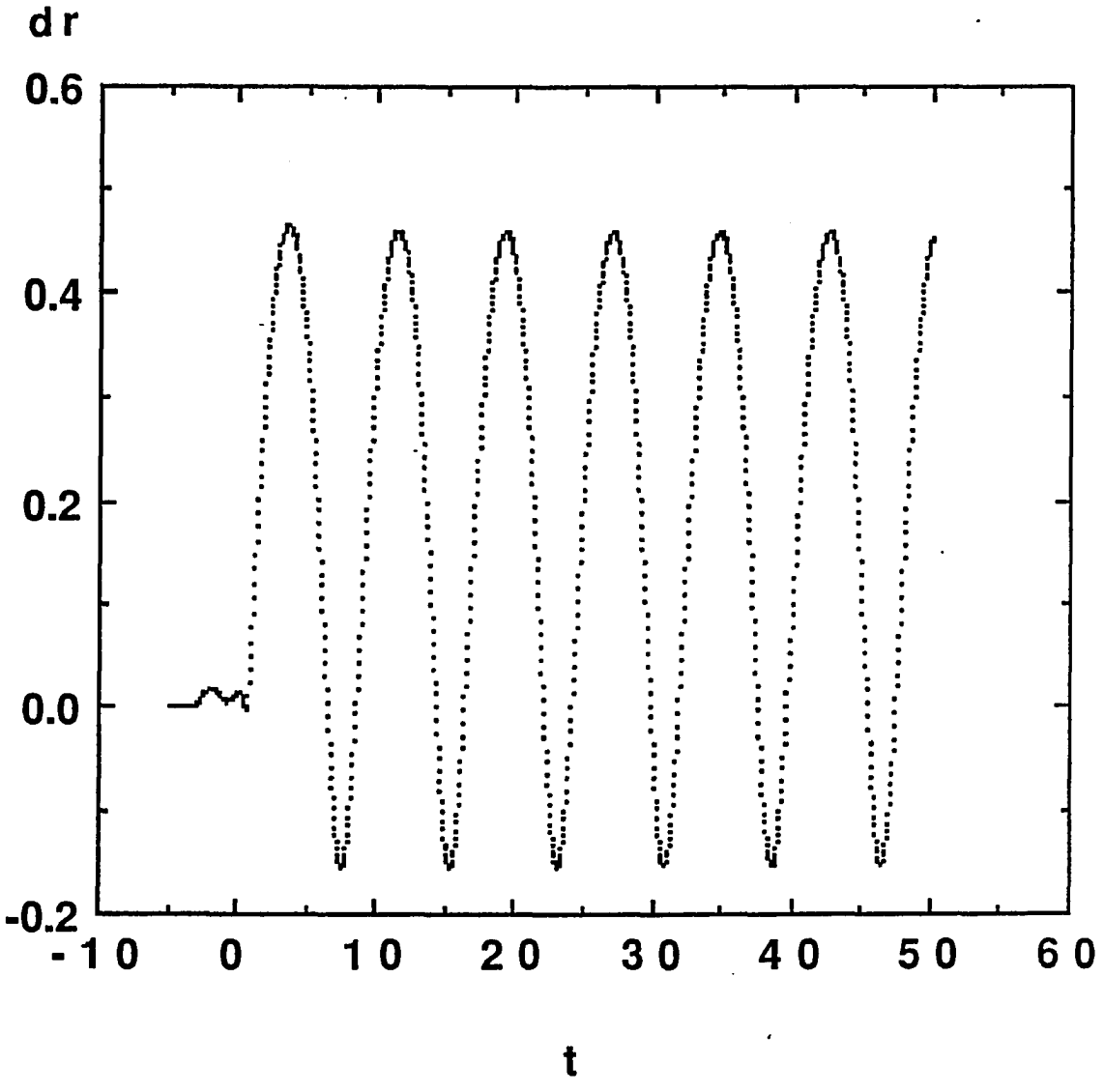

Fig. 9 - Same as Fig. 8, except for a retrograde co-planar encounter.

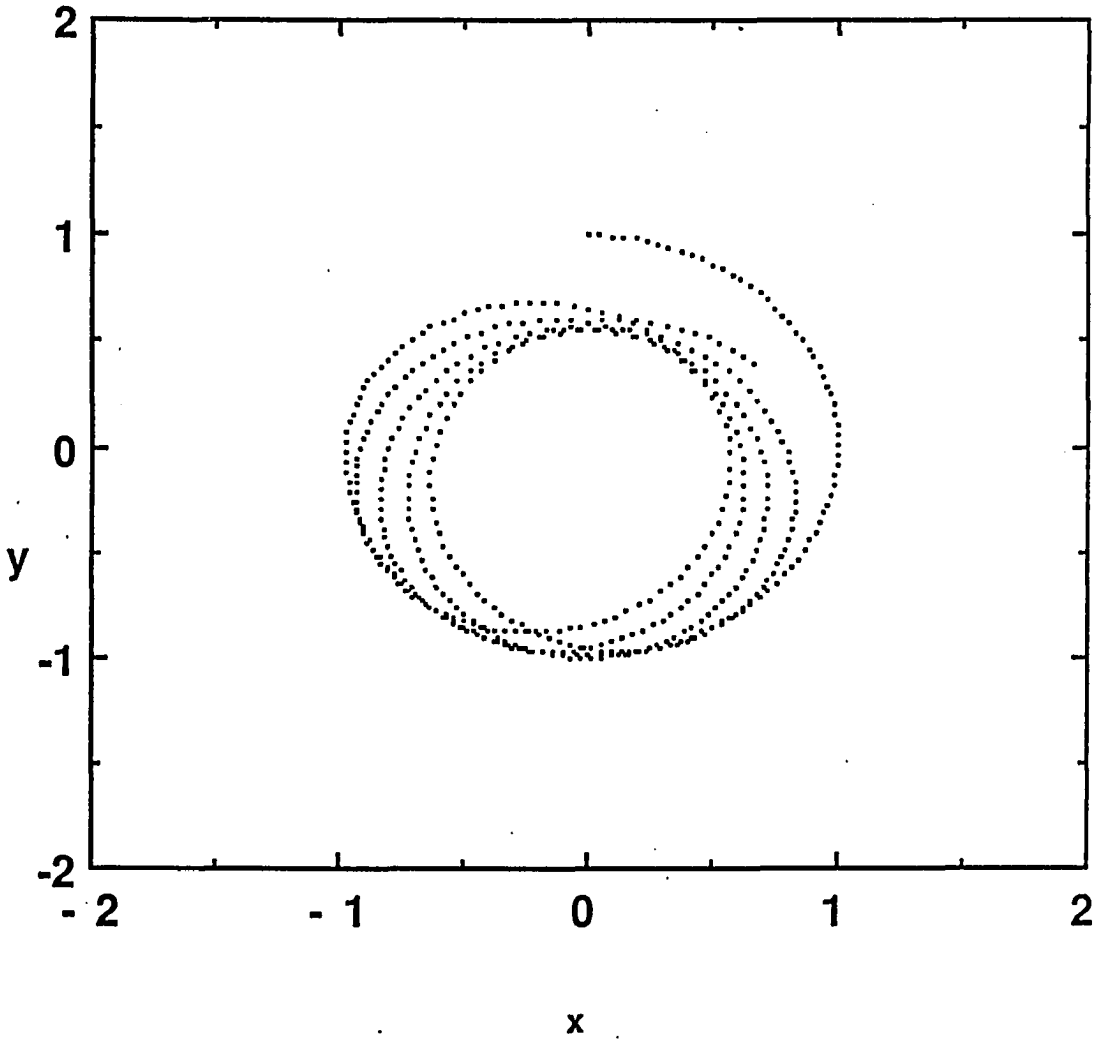

Fig. 10 - The projection of a test particle's trajectory onto the disk plane (the X-Y plane), for dimensionless time in the range $-5 < t < 20$, taken from run #1. The pre-collision radius of the particle was $r=1$.

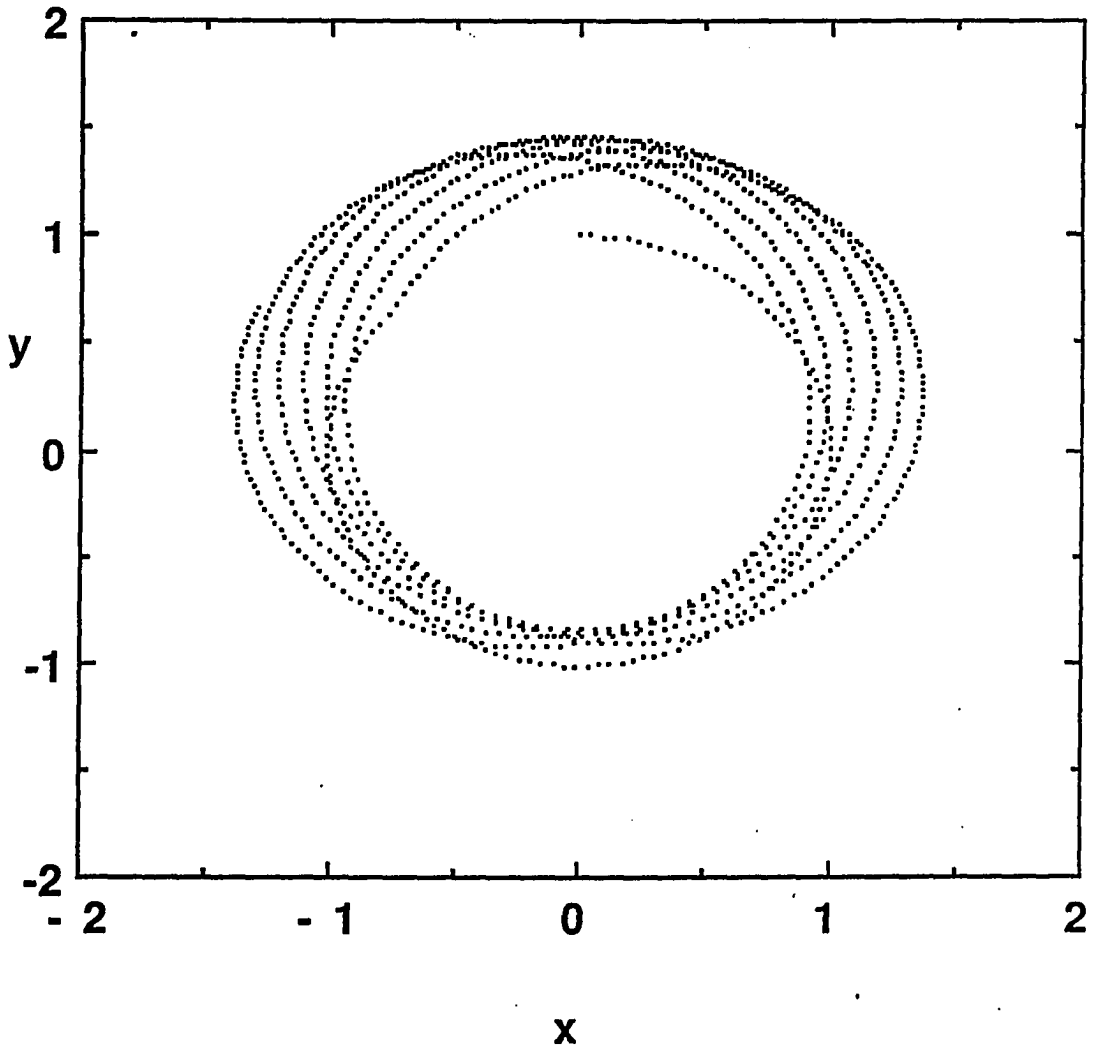

Fig. 11. - Same as Fig. 10, for a time range $-5 < t < 50$, except for a retrograde co-planar encounter.

particle following a head-on or a co-planar encounter. Specifically, following a strictly co-planar encounter the particle's motion in the z-direction (the z axis is defined as the disk axis of rotation) obviously remains unaffected, whereas a normal collision results in a perturbation of the particle's z motion. We find that the particle will execute sinusoidal oscillations in the z-direction, superimposed on its radial oscillatory motion. As a result, the envelope of the sinusoidal z-motion is itself sinusoidal, with a period determined by the radial motion. This behavior is clearly illustrated in Figure 12 which is a plot of z versus t of a test particle, initially located on the disk plane at a radial distance of 0.4.

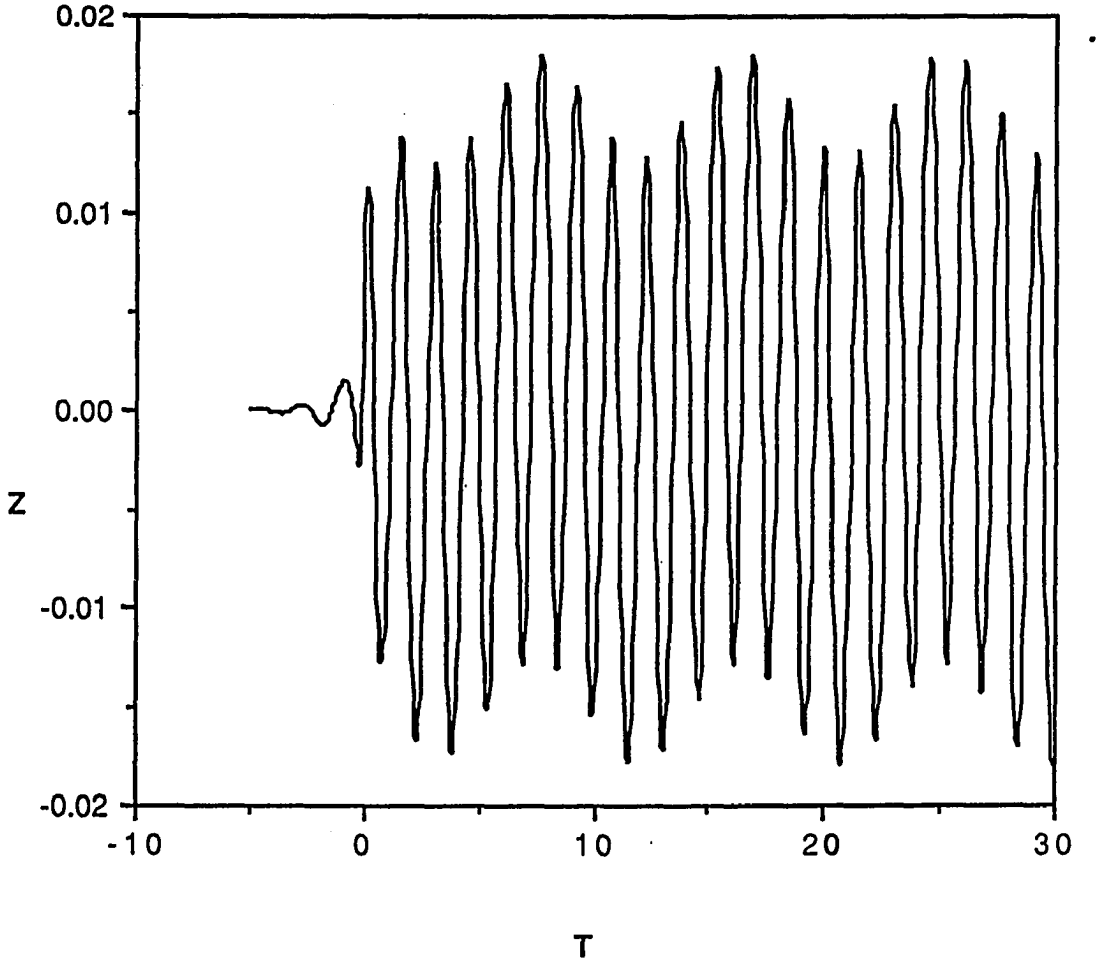

Fig. 12 - A plot of z versus t for a test particle, taken from run #1. The test particle had a pre-collision radial distance of 0.4 length units.

IV. LEADING ONE-ARM SPIRALS: KINEMATIC MODEL

In order to gain better insight into the nature of the leading one-arm spiral, we employed the kinematic model described in the second and third chapters of the thesis. As indicated there, this model is an elaboration of a simple kinematic model developed by Toomre (Lynds and Toomre 1976, Toomre 1978). For the present purpose, we used an extension of this model to two dimensions developed by Struck-Marcell (1990). The present version of this model uses a softened-point potential for the target galaxy (described by eq. [1], for p=1, in Section II of the second chapter "The Varieties of Symmetric..."). Indeed, for a certain range of collision parameters, a leading one-arm was reproduced by the kinematic model. However, by contrast to the long-lived one-arm formed in the restricted three-body code, the kinematic model arm is rather short-lived. The short duration of structures appears to be a generic property of the kinematic model. Understanding this behavior is a topic for future research.

The snapshots in Figure 13 show the development of the particle disk in the kinematic model following an impulsive disturbance. The target to companion mass ratio is 10, and the impact occurs at a distance of 5/7 in units of the potential softening length ε. Similar to the restricted three-body simulations, following the collision, a ring galaxy is formed ($t=10$, and $t=15$). At later stages the target disk is composed of an outer ring, and an inner leading one-arm ($t=15$). Eventually, it evolves into a short-lived (less than one rotation period) leading arm ($t=25$) which gradually expands, until it becomes unrecognizable ($t=40$).

Future research in the context of this project should concentrate on

Fig. 13 - Time evolution of points representing stars, following an off-center impulsive disturbance, calculated according to a simple two-dimensional kinematic model. The corresponding time is written in each frame.

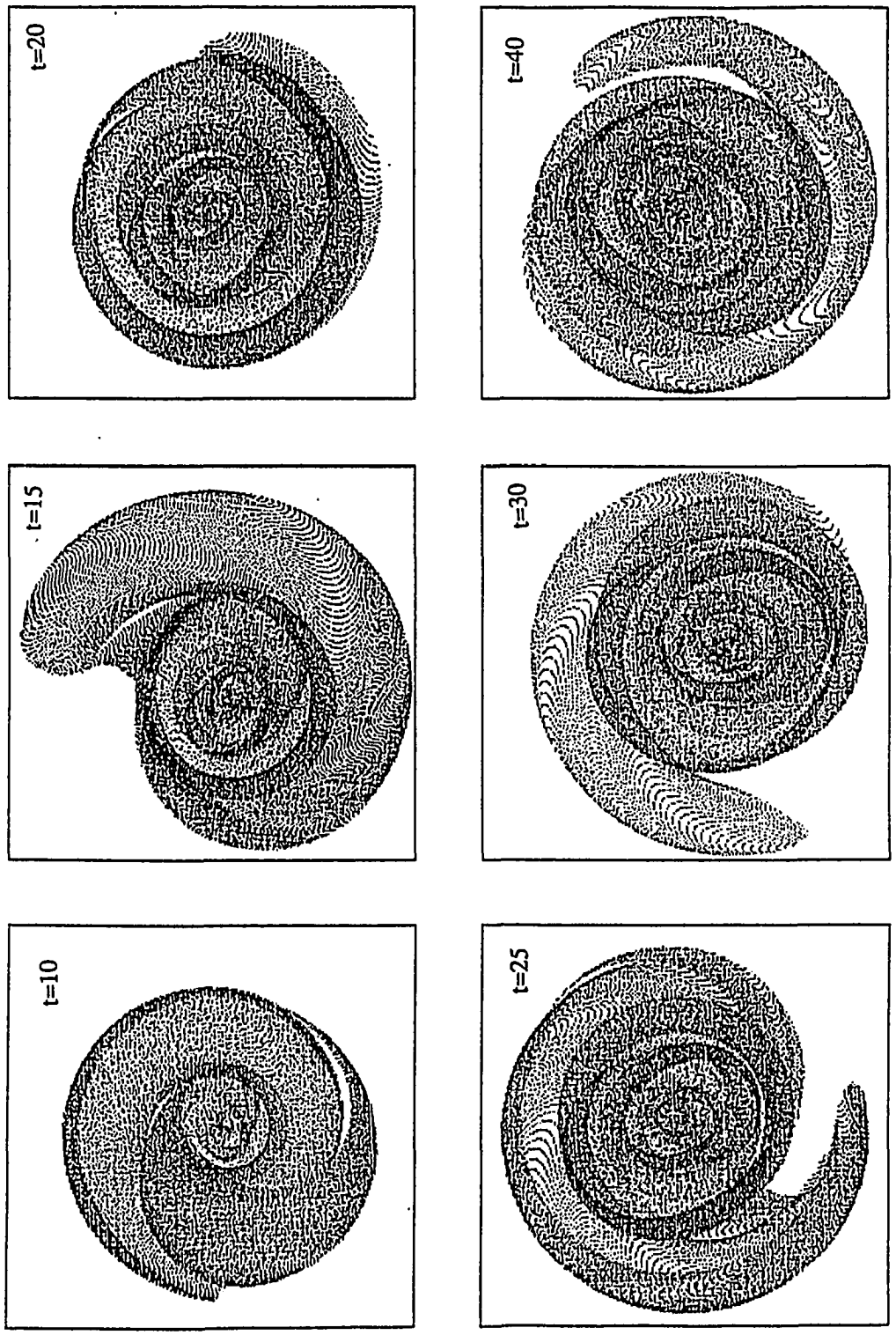
t=20
t=40
t=15
t=30
t=10
t=25

incorporating other potential forms into the kinematic model, in particular the "Hubble-like" potential, so that a direct comparison can be made with the restricted three-body simulations. Also, a successful simulation of the leading arm phenomenon in any model requires that the arm persist for at least several rotation periods. This has not been achieved yet with the present kinematic model.

V. COMPARISON WITH OBSERVATIONS

In order to distinguish between the head-on off-center production mechanism proposed in this paper, and the retrograde co-planar encounter scenario, one needs to determine the relative position of the companion with respect to the target disk. If the companion is obviously out of the disk plane, then a head-on collision is more probable, whereas if the companion is close to the plane, a co-planar encounter is more likely. Other types of evidence for the companion path, such as plumes of tidally stripped material along the companion's orbit can be used to distinguish between co-planar encounters and nearly head-on collisions. In addition, in our simulations we find that the thickness of the arm might also provide a clue for the formation mechanism. Specifically, thicker arms are more likely to be formed in head-on collisions. Narrower arms, by contrast, result from retrograde co-planar non-penetrating encounters.

In addition, in our simulations we find that at early stages following closest approach, the disk develops a propagating ring structure, much in the same way a collisional ring galaxy is produced. Subsequently, in intermediate stages the target will accomodate a ring in the outer parts of the disk, and a leading spiral arm interior to it. Although similar evolutionary paths were also found in some of our retrograde co-planar simulations, it appears that this behavior is more common in the more symmetric case of a head-on collision.

We are not aware of ring galaxies with a known inner leading spiral arm. However some ring galaxies possess "spokes" in their inner parts, such as the famous "Cartwheel" ring galaxy. The structure of these spokes should

be checked in view of the possibility that some of them might actually be leading spiral arms. In any event, the duration of this hybrid ring-spiral arm in our simulations is rather short which could makes this type of galaxy very rare.

As indicated above, a search for the existence of a dark spherical massive component in leading one-arm spirals, could test the collisional scenario, either a head-on or a co-planar. This property is expected from our simulations as well as those of Thomasson *et al.* (1989), since we find that the existence of a spherical component in the target galaxy is required for the arm formation. In fact, a nuclear bulge component could possibly constitute the spherical component, in particular in galaxies that contain a leading single-arm in their inner parts, such as M31.

Search for nearby companions in galaxies which possess a leading one-arm spiral, and determination of the orbits and properties of both galaxies, such as has been extensively done for M31 and M32, could clarify the origin of the arm, and specifically indicate whether an interaction is responsible for its formation.

V. CONCLUSIONS

Using restricted three-body simulations we find that a nearly head-on off-center collision, can result in a *long-lived leading one-arm spiral* in the target disk. In the existing literature, only co-planar retrograde mostly non-penetrating encounters are considered for the formation mechanism of leading one-arm spirals. Our proposed mechanism is possibly responsible for the leading one-arm situated in the inner disk of the Andromeda galaxy M31. Ample observational evidence exists which indicates that the dwarf elliptical satellite M32, crossed the disk of M31. Such a penetrating encounter is capable, according to our simulation results, of leading to the formation of a leading one-arm.

This family of one-arm spirals produced in a nearly head-on off-center collision, is intimately related to collisional ring galaxies (Theys and Speigel 1976, Lynds and Toomre 1976) believed to be formed in a central head-on collision. The two types of interacting galaxies are so closely related that often the post-collision disk starts out as a regular ring galaxy, which later transforms into a ring galaxy with an inner leading one spiral arm, and eventually into a long-lived pure grand design one-arm spiral. It is the degree of asymmetry (but depending on the other parameters as well) which determines whether the young ring galaxy will later evolve into a one-arm spiral, or remain a ring galaxy untill the rings have propagated out of the disk.

In comparing between simulations of head-on and co-planar collisions, we find that head-on collisions of low impact parameter *generally* result in more substantial, thicker arms than do co-planar encounters of large impact

parameter (of order the disk radius).

We propose several indicators which could possibly distinguish between a co-planar and a head-on collision in observed one-arm spirals. In particular, the position of the companion, or traces of its path, may be used to imply either a head-on collision or a co-planar retrograde encounter. Secondly, the presence of a ring around the one-arm which is found in our simulations for a brief period of time, implies that the formation mechanism is more likely a head-on collision rather than a co-planar one.

Future research should concentrate on analytic, possibly kinematic, methods, which we have only started to investigate. However, as described in Section IV above, as opposed to the restricted three-body simulations in which a very long-lived arm was formed due to the collision, the kinematic model was able to yield only a short-lived leading one-arm spiral. Since the arm formation is potential dependent, it is possible that incorporating the "Hubble-like" potential, invoked in our restricted three-body code, into the kinematic model (which currently uses a softened point potential), would result in the production of a *long-lived* arm. Even though self-gravity probably plays no role in the leading one-arm phenomenon, follow-up investigations with self-consistent methods are still desirable, and are part of our planned future research.

VII. REFERENCES

Athanassoula, E. 1978a, *Astron. Astrophys.*, **69**, 395.

Athanassoula, E. 1978b, *Structure and Properties of Nearby Galaxies*, IAU Symp. 77, eds. E. M. Berkhuijsen, R. Wielebinski, (Dordrecht: Reidel) p. 163.

Athanassoula, E. 1984, *Physical Reports*, **114**, 319.

Bertin, G. 1980, *Physical Reports*, **61**, 1.

Byrd, G. G. 1976, *Ap. J.*, **208**, 688.

Byrd, G. G. 1977, *Ap. J.*, **218**, 86.

Considère, S., and Athanassoula, E. 1982, *Astron. Astrophys.*, **111**, 28.

Elmegreen, D. M. and Elmegreen, B. G. 1982, *M.N.R.A.S.*, **201**, 1021.

Elmegreen, B. G. and Elmegreen, D. M. 1983, *Ap. J.*, **267**, 31.

Elmegreen, D. M. and Elmegreen, B. G. 1987, *Ap. J.*, **314**, 3.

Faber, S. M. 1973, *Ap. J.*, **179**, 423.

Fish, R. A. 1964, *Ap. J.*, **139**, 284.

Hernquist, L. and Quinn, P. J. 1988, *Ap. J.*, **331**, 682.

Kalnajs, A. J. 1975, *La Dynamique des Galaxies Spirales*, ed. L.Weliachew (Paris: CNRS), p. 103.

Keenan, D. W. and Innanen, K. A. 1975, *A. J.* **80**, 290.

King, I. R. 1962, *A. J.*, **67**, 471.

Kormendy, J. and Norman, C. A. 1979, *Ap. J.*, **233**, 539.

Lin, C. C., and Lau, Y. Y. 1979, *Studies Appl. Math.* **60**, 97.

Lotan, P. and Struck-Marcell, C. 1990, submitted to Ap. J.

Lynds, R., and Toomre, A. 1976, *Ap. J.*, **209**, 382.

Ostriker, J. P. and Peebles, P. J. E. 1973, *Ap. J.*, **186**, 467.

Pasha, I. I. 1985, *Soviet Astron. Letters*, **11**, 1.

Quinn, P. J., and Goodman, J. 1986, *Ap. J.*, **309**, 472.

Roberts, M. S. and Whitehurst, R. N. 1975, *Ap. J.*, **201**, 327.

Rubin, V. C., and Ford, W. K., Jr. 1970, *Ap. J.*, **159**, 379.

Sersic, J. L., and Agüero, E. L. 1972, *Astrophys. Space Sci.* **19**, 387.

Shu, F. 1982, *The Physical Universe* (Mill Valley: University Science Books) p. 274.

Struck-Marcell, C. 1990, *A. J.*, **99**, 71.

Struck-Marcell, C., and Lotan, P. 1990, *Ap. J.*, **358**, in press.

Theys, J. C. and Speigel, E. A. 1976, *Ap. J.*, **208**, 650.

Thomasson, M., Donner, K. J., Sundelius, B., Byrd, G. G., Huang, T.Y., and Valtonen, M. J. 1989, *Astron. Astrophys.*, **211**, 25.

Toomre, A. 1977, Ann. Rev. Astr. Ap., **15**, 437.

Toomre, A. 1978, *The Large Scale Structure of the Universe*, ed. M. S. Longair and J. Einasto (Dordrecht: Reidel), p. 109.

A COMPUTATIONAL METHOD FOR THE GRAVITATIONAL FIELD OF DISK GALAXIES

ABSTRACT

A numerical method is presented for calculating to high accuracy the gravitational potential V and field g for disk galaxies described by mass density distributions of the factorized form $\rho(r) = \sigma(r)\,\tau(z)$, where r and z are cylindrical coordinates. Most disk galaxies whose mass distributions have been investigated fall under this category. Due to this factorized form, V and g are expressible as one-dimensional integrals. For choices of observational relevance, in the vicinity ($|z|/r << 1$) of the galactic disk plane ($z = 0$) these integrals converge extremely slowly, thereby precluding accurate numerical evaluation by conventional methods. We show, however, that even for this problematic region, accurate evaluation of V and g can be achieved by invoking the Levin method for accelerating the convergence of infinite series.

I. INTRODUCTION

Calculation of the gravitational potential V and field $\mathbf{g} = -\nabla V$ due to a disk galaxy characterized by a continuous density function $\rho(r)$ is a topic of continuing importance in astrophysics. Knowledge of the gravitational field and potential is useful for several purposes, including the determination of the rotation curve of the disk as a function of its density distribution, and alternately, using the observed rotational curve, for inferring various disk properties. In addition, to incorporate effects of a disk component, various numerical simulation techniques, such as restricted N-body or restricted three-body methods, require knowledge of the disk field [e.g., Lotan and Struck-Marcell (1990), Struck-Marcell and Lotan (1990), Quinn and Goodman (1986), Villumsen (1985)]. Various convenient forms of the density function have been used, such as Toomre's (1962) disks, Mestel's (1963) disks, and others. (For a review and mathematical treatment see Chapter 2 of Binney and Tremaine 1987.) However, observational investigations of many disk galaxies (e.g., Freeman 1970; Kent 1984; Wevers 1984; Wevers, van der Kruit and Allen 1986) indicate that the radial intensity profile is well fitted by an exponential function. Further, normal to the disk plane (z-direction) the density has been fitted by the function $sech^2(z/z_o)$ (van der Kruit and Searle 1981a,b; 1982) for a sample of disk galaxies. A numerical calculation of the gravitational field created by the latter mass distribution was carried out by Villumsen (1985). For another sample of disk galaxies (Wainscoat, Freeman and Hyland 1989), as well as our Galaxy (Gilmore and Reid 1983; Pritchet 1983) an exponential in the z-coordinate was used to fit the density. The overall density distribution in the latter case

can be expressed as

$$\rho(r) = [M/(4\pi a^2 c)]\exp-[(r/a)+|z|/c] \ , \qquad (1)$$

where M is the total mass of the galaxy, and a and c are characteristic lengths. (The position vector r is conveniently described in terms of cylindrical coordinates r, ϕ, z.) The ratio $\xi = c/a$ is typically a small number. For example, Bahcall and Soneira (1980) find, on the basis of star counts, that for our Galaxy $\xi = 0.07$. Finally, an approximate analytic method for evaluating the g-field for the special case of a *strictly planar* mass distribution, and with an exponential dependence on r, was given by Ballabh (1973) and Chatterjee (1987).

In this paper, we present a numerical method for obtaining accurate values of V and g due to disk galaxies whose mass distributions possess rotational symmetry about the z-axis and, in addition, are of the factorized form

$$\rho(\mathbf{r}) = \sigma(r)\,\tau(z) \ . \qquad (2)$$

Fortunately, most mass distributions of observational significance fall under this category. Also, the assumption of rotational symmetry about the z-axis is valid for S0 galaxies. Finally, for some azimuthally asymmetric disks, such as those containing spiral arm structures, equation (2) describes the azimuthally averaged density distribution, and it might still provide a reasonable description.

For the class of disk galaxies with mass distributions described by equation (2), which includes as a special case equation (1), the quantities V

and g are expressible as one-dimensional integrals of the form given in equations (7), (10), and (11). To the best of our knowledge there is no known special case where these integrals can be evaluated, for arbitrary r and z, by analytical methods. Moreover, even the numerical evaluation of these integrals presents a major challenge for points in the near vicinity of the disk plane for most observationally relevant choices of the function $\sigma(r)$, due to the slow rate at which the oscillatory integrand in these equations decreases in magnitude to zero for large values of the integration variable. This is aggravated by the fact that the gravitational field changes most rapidly in the near vicinity of the disk plane ($z = 0$). Thus the evaluation of these slowly convergent integrals needs to be performed for a very large set of sampling points if one is to track the swift changes in the field components. Moreover, precisely the vicinity of the disk plane is of special importance in simulational studies, since the orbits of the disk particles generally remain in this region.

The purpose of the present work is to present a highly efficient numerical method for evaluating the one-dimensional integrals in equations (7), (10), and (11) even when they are slowly convergent, specifically, in the region $|z|/r << 1$. Our method entails relatively modest computations yet provides accuracies at the level of, at worst, parts in 10^6. This is to be compared with a typical accuracy of a few parts in 10^3 obtained by Ballabh (1973) and Chatterjee (1987) using an approximate analytical method. To describe our method we focus on equation (7) and we assume that the product $\Sigma(s)\psi(z,s)$ has the same sign for all s, or at most a finite number of sign changes. It is convenient to view the given integral as the infinite sum of the contributions between successive zeros of the Bessel function $J_0(rs)$. To fix the notation, let the integral be denoted by T and the individual contributions by t_n, so that $T = \Sigma_n t_n$ and the index n extends from 1 to ∞. Note that the successive contributions t_n alternate in sign. Furthermore,

for points in the near vicinity of the disk plane $|t_n|$ decreases very slowly in magnitude. As such, achieving an estimate of the infinite sum, by straightforward summation of the individual contributions t_n becomes impractical.

To overcome this obstacle, in Section III we employ the Levin method (1973) for accelerating the convergence of an infinite series. Utilizing the first N terms of an infinite series, the Levin method provides an estimate, to be denoted by $T[N]$, given by the formula in equations (14)-(16). It is remarkable that for values of N as small as 10-15 the estimate $T[N]$ can provide an exceptionally accurate estimate of the value of the infinite series. Generally, the requirement for the success of the Levin method is that the ratio of successive terms, i.e., t_n/t_{n+1}, be a slowly varying function of n, specifically, be well represented by an expansion in powers of $1/n$. Indeed, this requirement turns out to be met for the integrals appearing in equations (7), (10), and (11).

To utilize values of V and $\boldsymbol{g}$ due to the mass distribution of equation (2) in restricted N-body or restricted three-body numerical simulations, an efficient method of generating data must be employed. These simulations typically involve computing the orbits of several thousand test particles which comprise the disk. Obviously, evaluation of the field components at each test particle's position for each time step is impractical due to the enormous computation times required. Instead, one can evaluate and store, typically as a rectangular array, the components of the disk field for selected points (r_n,z_n) of a two-dimensional rectangular mesh within a domain, D, of interest. By applying interpolation methods to the entries of these stored arrays one can provide in an economical manner values of a field component or the potential for any point interior to D. A reasonable choice of this domain, in restricted N-body and restricted three-body methods, would be

the region where most of the test particles' orbits are confined. These issues are discussed further in Section IV. For points exterior to the chosen domain D, values of V and g can be obtained by asymptotically expanding the integrals in equations (7), (10), and (11) (Lotan and Luban 1990). The need for the asymptotic expressions arises, for example, in numerical simulations of interacting galaxies, in which values of the disk field at large distances (and thus exterior to the domain D) are usually required for calculating the orbit of an intruder galaxy. Also to be found in that paper are the derivations of analytic expressions for g_z along the z axis and on the disk plane, as well as g_r along the disk plane. In the last part of Section IV, we review the major features of the disk field derived using the present method. Finally, in Section V, we present a summary of our results.

II. BASIC EQUATIONS

A. General Results

In the first part of this section, we derive formulas, expressed as one-dimensional integrals, for the gravitational potential V and field g due to disk galaxies with a density function of the factorized form shown in equation (2). After providing these derivations we discuss the problematics of the integrals, specifically their slow convergence, which can arise for points in the vicinity of the disk plane ($z = 0$). In the following section, a method is presented for overcoming these difficulties.

Without loss of generality we impose the normalization condition

$$\int_{-\infty}^{\infty} dz\, \tau\,(z) = 1\,. \tag{3a}$$

Thus the quantity $\sigma(r)$, which is often called the disk surface density, satisfies the equality

$$\int_{0}^{\infty} dr\, r\, \sigma\,(r) = M/(2\pi)\quad . \tag{3b}$$

The gravitational potential associated with ρ can be written as

$$V(r\,,\,z) = 2G\int_{0}^{\infty} dR\, R\, \sigma\,(R)\int_{-\infty}^{\infty} dZ\, \tau\,(Z)\;\; W(r, R, Z - z)\,, \tag{4}$$

where G is the gravitational constant. Due to cylindrical symmetry, it suffices to choose the field point to be situated directly above the x axis. In equation (4), the quantities R and Z are integration variables, r and z are cylindrical coordinates of a field point, and W is defined by

$$W(r, R, u) = \int_0^{2\pi} d\Phi \, [r^2 + R^2 + u^2 - 2rR\cos\Phi]^{-1/2} \quad . \tag{5}$$

In equation (5) and henceforth, we can require that $u \geq 0$. A very convenient representation of the function W is provided by the identity (Watson, 1958, pg. 389, eq. [2])

$$W(r,R,u) = 2\pi \int_0^{\infty} ds \, J_0(rs) \, J_0(Rs) \, exp(-|u|s) \quad . \tag{6}$$

We may thus rewrite equation (4) as

$$V(r,z) = G \int_0^{\infty} ds \, J_0(rs) \, \Sigma(s) \, \psi(z,s) \quad . \tag{7}$$

The functions $\Sigma(s)$ and $\psi(z,s)$ are defined by

$$\Sigma(s) = 2\pi \int_0^{\infty} dR \, R \, \sigma(R) \, J_0(Rs) \quad , \tag{8}$$

$$\psi(z,s) = \int_{-\infty}^{\infty} dZ \, \tau(Z) \, exp(-|Z-z|s) \quad . \tag{9}$$

Note that $\Sigma(0) = M$ and $\psi(z,0) = 1$ by virtue of equations (3a) and (3b).

The gravitational field associated with the potential of equation (7) has two nonzero components given by

$$g_r(r,z) = G\int_0^\infty ds\, s\, J_1(rs)\, \Sigma(s)\, \psi(z,s) \quad , \tag{10}$$

$$g_z(r,z) = -G\int_0^\infty ds\, J_0(rs)\, \Sigma(s)\, \frac{\partial\psi(z,s)}{\partial z} \quad . \tag{11}$$

These components satisfy the symmetry properties,

$$g_r(r,-z) = g_r(r,z)\ ,\ g_z(r,-z) = -\,g_z(r,z)\ . \tag{12}$$

For circularly symmetric, strictly planar mass distributions, i.e., $\tau(z) = \delta(z)$, where δ denotes the one-dimensional Dirac delta function, the function ψ reduces to $\psi(z,s) = exp(-|z|s)$ and equation (7) has the form given by Binney and Tremaine (1987, pg. 76). In the following, we assume that both Σ and ψ can be evaluated analytically.

B. Problematics

Inspection of equations (7), (10), and (11) shows that the rate of convergence of these integrals is determined by the rate at which the products $\Sigma\psi$ and $\Sigma\partial\psi/\partial z$ decrease to zero for large values of s. To illustrate the problematics concerning the convergence of the integrals we focus on equation (7) and consider points on the disk plane ($z = 0$) and assume for the moment that the mass distribution is strictly planar, so that the factor

$\psi(0,s) = 1$ for all s. The rate of convergence is thus determined solely by the function Σ.

In the following, we will concentrate on disk galaxies for which σ depends on r exponentially. Normalized in accordance with equation (3), we have $\sigma(r) = [M/(2\pi a^2)]\ exp(-r/a)$ and thereby $\Sigma(s) = M[1 + (as)^2]^{-3/2}$. Note that Σ is positive for all values of s. (As will be seen in the following section this property is essential for the success of the method we have developed for evaluating the integral in eq. [7].) For large values of s, to leading order, the integrand of equation (7) is proportional to $s^{-7/2}\ cos(sr-\pi/4)$ and, due to this slow oscillatory decrease, accurate evaluation of the integral (again, for $z \approx 0$) by standard numerical methods is essentially impractical.

A second example, though only of mathematical interest, presents even greater difficulties. Consider the choice $\sigma(r) = M/(\pi a^2)$ for $r/a < 1$, and $\sigma(r) = 0$ for $r/a > 1$. For this choice $\Sigma(s) = 2M[J_1(as)/(as)]$. Here the function Σ alternates in sign between successive zeros (infinite in number) of J_1, and the method presented in the following section is inapplicable.

As a third and final example, consider $\sigma(r) = [M/(\pi a^2)]\ exp(-r^2/a^2)$. For this choice $\Sigma(s) = M\ exp(-a^2s^2/4)$. The integrand in equation (7) decreases so rapidly to zero for large values of s that numerical integration can be executed effectively even for points in the immediate vicinity of the disk plane.

In the remainder of this work, we specifically consider the mass distribution given in equation (1), because of its excellent fit to observational data.

III. THE LEVIN METHOD

In this section, we describe a method for successfully evaluating the integrals in equations (7), (10), and (11) even in the problematic region where $|z|/r << 1$. In order to evaluate equation (7), we suppose that the product $\Sigma\psi$ has the same sign for all s. (The corresponding requirement applies for the two integrals in eqs. [10] and [11] as well.) The present method can be generalized to include cases where this product has a *finite* number of sign changes. We denote the positive zeros of $J_0(u)$ by u_n for $n = 1,2,3,...$, and the interval (u_{n-1},u_n) by I_n, for $n = 2,3,...$. We also define I_1 as the interval $(0,u_1)$, and t_n as the contribution from I_n to the infinite integral, denoted by T. Using this notation we have

$$T = \sum_{n=1}^{\infty} t_n \tag{13}$$

Highly accurate values of t_n can be obtained by Gaussian numerical integration. Since we assume that $\Sigma\psi$ does not change sign, it follows that the integrand is of the same sign throughout any interval I_n, and that successive values of t_n alternate in sign. Further, for large enough values of n , the magnitude of t_n decreases monotonically in magnitude. However, for the regime $|z|/r << 1$, the decrease occurs at a slow rate, which rules out accurate evaluation of the sum in equation (13) by straightforward summation.

A highly accurate estimate for the infinite sum, even for this problematic regime, is provided by applying the Levin (1973) series acceleration method to the first N subintegrals t_n. Although other series

acceleration methods exist in the literature, the Levin method appears to provide (Luban 1990) the most accurate estimates for the value of many infinite series whose terms alternate in sign. This conclusion is verified by comparing the accuracy of various acceleration methods, in those cases where the series can be summed analytically. We denote by $T[N]$ the Levin estimate of the infinite series T of equation (13) as obtained by employing the first N terms of the series. The value of this quantity is given by

$$T[N] = P[N]/Q[N] \quad , \tag{14}$$

where

$$P[N] = \sum_{k=1}^{N} (-1)^k \, k^{N-1} \, (T_k / t_k)/[k! \, (N-k)!] \tag{15}$$

$$Q[N] = \sum_{k=1}^{N} (-1)^k \, k^{N-1} \, (1/t_k)/[k! \, (N-k)!] \quad , \tag{16}$$

and $T_k = t_1 + t_2 + \ldots + t_k$. In our numerical work we found that the estimates $T[14]$ and $T[15]$ typically agreed with each other to an accuracy of a few parts in 10^8, and the common digits can be taken as providing the value of T to nine significant figures.

At first sight it may appear quite mysterious that summing a very large number of terms of the series in equation (13) fails to provide an accurate estimate of T, whereas if one uses the Levin formulas, equations (14)-(16), in conjunction with a mere dozen or so terms t_n, one obtains estimates of T with an accuracy no worse than parts in 10^6. However, it should be noted that, rather than sum the terms of the series, the Levin method exploits a property of many infinite series, that the error in approximating the full

series by the sum of the first n terms is of order the last term retained. This may be expressed quantitatively by the relation $T_n = T + t_n f_n$, for all positive integers n, where f_n is a slowly-varying function of $1/n$ with a unique, finite limit for $n \to \infty$. It can be shown that necessary requirements for the sequence $\{f_n\}$ to have these properties are that the ratio of successive terms of the given series, namely t_n/t_{n+1}, should be a slowly-varying function of $1/n$, and, secondly, the ratio should approach a unique finite limit unequal to unity for $n \to \infty$. For series where f_n has these properties one can expect that approximating this quantity by a polynomial in the variable $1/n$ should lead to accurate estimates of the value of the series. Specifically, if we write

$$f_n = \sum_{k=0}^{N-2} c_k (1/n)^k \tag{17}$$

and require that $T_n = T[N] + t_n f_n$ for $n = 1, 2, \ldots, N$, we have N equations which determine the N unknowns, $T[N]$, $\{c_k\}$, $(k = 0, 1, \ldots, N-2)$. In fact, equations (14)-(16) provide the value of $T[N]$.

IV. EVALUATION OF INTEGRALS

A. Procedures

As explained in the previous section, our method for evaluating the integrals in equations (7), (10), and (11) is based on two ingredients: (1) numerical integration methods are used to determine the individual contributions, t_n, to the integrals from each arch of the Bessel function J_0 (or J_1). (2) if the individual terms decrease slowly in magnitude, we invoke the Levin series acceleration method so as to obtain highly accurate estimates of the infinite sum in equation (13). Because of the slow variation of the factors $\Sigma\psi$ and $\Sigma\partial\psi/\partial z$ between successive zeros of the Bessel functions we utilized Gauss's 21-point integration method for each arch so as to obtain values of t_n with an accuracy of a few parts in 10^{10}. Such a high level of accuracy is desirable since the Levin method tends to greatly magnify small errors in the values of the individual terms of a given series. The zeros of J_0 and J_1 are provided by Gray, Mathews, and MacRoberts (1931) to 12 and 18 significant figures, respectively. The ratio of successive terms, t_n/t_{n+1} was found to be an extremely slow-varying function of 1/n, thus providing a large degree of confidence that the Levin method should indeed provide highly accurate estimates of the infinite integrals.

We have evaluated the components of the disk field for the points of a two-dimensional square mesh, with mesh spacing h, within a domain D defined by $|Z| < 10$, $0 < R < 20$. The dimensionless quantities Z and R denote the coordinates of a field point measured in units of the disk scale length a appearing in equation (1). The resulting values of g_z and g_r are stored as the entries of two rectangular arrays. Interpolation using the entries

of these arrays provides values of the field components for any point interior to the domain D. The mesh spacing h was adjusted to insure a desired level of accuracy. For the regime $0 < Z < 0.2$, where g_Z and g_r vary rapidly, we chose $h = 0.01$ whereas for $Z > 0.2$ our choice was $h = 0.05$. For points exterior to the domain D we used asymptotic expansions of equations (10) and (11) derived in Lotan and Luban (1990). This procedure was necessary only for the intruder since the test particles were always confined to the near vicinity of the disk plane $Z = 0$. A copy of our Fortran code for evaluating these integrals is available upon request.

B. Behavior of Field Components

1. Planar disk

A strictly planar disk is described by equation (1) with $\xi = c/a = 0$. In Figure 1 we show the dependence of g_Z on Z for several fixed values of R. The first interesting feature is that g_Z exhibits a discontinuity at $Z = 0$, by virtue of the symmetry relation in equation (12). Specifically, g_Z changes sign as one crosses the disk plane. Second, for increasing values of Z, the curves shown tend to merge, i.e., for that region the quantity g_Z is essentially independent of R. In fact, one expects that sufficiently far from the disk the value of g_Z should decrease proportional to $1/Z^2$ due to the finite total mass of the galaxy.

In Figure 2, g_Z is shown as a function of R, for several fixed values of Z. Evidently, g_Z decreases monotonically with R, which is to be expected because of the monotonic decrease with R of the local mass density. Also, g_Z is seen to be independent of (fixed) Z for large values of R, and the asymptotic dependence is proportional to $1/R^2$.

In Figure 3, we show the dependence of g_r on R for several fixed values of Z. Note that g_r vanishes for all points on the Z axis, as is to be

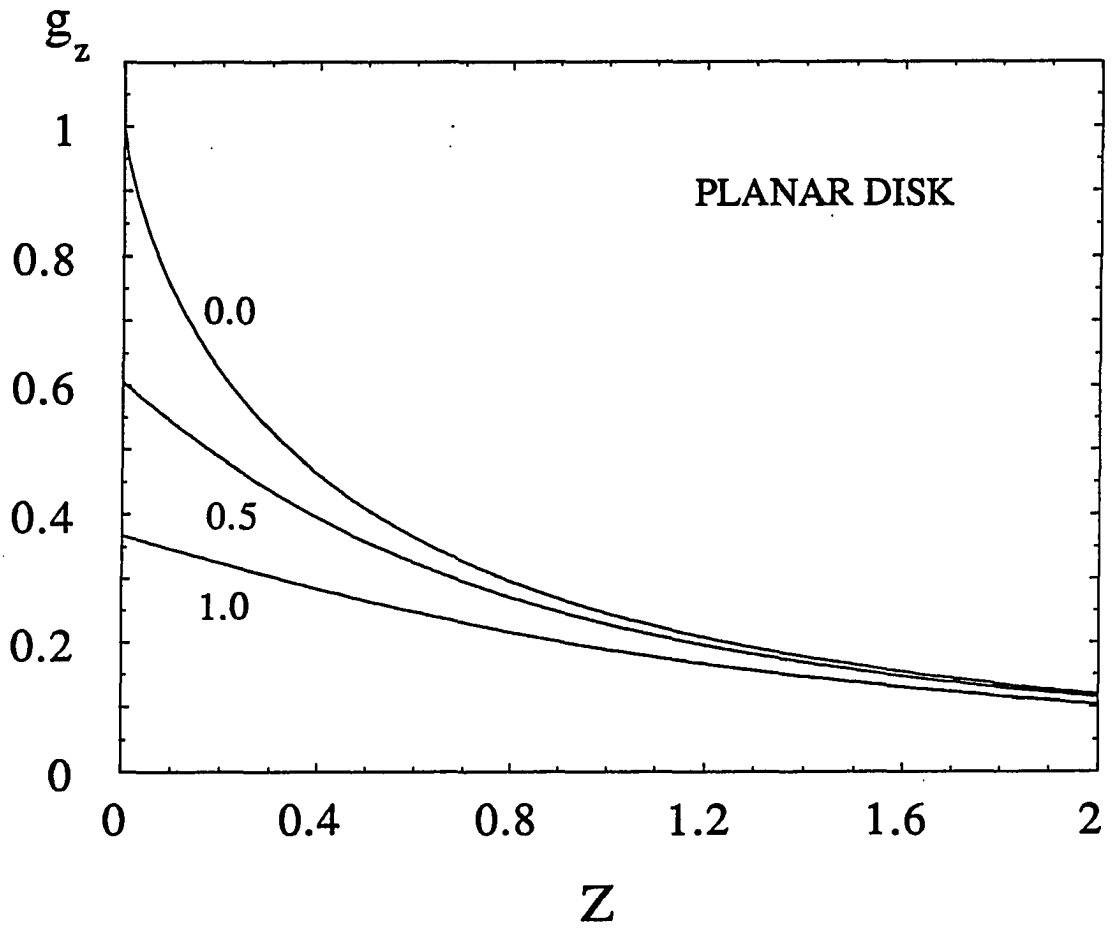

Fig. 1 - *Z*-component of the gravitational field due to a planar mass distribution given by a decreasing exponential function of the radial coordinate, as a function of the field coordinate *Z* for the listed values of *R*.

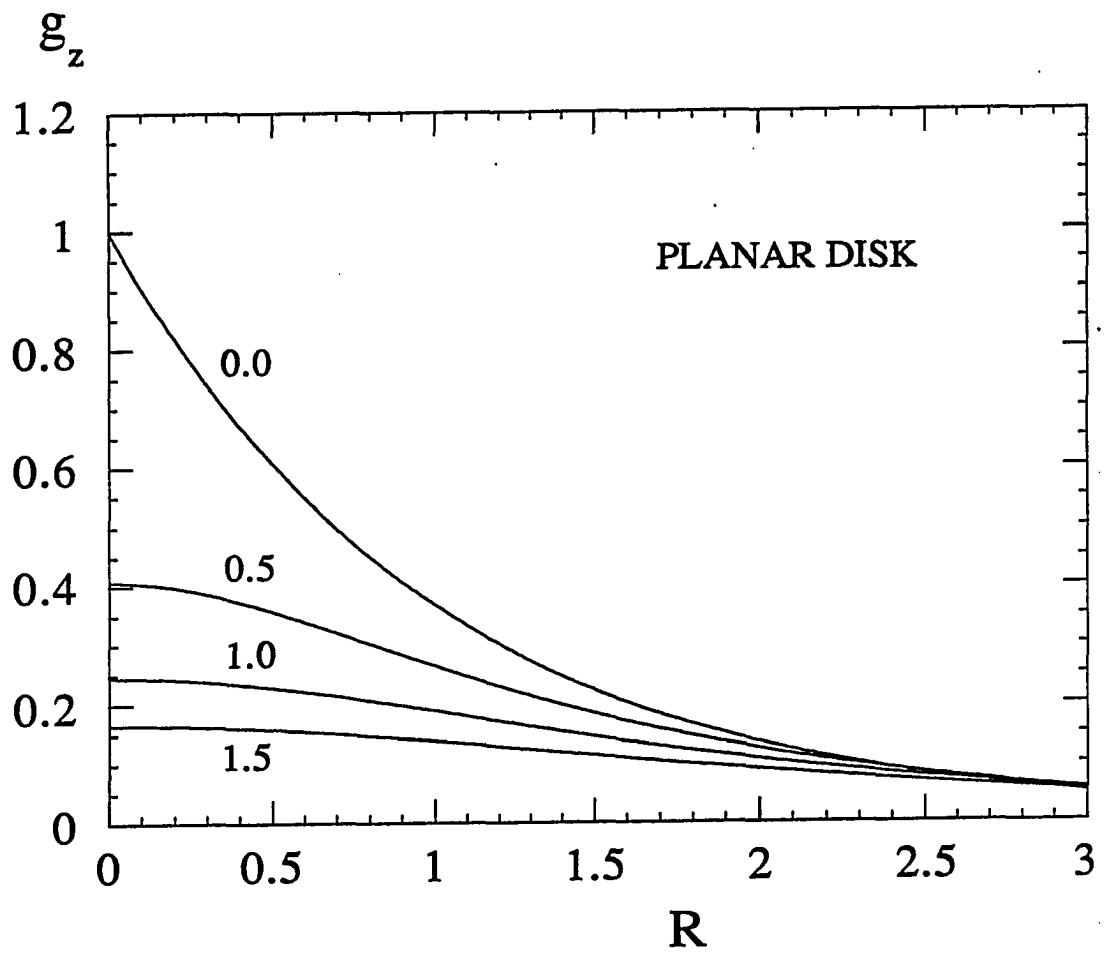

Fig. 2 - Same as Fig. 1 except as a function of the field coordinate *R* for the listed values of *Z*.

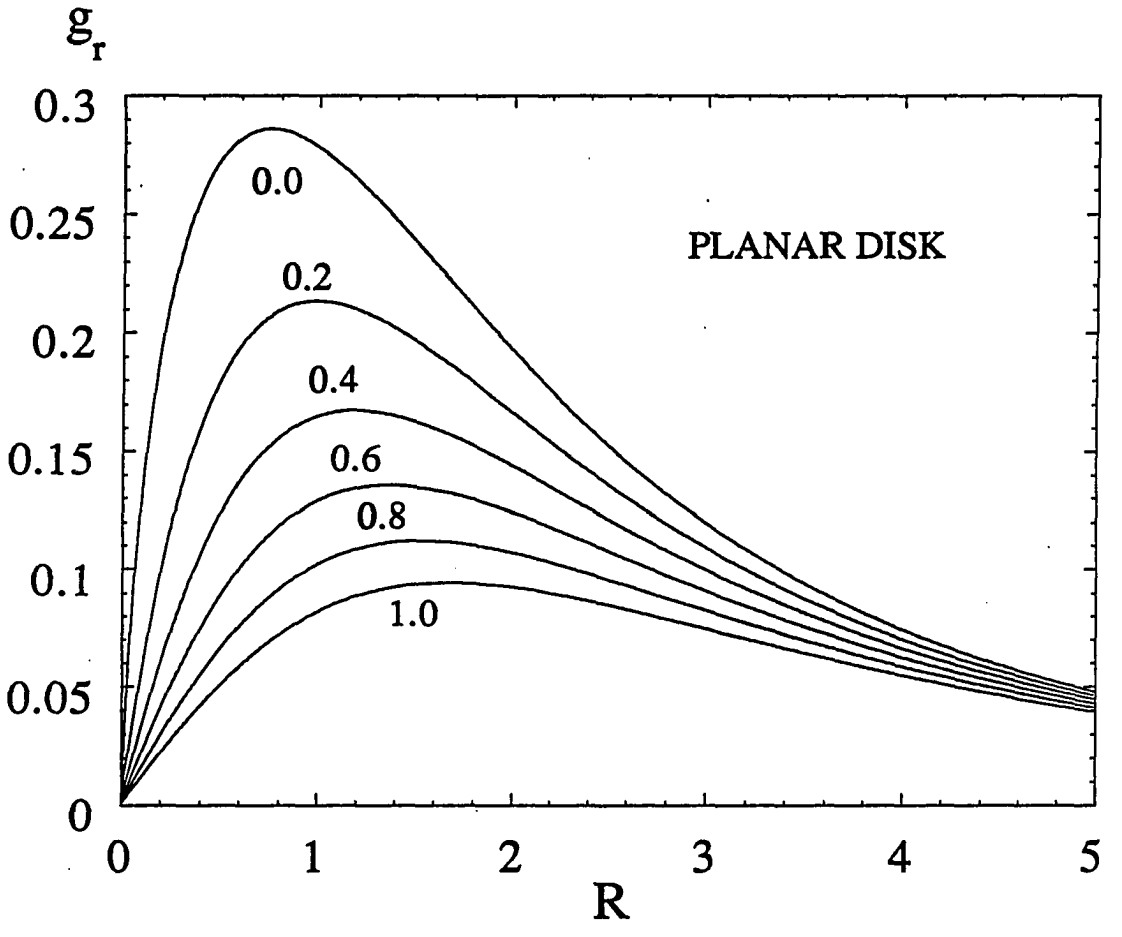

Fig. 3 - *R*-component of the gravitational field due to a planar mass distribution given by a decreasing exponential function of the radial coordinate, as a function of the field coordinate *R* for the listed values of *Z*.

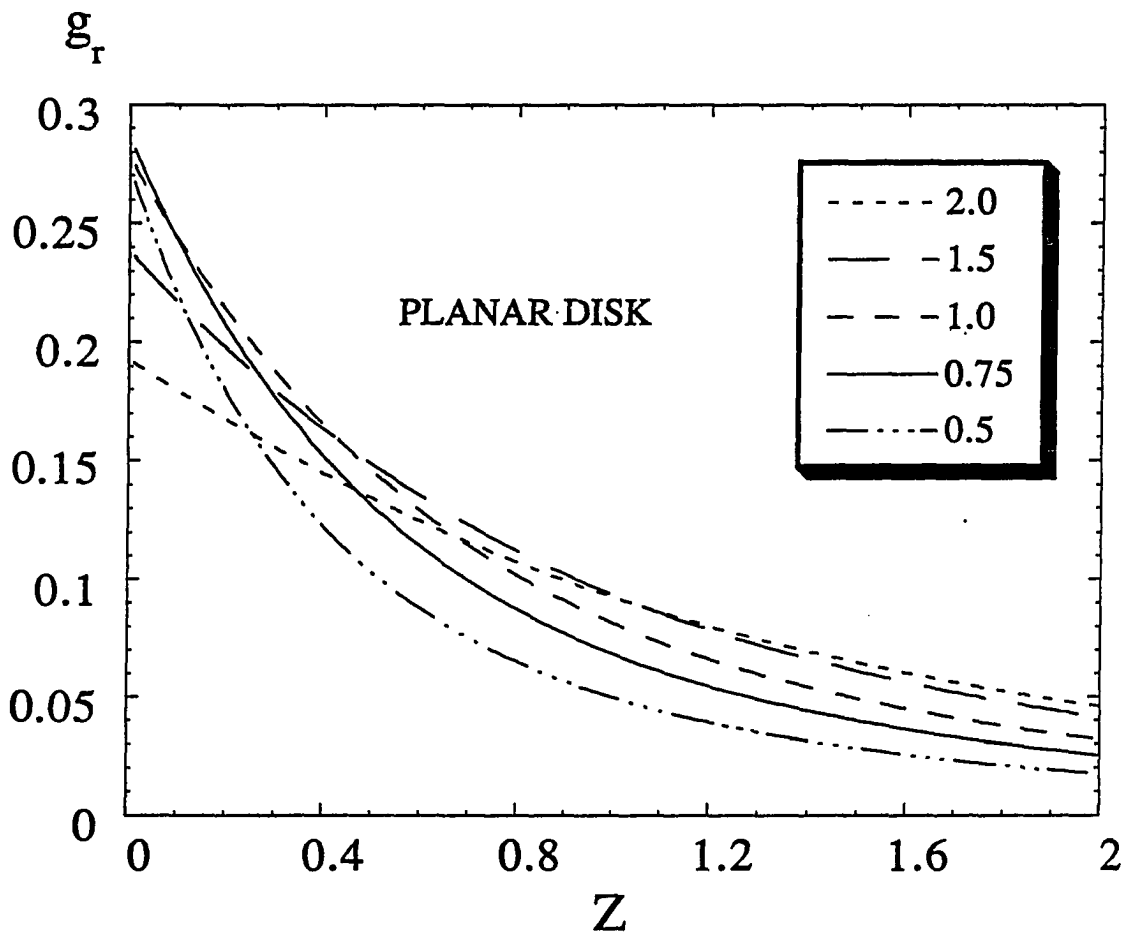

Fig. 4 - Same as Fig. 3 except as a function of Z for the listed values of R.

expected by symmetry. The fact that g_r is non-zero everywhere off the Z axis is due to the fact that the chosen mass distribution is dependent on R. (Recall that g is directed strictly along the Z direction for a planar disk with a uniform surface distribution.) Also note that as expected, the initial slope of g_r is larger the smaller the value of Z. In the Keplerian limit, namely for large values of R, the family of curves in Figure 3 tend to merge and decay as $1/R^2$ as expected. Note that the same value of g_r occurs for two different values of R on each curve of fixed Z. This property is responsible for the mutual intersection of the curves of g_r versus Z seen in Figure 4.

2. "Fattened" Disk

A "fattened disk" is defined by a mass density distribution in which $c \neq 0$ (eq. [1]). In Figure 5 we show g_Z for points on the axis of symmetry (Z axis) for $\xi = 0.0, 0.035,$ and 0.07. Note that g_Z decreases to zero monotonically as Z approaches 0, as is expected on the basis of the symmetry relations of equation (12) for a continuous matter distribution (i.e., $\xi \neq 0$). Also, the monotonic decrease of g_Z for fixed Z as ξ is increased can be understood, since less material lies between the point Z and the disk plane, as the disk grows increasingly fatter. Note that the value of g_Z is essentially independent of ξ when $z > 4c$ simply because high above or below the disk, the effect of "fattening" cannot be felt anymore.

The effects of disk "fattening" on the R dependence of g_Z are shown in Figures 6-8. The main result is that the dependence on R is sensitive to the value of ξ only close to the region of "fattening", since exterior to that region, the actual width of the mass distribution in the z-direction is basically irrelevant.

The effects of disk "fattening" upon g_r can be seen in Figures 9, and 10. In Figure 9, we display the behavior of g_r as a function of R for points along the disk plane. The role of increasing ξ is to give rise to a monotonic decrease of g_r for any given value of R. This too is in accord with intuition. A similar monotonic decrease with increasing ξ occurs for g_r as a function of Z, as seen in Figure 10. Overall, the effects of increasing ξ are much more pronounced for the field component g_z than for g_r.

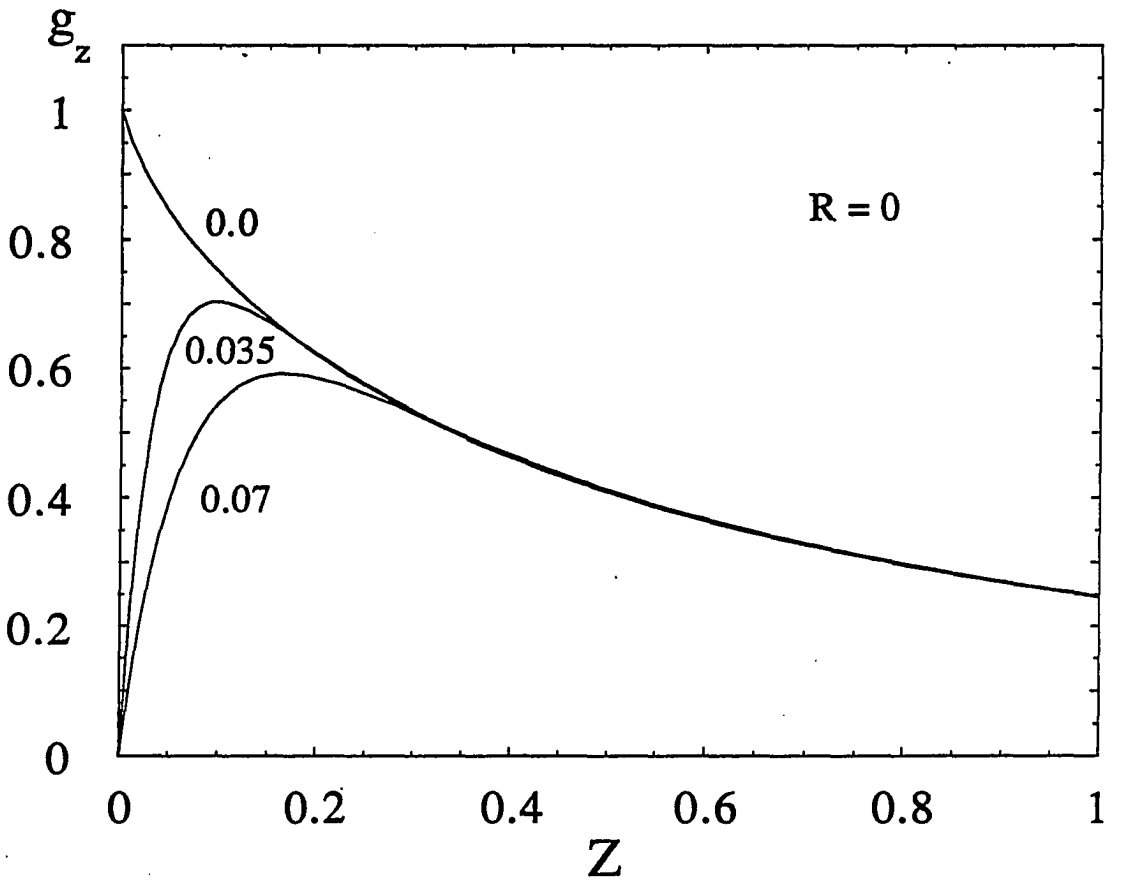

Fig. 5 - Z-component of the gravitational field due to the mass distribution given in eq. (1), for field points on the Z axis and for the values of ξ (=c/a) listed.

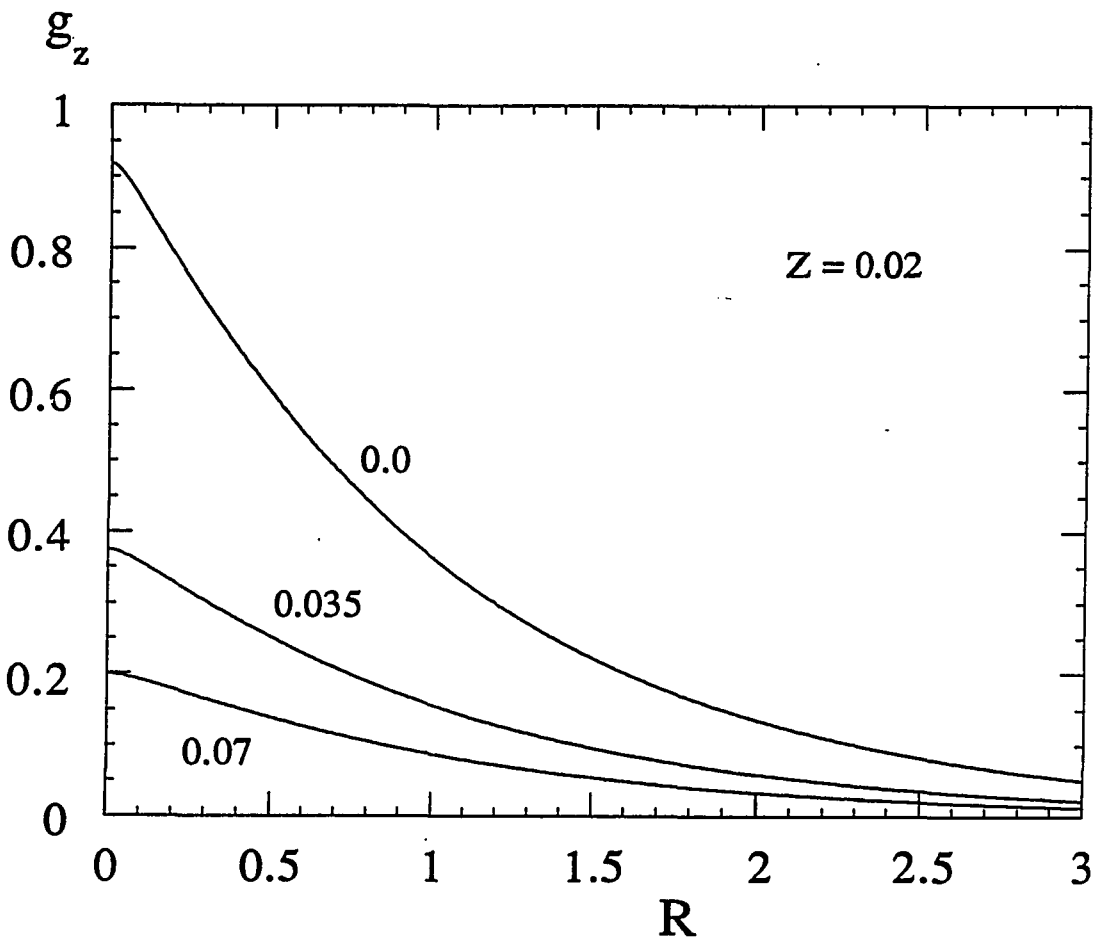

Fig. 6 - *Z*-component of the gravitational field due to the mass distribution given in eq. (1), for field points in the plane $Z = 0.02$ and for the values of ξ (=c/a) listed.

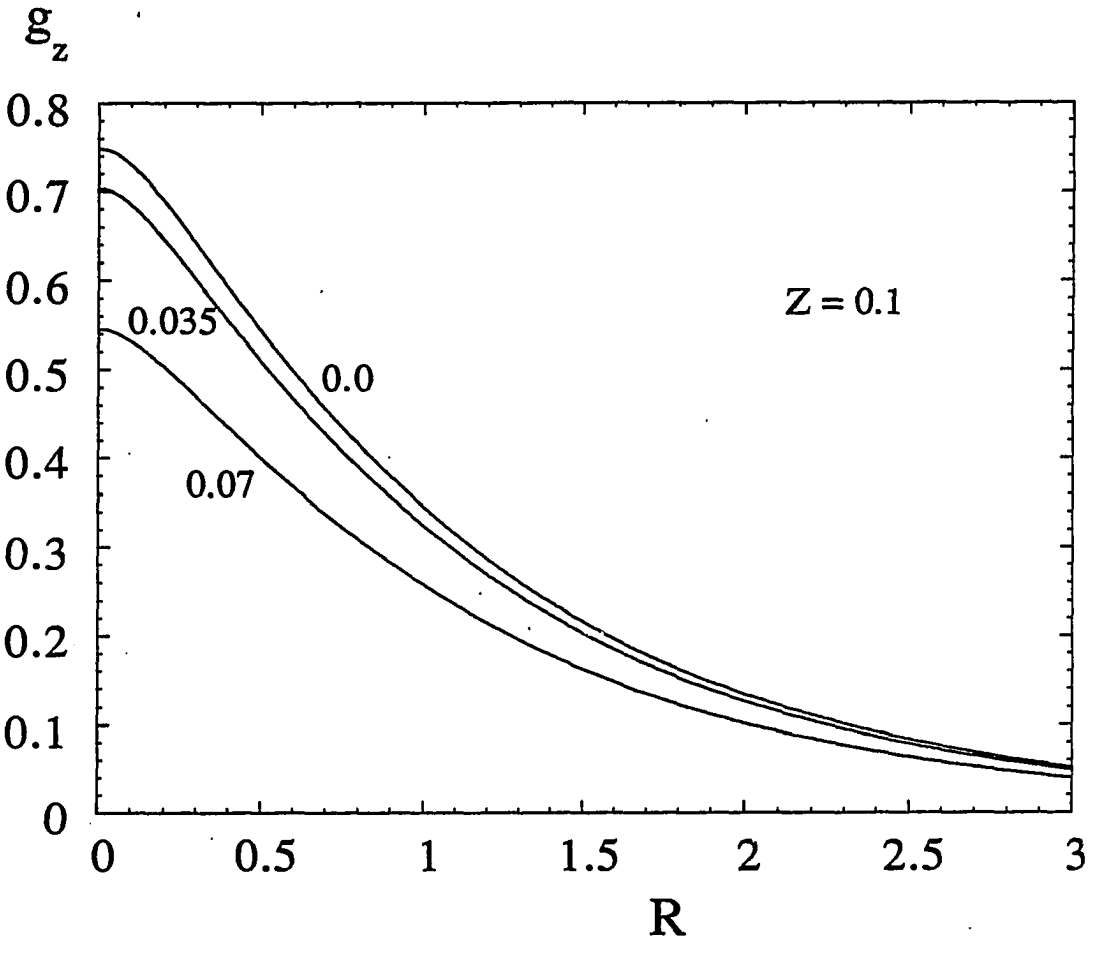

Fig. 7 - Same as Fig. 6 except for the plane $Z = 0.1$.

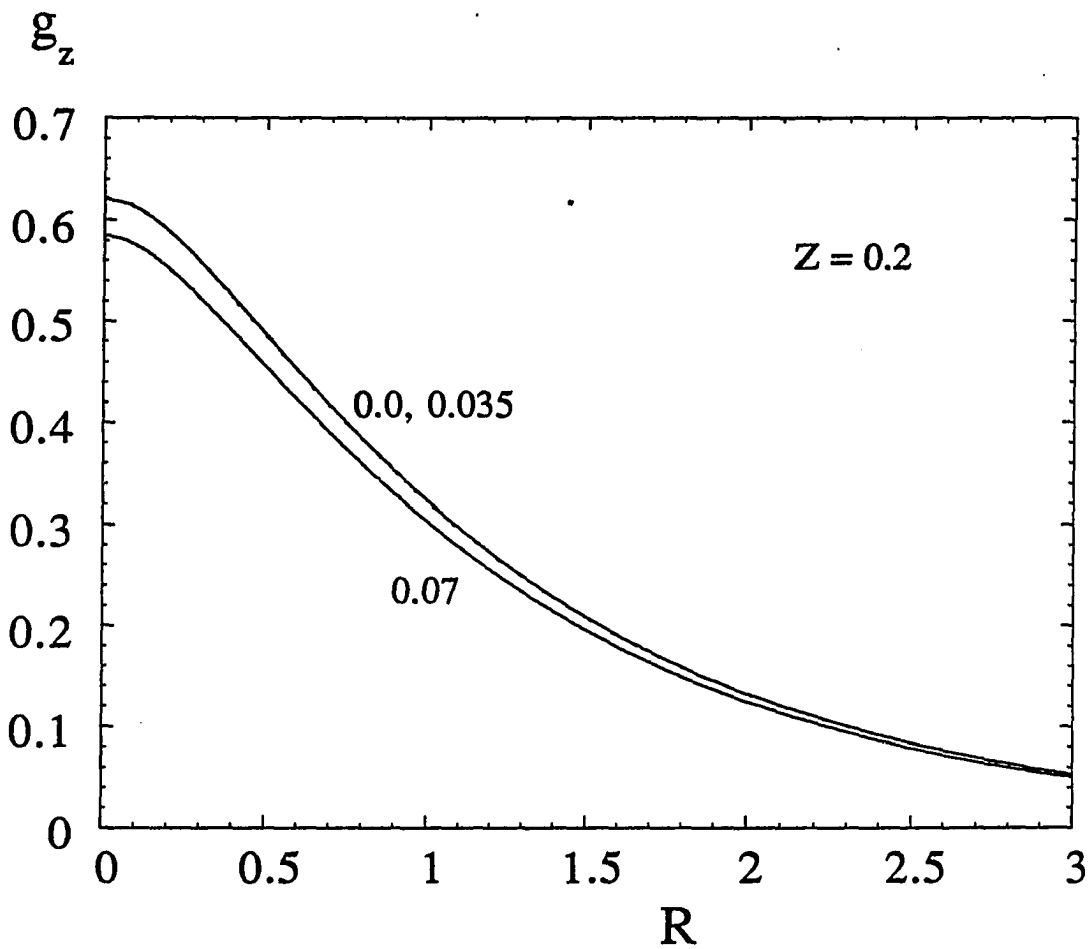

Fig. 8 - Same as Fig. 6 except for the plane $Z = 0.2$.

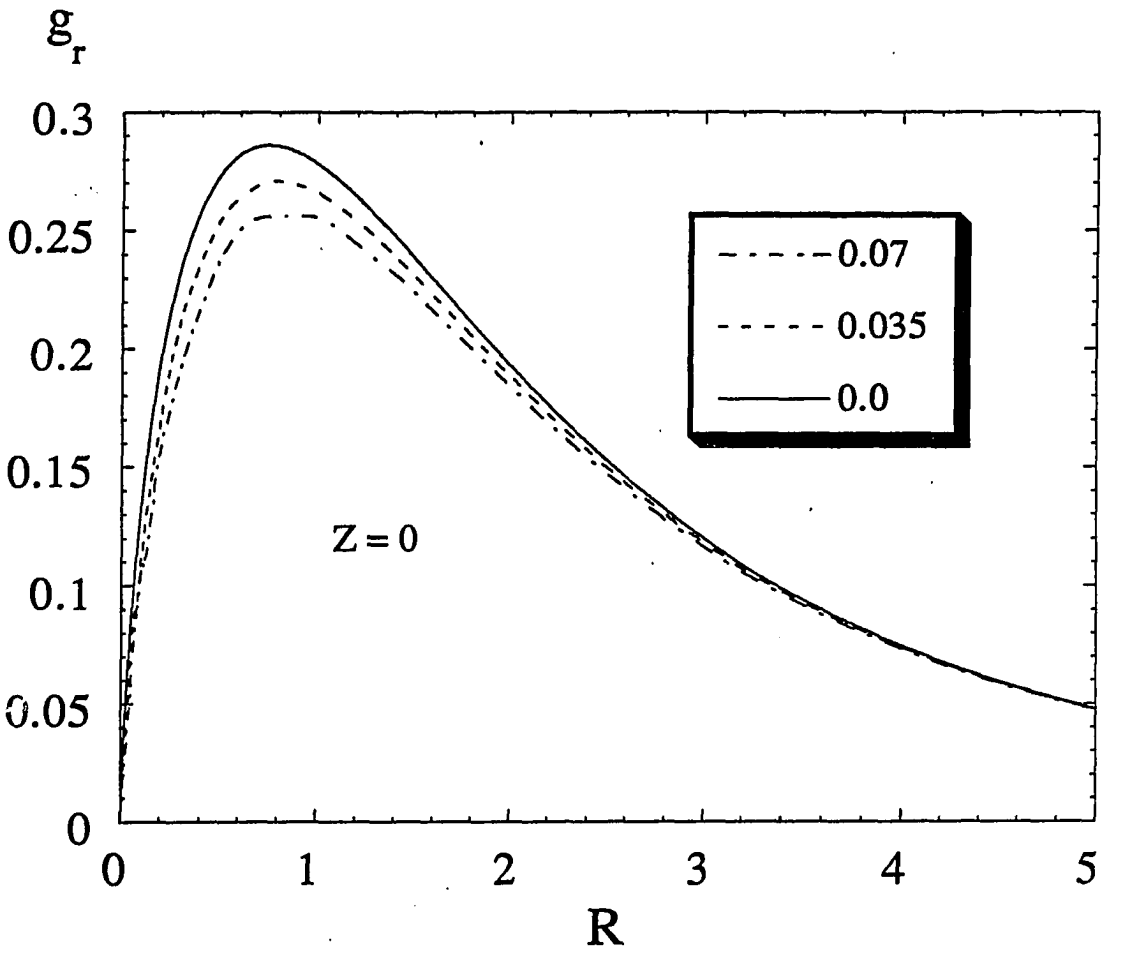

Fig. 9 - *R*-component of the gravitational field due to the mass distribution given in eq. (1), for field points in the disk plane ($Z = 0$) and for the values of ξ ($=c/a$) listed.

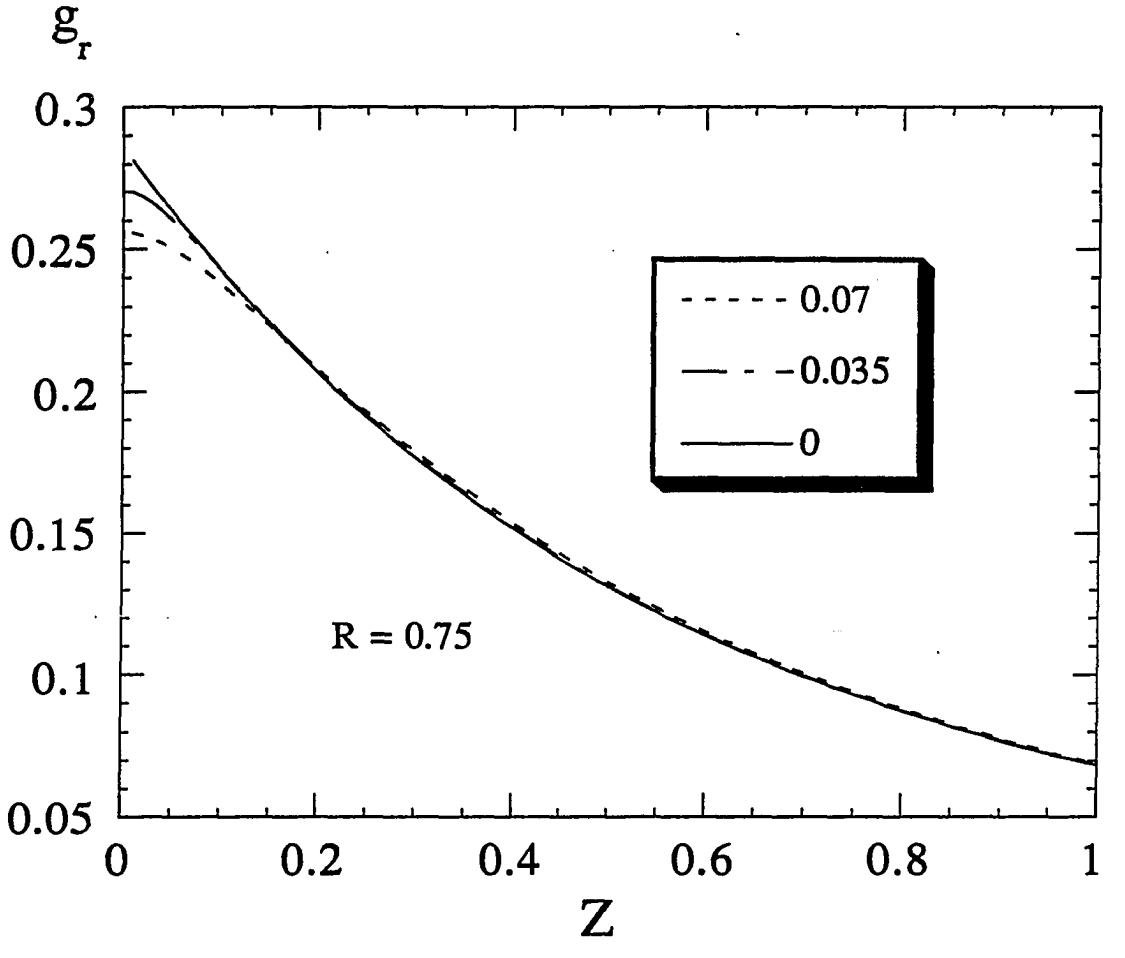

Fig. 10 - Same as Fig. 9 except as a function of the field coordinate Z for R = 0.75 and and for the values of ξ *(= c/a)* listed.

V. CONCLUSIONS

In this paper, we have presented a numerical method providing accurate values of the gravitational potential V and field $\boldsymbol{g}$ due to a disk galaxy characterized by any mass distribution of the separable form given in equation (2). Of special importance, for mass distributions of observational relevance, conventional integration methods encounter the difficulty that the infinite integrals providing V and $\boldsymbol{g}$ converge extremely slowly for the region in the vicinity of the disk plane. We have overcome this difficulty by employing the following method. The first step consists of dividing the infinite integration range into an infinite number of intervals whose boundaries are the zeros of the Bessel function J_0 (or J_1). The value of the infinite integral can be written as the infinite sum of the contributions of the separate intervals. For the region $|z|/r << 1$ accurate estimates of the values of the resulting slowly-convergent sum are obtained by invoking the Levin series acceleration method (1973). The present method should be of special interest for simulational studies of disk galaxies, in particular restricted N-body and restricted three-body methods, in cases where accurate values of V and $\boldsymbol{g}$ in the immediate vicinity of the disk plane are of particular importance. We have also derived useful asymptotic formulas for V and $\boldsymbol{g}$ for points far from the disk plane but the derivation and the major formulas will be presented elsewhere (Lotan and Luban, 1990). These formulas are of value if one wishes to determine the orbit of an initially distant intruder galaxy. The majority of our numerical results have been obtained for the mass distribution given by equation (1), although it would be equally straightforward to evaluate the disk field and potential energy for other choices, if shown to be of observational relevance.

VI. REFERENCES

Bahcall, J. N., and Soneira, R. M. 1980, *Ap. J. Suppl.*, **44**, 73.

Ballabh, G. M. 1973, *Astrophys. Space Sci.*, **24**, 535.

Chatterjee, T. K. 1987, *Astrophys. Space Sci* , **139**, 243.

Binney, J. C., and Tremaine, S. 1987, *Galactic Dynamics* (Princeton: Princeton University Press).

Freeman, K. C. 1970, *Ap. J.*, **160**, 811.

Gilmore, G. and Reid, N. 1983, *M.N.R.A.S.*, **202**, 1025.

Gray, A., Mathews, G. B., and MacRobert, 1931, *A Treatise on the Theory of Bessel Functions*, 2nd ed. (London: Macmillan).

Kent, S. M. 1984, *Ap. J. Suppl.*, **59**, 115.

Levin, D. 1973, *Int. J. Computer Math.*, **3**, 371.
University.

Lotan, P., and Luban, M. 1990, in preparation, Department of Physics, Iowa State University.

Lotan, P., and Struck-Marcell, C. 1990, submitted to *Ap. J.*.

Luban, M. 1990, in preparation, Department of Physics, Iowa State University.

Mestel, L. 1963, *M.N.R A S.*, **126**, 553.

Mihalas, D., and Binney, J. 1981, *Galactic Astronomy* (New York: W. H. Freeman).

Pritchet, C. 1983, *Ap. J.*, **88**, 1476.

Quinn, P. J., and Goodman, J. 1986, *Ap. J.*, **309**, 472.

Struck-Marcell, C., and Lotan, P. 1990, *Ap. J.*, **358**, in press.

Toomre, A. 1962, *Ap. J.*, **138**, 385.

van der Kruit, P. C. and Searle, L. 1981a, *Astr. Ap.*, **95**, 105.

van der Kruit, P. C. and Searle, L. 1981b, *Astr. Ap.*, **95**, 116.

van der Kruit, P. C. and Searle, L. 1982, *Astr. Ap.*, **110**, 61.

Villumsen, J. V. 1985, *Ap. J.*, **290**, 75.

Wainscoat, R. J., Freeman, K. C., and Hyland, A. R. 1989, *Ap. J.*, **337**, 163.

Watson, G.N. 1958, *A Treatise on the Theory of Bessel Functions*, 2nd ed. (Cambridge: Cambridge University Press).

Wevers, B. M. H. R. 1984, Ph. D,, thesis, University of Groningen.

Wevers, B. M. H. R., van der Kruit, P. C., and Allen, R. J. 1986, *Astron. Astrophys. Suppl.*, **66**, 505.

SUMMARY AND CONCLUDING REMARKS

Numerical studies of two rare, yet intriguing, types of collisional galaxies are the topic of this dissertation. Several numerical methods are employed in order to investigate the formation and properties of the colliding galaxies. These methods include, restricted three-body simulations, kinematic model calculations, and hydrodynamical calculations. Various aspects of the colliding galaxies are explored. The first project is a thorough investigation into the dependence of the morphology and kinematics of colliding ring galaxies, on the collision parameters, and the pre-collision structure of the colliding galaxies. The second project concentrates on effects of multiple central passages and merger on a disk galaxy. The main result of this investigation is a proposed classification of collisional ring galaxies, which appears similar to an empirical classification reported in the existing literature. The third project deals with a different, yet closely related type of interacting galaxies, namely leading one-arm spirals. We find that perpendicular off-center collisions give rise to this wave morphology. This type of collision is different from the retrograde co-planar encounters previously reported in the literature. Furthermore, our proposed new formation scenario establishes a close relationship between collisional ring galaxies and leading one-arm spirals. The type of collision producing the two types of interacting galaxies, differs merely in the size of the impact parameter of the collision.

Despite the rich spectrum of phenomena described in this dissertation, the range of collisional parameters investigated in the various projects reported, makes up only a small fraction of possible collisions between two

or more galaxies. Other types of collisions include: co-planar encounters, non-penetrating encounters, high-speed encounters, effects of collisions on spherical systems (only disk galaxies are considered in the dissertation), collisions between three or more galaxies, and others. In addition, other physical effects, not included in our investigation, may be of great importance, such as gas-dynamics, star formation activity, star-gas interactions and other phenomena. More sophisticated numerical methods, in particular self-consistent N-body methods, and hydrodynamical investigations, are needed to explore additional physical phenomena such as the effects of star-star interaction (not included in our restricted three-body code), changes in the potentials of the colliding galaxies due to tidal distortions brought about by the encounter, and effects of realistic velocity dispersions, which tend to wash out structures. These research directions are natural extensions of this thesis, and I plan to extend our investigation in these directions, and others, in future work.

ACKNOWLEDGEMENTS

I wish to thank my thesis advisor Dr. Curtis Struck-Marcell for guiding me throughout my graduate studies with much dedication and expertise.

Special thanks go to the Applied Mathematical Sciences Group of the Ames Laboratory, Iowa State University for providing me with generous computing facilities. Thanks also to Dr. Phil Appleton for use of his computing equipment.

I wish to thank Dr. John F. Wallin for making available to me a restricted three-body code which provided the basis for the code used in this project.

I am also grateful to the entire Astrophysics group at the Department of Physics at Iowa State University for providing me with scientific education combined with a very pleasant atmosphere throughout my graduate studies.

Thanks go to my thesis commitee members John P. Basart, George H. Bowen, Derek L. Pursey, Curt Struck-Marcell, and Lee Ann Willson, for comments and corrections which led to an improved final manuscript.

Part of this project was supported through NASA grant NAGW 1009, for which we are grateful.

Finally, special thanks to my husband, Dr. Marshall Luban, for his deep abiding friendship and love. To our children Dekel, Aviv, and Sarit, I am grateful for making these years of my graduate studies a true challenge.